From normal right ventricle to pathology : shape and function analysis with different loading conditions using imaging and modelling

Pamela Moceri

École doctorale Sciences et Technologies de l'Information et de la Communication

Unité de recherche : INRIA Equipe Asclepios

Thèse de doctorat

Présentée en vue de l'obtention du grade de

Docteur en Sciences

de l'UNIVERSITE COTE D'AZUR

par

Pamela MOCERI

Du cœur droit normal au pathologique – analyse de la forme et de la fonction dans différentes conditions de charge à l'aide de l'imagerie médicale et de la modélisation

Dirigée par Maxime SERMESANT

Co-Encadrée par Nicolas DUCHATEAU

Date de soutenance : 25 Janvier 2018

Jury :

Philippe ACAR	Université de Toulouse	Rapporteur
Patrick CLARYSSE	CREATIS, CNRS, Inserm, Lyon	Rapporteur
Mathieu DE CRAENE	Philips Medical System, Suresnes	Examinateur
Nicolas DUCHATEAU	CREATIS, CNRS, Inserm, Lyon	Co-encadrant
Emile FERRARI	Université de Nice	Examinateur
Maxime SERMESANT	INRIA, Sophia-Antipolis	Directeur de thèse

From normal right ventricle to pathology: shape and function analysis with different loading conditions using imaging and modelling

ABSTRACT

The aim of this thesis is to study the right ventricle (RV) in different loading conditions using imaging and modelling.

The first axis of this work was a prospective study in which we studied RV deformation in healthy controls and pulmonary hypertension (PH) patients (pressure overload) using 3D transthoracic RV echocardiographic sequences. Output RV meshes; obtained after myocardial tracking; were post-processed to extract area strain and spatiotemporal correspondences were checked before computing statistics on these meshes. RV shape and strain patterns were gradually deteriorated with the severity of PH and provided independent prognostic information.

The second axis of this work focused on the role of a longitudinal evaluation in comparison with a single assessment at baseline, using the same methodology. We demonstrated the additional prognostic value of changes in RV area strain and the importance of septal segments.

In the third axis, we assessed the complementary aspects of RV deformation and shape (using curvature index) in RV volume overload patients. While shape and strain are both altered in tetralogy of Fallot patients, only RV shape allows to differentiate atrial septal defects from normal controls.

Finally, in the last axis, we focused on the added value of the personalisation of a 0D circulation model to characterize the pathology and predict the response to therapy in pulmonary arterial hypertension. The model was personalised to 11 PH patient data before and after advanced specific PH therapy. The model parameters reflected accurately the expected changes with therapy.

RESUME

L’objectif de cette thèse est d'étudier le ventricule droit (VD) dans différentes conditions de charge en utilisant imagerie et modélisation.

Le premier axe de ce travail est une étude prospective dans laquelle nous avons étudié la déformation VD chez des patients sains et avec hypertension pulmonaire (HTP; surcharge barométrique) en utilisant l’échocardiographie trans-thoracique 3D. Les maillages VD ont été obtenus par tracking myocardique et post-traités afin d’extraire le strain de surface. Les correspondances spatiotemporelles ont été vérifiées avant de réaliser les statistiques sur ces maillages. La forme globale et la déformation VD sont associées à la sévérité de l'HTP et donnent des informations pronostiques indépendantes.

Le deuxième axe de ce travail présente le rôle d'une évaluation longitudinale par rapport à celui d’une évaluation instantanée, en utilisant la même méthodologie. Nous avons démontré la valeur ajoutée pronostique des modifications dans le temps de déformation VD et l'importance du septum.

Dans le troisième axe, les aspects complémentaires de la forme (définie par la courbure) et déformation VD ont été évalués dans des populations de surcharge en volume VD. Alors que forme et déformation sont altérés chez les patients avec tétralogie de Fallot, seule la forme a permis de différencier les patients avec communication inter-atriale des témoins.

Enfin, dans le dernier axe, nous avons travaillé sur la valeur ajoutée de la personnalisation d'un modèle circulatoire 0D afin de caractériser la pathologie et prédire la réponse au traitement dans l’hypertension artérielle pulmonaire. Le modèle a été personnalisé pour 11 patients avant et après traitement spécifique de l’HTP. Les paramètres du modèle reflètent bien les changements attendus avec la thérapie.

REMERCIEMENTS

Tout d'abord, j'aimerais remercier chaleureusement mon directeur de thèse, Maxime Sermesant, pour ses conseils et son soutien, y compris lors des derniers moments de retard ! Tu as toujours été là pour répondre à mes questions et me guider. J'ai beaucoup appris à ton contact et surement gagné en ouverture d'esprit ! A mon co-encadrant, Nicolas Duchateau, je souhaiterai vivement te remercier pour ta disponibilité, ton travail, ta réflexion et ta sympathie (sans parler des quelques mots d'espagnol que j'ai appris à ton contact). J'en profite également pour t'exprimer mon admiration pour tes compétences. Je suis certaine que Maxime et toi, par vos connaissances approfondies en Cardiologie, pourriez faire des envieux parmi nos internes. La Cardiologie numérique a de beaux jours devant elle ! Je souhaite également remercier profondément Nicholas Ayache pour son accueil enthousiaste au sein de l'équipe Asclepios, ainsi qu'Hervé Delingette et Xavier Pennec. Je voudrai remercier également tous les membres de l'équipe Asclepios qui m'ont accueilli et aidé, Isabelle, Sophie, Rocio, Roch, Marco, Nicolas, Shuman et les autres !

Je souhaiterai également remercier Mr Patrick Clarysse d'avoir accepté de rapporter ce travail de thèse et participer à mon jury de soutenance de thèse. Un grand merci également à Mr Mathieu De Craene d'avoir accepté de participer à ce jury.

J'adresse des remerciements particuliers au Pr Philippe Acar pour avoir accepté de rapporter et siéger dans ce jury. Ces dernières années vous avez beaucoup œuvré pour le développement de travaux de recherche en imagerie des cardiopathies congénitales au sein de la filiale et vous avez permis le développement de plusieurs collaborations toujours en cours. Merci encore de soutenir nos idées et projets de recherche.

Un grand merci au Pr Emile Ferrari, pour participer au jury mais aussi supporter mes emails, mes demandes de cathétérisme bizarres et mes coups de gueule. Je vous remercie surtout pour votre soutien, puisque sans secousse de votre part, je ne soutiendrai pas ma thèse aujourd'hui… Merci d'avoir le moral quand on ne l'a pas, d'espérer quand on n'y croit plus et d'avoir la vision des choses qui nous échappe encore.

J'ai aussi une pensée plus triste pour les patients dont parle ce travail. On mêle la recherche à la clinique, on connaît les gens, leur histoire, leur famille. En espérant qu'un jour on les aidera, plus, mieux … Merci à tous ceux qui participent à leur prise en charge ! Nos IDE (Françoise, Andrée, Virginie, Julie !), secrétaires (Marie-Pierre, Danielle, Anaïs), à Katia et Aline, Céline, Sylvie, Viviane, Charles-Hugo, Pierre, Olivier et Camille. Au « double » Dr Baudouy … Merci à tous mes collègues de Pasteur, L'Archet et Lenval que je n'ai pas cité mais avec qui c'est un plaisir de travailler.

A ma famille. A mes parents, j'arrête de promettre que c'est le dernier examen que je passe. Ça fait 10 ans que je vous fais le coup, je sais … Merci d'avoir toujours cru en moi et de m'avoir donné les moyens de réussir. Outre l'entêtement familial dont j'ai hérité, c'est grâce à vous que j'en suis là. Je n'ai pas de mots assez forts pour vous remercier. De même je ne vous remercierai jamais assez de vous occuper d'Alexandre comme vous le faites. A ma grand-mère, peut-être que si j'ai 2 titres de docteur, tu finiras par écouter mes conseils ! Merci pour ton soutien indéfectible !

Stéphane, merci de me supporter et de croire en moi… On en rigolera surement dans quelques temps, après tout, déménager et rendre sa thèse en même temps ça passe … ;)

A mon fils, j'ai beau ne pas être toujours là, il ne se passe pas un instant sans que je ne pense à toi. Tu es mon soleil. Et tu n'as pas réussi à noyer mon ordinateur. Merci d'être là, je t'aime.

CONTENTS

ABBREVIATIONS

AS	Area strain
ASD	Atrial septal defect
BAS	Baseline
BNP	Brain natriuretic peptide
CS	Circumferential strain
EDV	End-diastolic volume
EF	Ejection fraction
FU	Follow-up
HR	Hazard ratio
IVA	Myocardial acceleration during isovolumic contraction
IVV	Peak velocity during isovolumic contraction
LV	Left ventricle
LS	Longitudinal strain
mPAP	mean pulmonary artery pressure
MPI	Myocardial performance index
PA	Pulmonary artery
PAH	Pulmonary arterial hypertension
PGI2	Prostaglandin I2
PH	Pulmonary hypertension
RV	Right ventricle
RVOT	Right ventricular outflow tract
SD	Standard deviation
SV	Stroke volume
TAPSE	Tricuspid annular plane systolic excursion
TOF	Tetralogy of Fallot
TV	Tricuspid valve
VTI	Velocity time integral
WHO	World Health Organization

CHAPTER 1.
INTRODUCTION:
CLINICAL AND TECHNICAL CONTEXT

CONTENTS

1. The right ventricle, the forgotten chamber

The study of the right ventricle is still shadowed by the study of the left ventricle, the systemic chamber. The right ventricle has long been viewed as less important than the left ventricle. Going back to the history of medicine, Claude Galien (*Galenus 129-216*) discovered the pulmonary circulation at the age of 28, when he was chief physician to the Pergamon's gladiators. However, he thought that the liver pumped venous blood to the circulation. Matteo Realdo Colombo (1515-1559); an Italian professor of anatomy and surgeon at the University of Padua; confirmed the pulmonary circulation on vivisection and discovered that the heart's valves permitted blood circulation in only one way: from the right ventricle to the lungs and from the left ventricle to the aorta. William Harvey (1578-1657), an English physician who graduated at the University of Padua, was the first known physician to describe in detail the blood circulation. His manuscript « *Exercitatio Anatomica de Motu Cordis et Sanguinis in Animalibus* » (1) describes the circulatory system of the blood in the body. Harvey proved that blood flows separate in two distinct loops, the pulmonary circulation and the systemic circulation and from experimentations using the forearm veins; he also proved that the venous blood flowed to the heart. He was thus the first to describe the right ventricular importance: *"Thus the right ventricle may be said to be made for the sake of transmitting blood through the lungs, not for nourishing them"*. Studies such as Starr et al.(2) previously conclude that in the presence of normal lung function, a normal right ventricular function is unnecessary for circulatory stability. The RV was at that stage considered as a passive conduit between the systemic venous circulation and the lungs (3, 4). Later, the description and the prognosis of right ventricular hypoplasia underlined the importance of right ventricular function and interactions with the left ventricle. Right ventricular myocardial infarction has also been clinically recognized and suggested that RV dysfunction could lead to heart failure. More recently, the importance of RV function has been recognized in left heart disease such as heart failure, dilated cardiomyopathy, myocardial infarction and diseases affecting the right ventricle are receiving more and more attention.

2. Right ventricular anatomy

The right ventricle is the most anterior cardiac chamber, situated immediately behind the sternum. In contrast to the LV elliptic shape, the RV has an almost triangular shape. The RV is delimitated by the tricuspid (posterior) and pulmonary valve and composed by 3 distinct chambers: the inlet (admission of the RV with the tricuspid valve and chordae tendinae), the apex (trabecular RV) and the RV outlet also called infundibulum or outlet (smooth myocardial outflow region) (5). The tricuspid valve is composed by three different leaflets. The septal leaflet of the tricuspid valve has multiple tendinous cords attaching it directly to the ventricular septum, in contrast to the mitral valve also called "septo-phobic" without any septal attachments. The tricuspid hingeline is also closer to the ventricular apex as compared to the mitral valve. Three muscular bands are present in the RV: the parietal band, the septo-marginal band and the moderator band. Muscular trabeculations in the apical part of the right ventricle are larger than those in the left ventricle. A muscular fold (the infundibular fold) separates the pulmonary valve from the tricuspid valve, explaining the absence of tricuspid-pulmonary continuity in contrast to the mitro-aortic fibrous continuity in normal hearts.

When viewed from the side, the RV has a triangular shape. In cross section, the RV cavity shape is described as a crescent, wrapping around the left ventricle (5). The shape is also influenced by the position of the interventricular septum and loading conditions. Under normal loading conditions, the inter-ventricular septum is concave toward the LV during the whole cardiac cycle. This is not the case under pathological conditions: with volume overload, the concavity of the interventricular septum is reduced

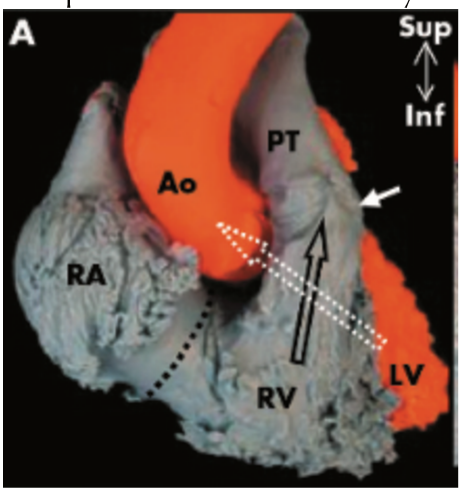

From Ho Y, Heart 2006. RA right atrium, RV right ventricle, PT pulmonary trunk. This figure illustrates the triangular shape of the right ventricle.

in diastole whereas in patients with pressure overload, the septum becomes convex with the severity of the disease in both systole and diastole (6-8).

The ventricles are composed of multiple layers that form a network of fibres. The RV wall is mainly composed of superficial and deep muscle layers. Per Ho Y, *et al* (5), the superficial fibres turn obliquely toward the cardiac apex to cross the interventricular groove and continue into the superficial myofibres of the left ventricle. At the apex, superficial myofibres invaginate in spiral fashion to form the subendocardial deep myofibres. These deep myofibres are longitudinally aligned, apex to base. In normal hearts, the muscular wall of the right ventricle, excluding trabeculations, is relatively thin and is composed of both circumferential and longitudinal fibres. In contrast, the thicker left ventricular wall contains superficial obliquely arranged myofibres, deep longitudinal fibres (subendocardium) and circular fibres in the middle layer. Some studies showed that in pathological right ventricles such as tetralogy of Fallot, there was a shift in RV myofibres toward an "LV type" arrangement (9, 10).

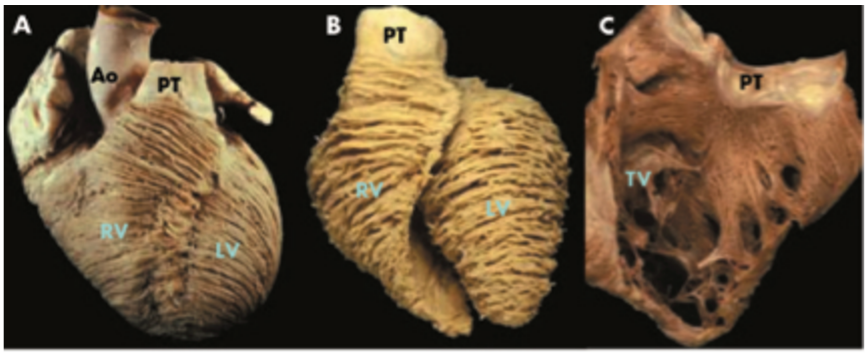

Myofibres organisation of the right ventricle, from Y. Ho (5)

Several segmentations have been proposed. We will here present the most widely used RV segmentations:

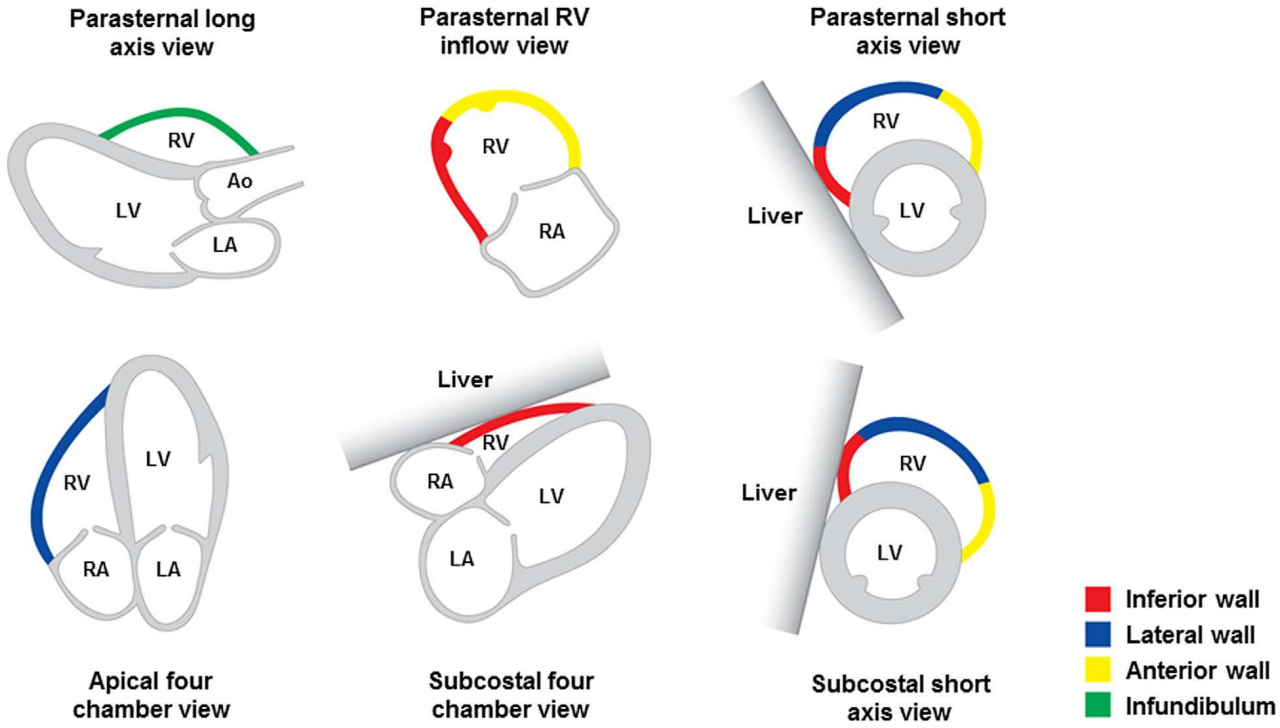

Along with the segmentation of the interventricular septum:

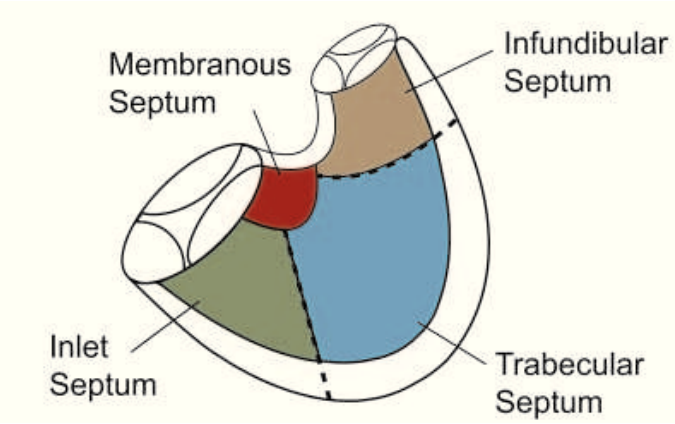

From Jiang L. Right Ventricle. In: Weyman AE, ed. Principle and Practice of Echocardiography. Baltimore, MD: Lippincott Williams & Wilkins; 1994: 901– 921 (11).

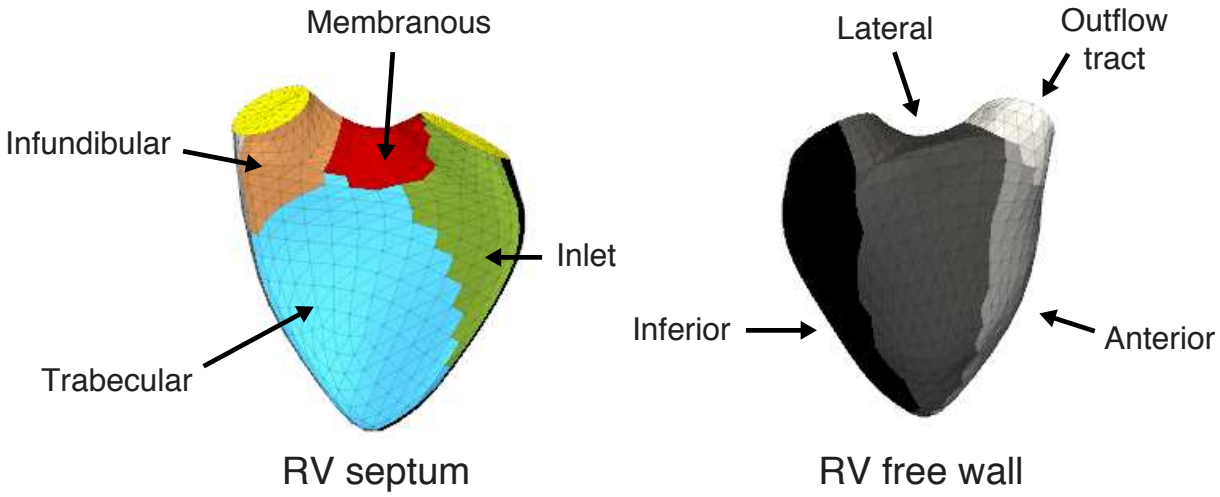

Three-dimensional RV segmentation represented on an RV mesh exported from TomTec RV Function 2.0

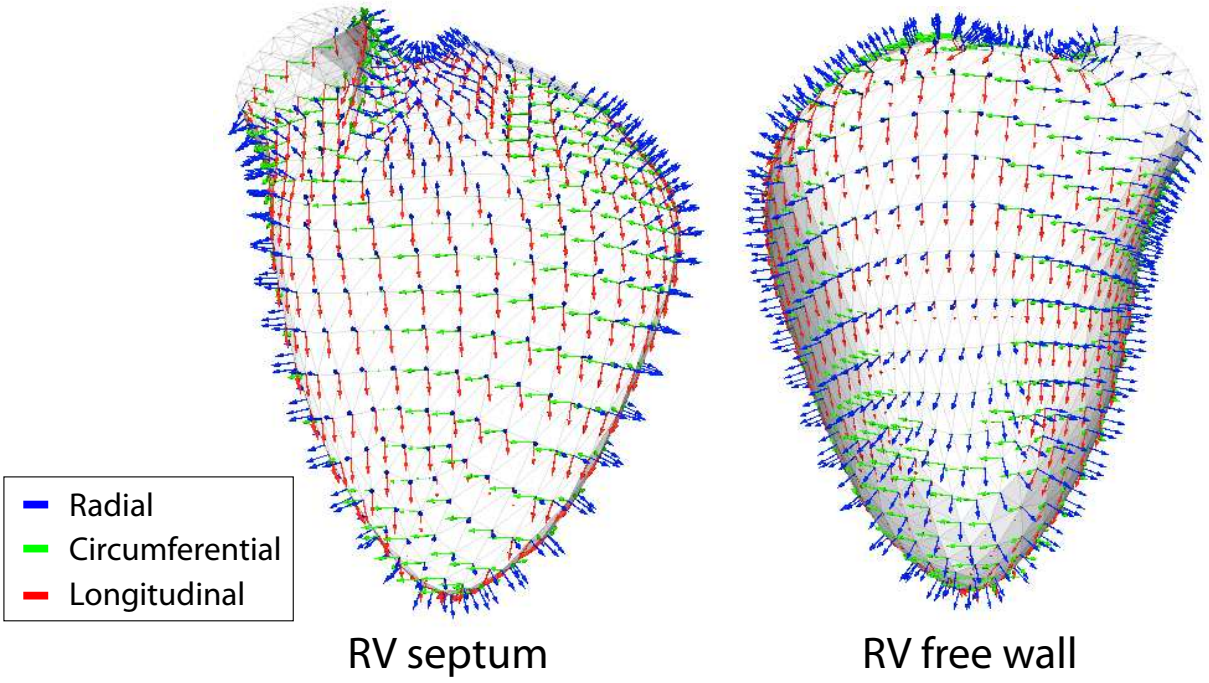

Three-dimensional RV map presenting local anatomy directions along the 3 different axis: radial, circumferential and longitudinal (N. Duchateau)

3. Right ventricular physiology

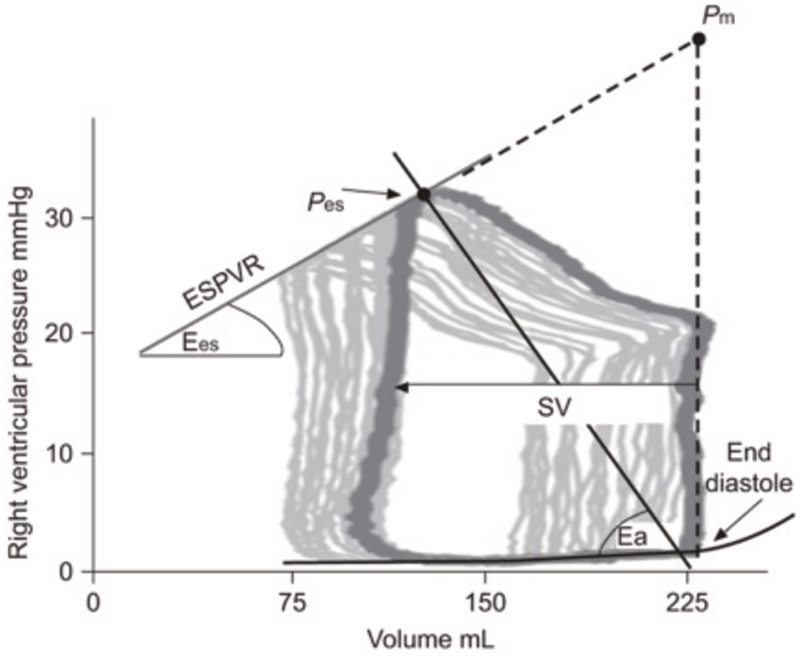

Adapted from (Vonk Nordegraaf, *et al*. (15)) The pressure–volume relationship in the RV. A pressure–volume loop includes four phases: starting at end-diastole: isovolumic contraction, ejection, isovolumic relaxation and filling. The figure shows that a large increase of volume induces only a small increase in pressure. The line connecting the end-systolic pressure–volume points is the end-systolic pressure–volume relationship (ESPVR). Its slope, E_{es}, is a measure of systolic RV function. The slope of the line connecting end-diastolic volume and end-systolic pressure, E_a, arterial elastance, is very close to pulmonary vascular resistance over heart period: *R*/T. The ratio E_{es}/E_a is a measure of ventriculo-arterial coupling. SV, stroke volume.

The right ventricle-pulmonary artery unit can be assimilated to a series of pumps (12). The right ventricular energy is supplied by RV myocyte contraction. The contraction depends on the preload (stretch), the afterload imposed (stress) and the bioenergetics status. The pulmonary vascular system is a low-impedance, highly distensible circuit. Compared with the systemic circulation, pulmonary circulation has a lower resistance, greater distensibility and a lower pulse wave reflection coefficient (13). The RV pump function also depends on the left ventricular pump function given the inter-relation at the septum level. RV pressure-volume loops (14) help understand the influence of different loading conditions on the right ventricle.

4. Importance of right ventricular function in clinical practice

Classical determinants of the RV function are RV load, myocardial contractility and LV-RV interaction. Thus, numerous studies demonstrate the role of RV function (especially dysfunction) in the patient prognosis for various cardiac conditions (15).

In heart failure, RV function is a long-known predictor of outcomes. For example, an index of RV length-force relationship, the ratio TAPSE (tricuspid annular plane systolic excursion)/PA systolic pressure predicts outcome in left ventricular systolic dysfunction and is associated with left ventricular dysfunction (16). RV function is also of prognostic importance in ischemic cardiomyopathy (17). Recent data underline the need to understand and assess RV function in heart failure with preserved ejection fraction (18) as it has many prognostic and therapeutic implications. In this situation of diastolic left ventricular dysfunction, RV dysfunction is related to myocardial impairment and afterload increase (post-capillary pulmonary hypertension). It is favoured by increased pulmonary pressures, non-sinus rhythm and is associated with left ventricular dysfunction and male sex (19). In patients with heart transplant, right heart failure is the major cause of death together with graft reject in the early period after surgery (20). Impaired RV function is observed in all patients after heart transplant but a longitudinal index of RV function does not seem to well reflect the RV global function (as assessed by 3D echocardiography) (21). Improvements in patients with cardiac resynchronization therapy can be monitored using RV function (22).

In patients with right heart valvar diseases, RV function is of critical importance as it determines the timing of surgery or catheter intervention (23). In severe primary tricuspid regurgitation, surgery is recommended in asymptomatic patients with progressive RV dilatation or dysfunction is observed. Thus, RV function assessment and follow-up is fundamental, to avoid any irreversible RV damage. RV function also determines outcomes in left heart valvar disease as the RV is affected by changes in loading conditions such as in aortic stenosis (24) and mitral regurgitation (25). In mitral regurgitation, the constraint on the septum, secondary to left ventricular remodelling, leads to RV function impairment that recovers after mitral valve repair or replacement.

Congenital heart defects often involve the RV such as in pulmonary valve stenosis, tetralogy of Fallot (TOF), Ebstein's anomaly, RV volume overload such as in atrial septal defect or abnormal pulmonary vein return. There are also patients with systemic right ventricles (sub-aortic position) such as in double discordance or more frequently in patients with transposition of the great arteries corrected with an atrial switch (before the advent of the arterial switch, approximately 30 years ago) and also patients with a single right ventricle (univentricular physiology, mitral atresia, Shone syndrome…). In all these situations, the RV function is of critical importance as it determines the patients' exercise capacity, symptoms and survival.

In pulmonary hypertension, the role of RV function will be developed in the next section and chapter. It is a major determinant of both exercise capacity, symptoms and prognosis.

5. Assessment of right ventricular function

Partly adapted from the article by Moceri *et al.* (26). Multimodality imaging is often used in clinical practice, but given the aim of this thesis and despite the cardiac magnetic resonance gold standard, we deliberately chose to only describe the echocardiographic assessment of RV function.

Right ventricular scalar dimensions

Measurement of the dimensions of the RV is a crucial component of echocardiography in clinical routine, as they describe global RV remodelling. RV free wall thickness reflects the degree of RV hypertrophy; it should be measured at the end of diastole in subcostal or parasternal long-axis view, preferably at the level of the tip of the anterior tricuspid leaflet. The normal cut-off for RV wall thickness, excluding trabeculations and papillary muscle, is 5 mm. As there may be beneficial and detrimental RV hypertrophy regarding different metabolic pathways (27), RV wall thickening is not independently associated with survival in pulmonary hypertension. As the RV dilates in response to RV failure and increased pressure overload, RV enlargement is a predictor of mortality in patients with pulmonary disease and pulmonary hypertension (28, 29). RV dimensions should be measured at the basal mid-cavity level as well as longitudinally using the four-chamber view. The basal diameter (RV D1, upper limit 42mm; Figure 2A) should also be compared with LV dimensions, to help distinguish enlarged RV from global heart dilatation. One major limitation of this two-dimensional (2D) technique is that it highly depends on the probe and patient position. Beyond RV dilatation, PA dilatation is crucial to detect because of its prognostic importance (30).

Tricuspid regurgitation

In RV volume or pressure overload, TR occurs as the result of increased RV afterload on RV dilatation and function. TR is usually caused by tricuspid annular dilatation, altered RV geometry and apical displacement of tricuspid leaflets, failing to

adapt. Moderate or greater degrees of TR are commonly seen, especially in advanced pulmonary hypertension (31), the severity of TR being correlated with functional capacity. TR also contributes to reduced cardiac output.

Right ventricular fractional area change

RV fractional area change, defined as (end-diastolic area — end-systolic area)/end-diastolic area × 100 (Figure 1A), is a simple 2D way to assess RV systolic function using the apical four-chamber view. Despite the limitations inherent to the method (challenging contour tracing, foreshortened apical view because of RV dilatation), it has been correlated with cardiac magnetic resonance data (32) and is considered the gold standard in RV assessment. A RV fractional area change of <35% indicates RV systolic dysfunction and changes in time correlate with clinical deterioration (33). However, the significant variability, when measured by echocardiography and compared with cardiac magnetic resonance, explains why it requires multiple measurements.

Longitudinal right ventricular function

Longitudinal systolic RV function can be estimated using tricuspid annular plane systolic excursion (TAPSE) and S′ (also called tricuspid valve Sm). TAPSE (Figure 1B) is one of the simplest measurements, an M-mode measure obtained from the apical view, which is of critical importance. Beyond reflecting longitudinal function, TAPSE also correlates with global indices of RV global function (34-36). RV dysfunction is considered for TAPSE < 16 mm. TAPSE has significant prognostic importance in PAH (37), especially in patients with idiopathic PAH, systemic sclerosis-associated PAH (38) and Eisenmenger syndrome (39). TAPSE seems preserved in atrial septal defect patients but is lower in tetralogy of Fallot patients (40). Impaired TAPSE over time is observed in tetralogy of Fallot patients, where TAPSE is correlated with both right ventricular ejection fraction and end-diastolic volume (41). However, TAPSE is angle and operator dependent and varies per heart motion (the reference point being located outside the heart) and the severity of TR and RV-LV interactions (42). Tissue Doppler imaging can also determine

S′, the peak systolic velocity of the lateral tricuspid annulus (by pulsed tissue Doppler and/or color-coded tissue Doppler) (Figure 1D). S′ is well correlated with TAPSE and the lower reference limit in normal control patients has been established as 10 cm/s (43, 44). However, these variables remain limited, given that, as shown by a 3D study (45), under pathological conditions the RV has differential regional function, with distinct features for each compartment, thus having a different effect on the overall systolic function.

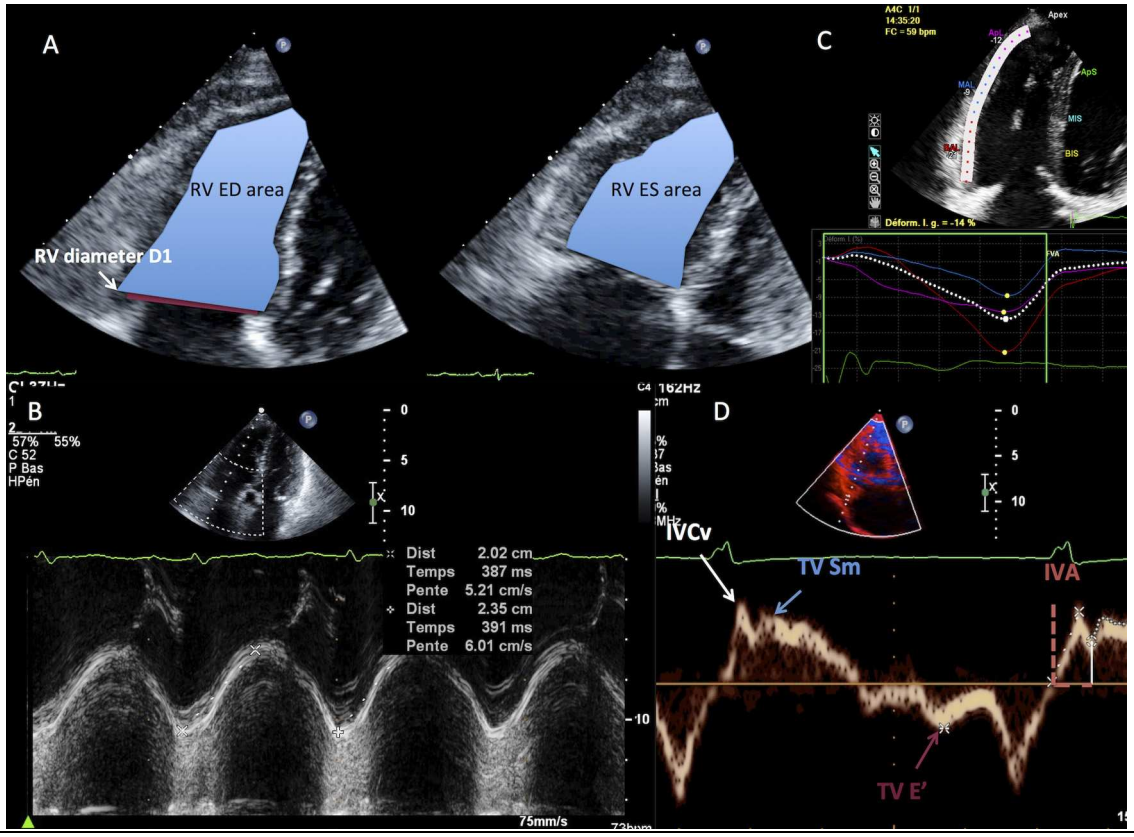

Figure 1. Assessment of right ventricular function. (A) Apical view focused on the right ventricle (RV) with RV inlet end-diastolic measurement (D1) and end-diastolic area (RV ED area) and end-systolic area (RV ES area) tracing, allowing calculation of the RV fractional area change (RV ED area—RV ES area)/RV ED area. (B) Measurement of TAPSE using the four-chamber view. (C) Example of RV free wall speckle-tracking study showing a decreased longitudinal strain. (D) Tissue Doppler imaging with pulsed Doppler at the tricuspid lateral annulus; the example shows the measurement of S′ (tricuspid valve [TV] Sm), the isovolumic contraction peak velocity (IVCv) and acceleration during isovolumic contraction (IVA).

Another tissue Doppler variable derived from the basal RV free wall that is useful in clinical practice is myocardial acceleration during isovolumic acceleration (IVA) (46) (Figure 2D). IVA is defined by the peak isovolumic myocardial velocity (IVCv) divided by time to peak velocity, the zero-crossing line defining the onset of myocardial acceleration. IVA is less load-dependent than other indices (47), but is frequency dependent, explaining why it should be indexed to the heart rate (divided by √RR [ms]). The lower reference limit by pulsed-wave tissue Doppler imaging is 2.2 m/s^2. Despite being a reliable indicator of RV function (48), IVA has not yet been related to prognosis in patients with PAH; however, IVCv (peak velocity) has been identified recently as an independent predictor of clinical outcomes in group 1 pulmonary hypertension patients (49). In tetralogy of Fallot, IVA has been correlated to the severity of pulmonary regurgitation (50).

Right ventricular adaptation

The RV myocardial performance index (MPI) or Tei index (51) (Figure 2A), defined by the ratio of isovolumic time divided by ejection time, reflects the global RV performance and adaptation. It can be obtained either by pulsed Doppler on RV outflow and the tricuspid valve (using similar RR intervals) or by tissue Doppler imaging. Reference values differ between these two methods (52) (upper reference limits 0.40 [pulsed Doppler] and 0.55 [tissue Doppler]). This index is related to prognosis in PAH and is associated with clinical improvement following advanced therapies (53). In chronic thromboembolic pulmonary hypertension, RV MPI is correlated with disease severity and associated with outcomes (54). RV MPI has also been validated in paediatric pulmonary hypertension, MPI being correlated with mPAP and response to therapy (55). MPI has also been studied in congenital heart disease: it is correlated with peak oxygen uptake and right ventricular function in patients with systemic right ventricles (56, 57). In the situation of tetralogy of Fallot, MPI can be "pseudo-normalized" (58): in patients with severe pulmonary regurgitation, isovolumic relaxation is absent or at least shortened and the increased end-diastolic volume due to volume overload increases the pulmonary ejection time thus lowering the MPI. When compared with cardiac magnetic resonance,

MPI followed the right ventricular ejection fraction but is lower as compared to standard values (59). In atrial septal defect, differences were observed between children and adults (with long-standing right ventricular overload and significant right ventricular remodelling), MPI was considered normal in children, whereas it was slightly but significantly prolonged in adults with atrial septal defect (57).

The measure of the total isovolumic time provides with the same indications than MPI; it has been related to outcomes in Eisenmenger syndrome (39), is prolonged in patients with systemic right ventricles (60) and is overall related to the disease severity and degree of pulmonary hypertension (61, 62). Calculation of the systolic to diastolic duration ratio (S/D ratio) is another means of assessing RV adaptation. Durations of systole and diastole are measured from the apical view (Figure 2B). Systolic duration is measured as the duration of the TR flow, whereas diastolic duration is considered from termination to onset of TR. An increase in the S/D ratio reflects a certain degree of RV dysfunction, with longer systole and abnormal cardiac performance; it is one of the strongest independent predictors of death in Eisenmenger syndrome and independently predicts lung transplantation and death in paediatric PAH (cut-off 1.4) (63). This ratio is also an indicator of right ventricular function in hypoplastic left heart syndrome (64)

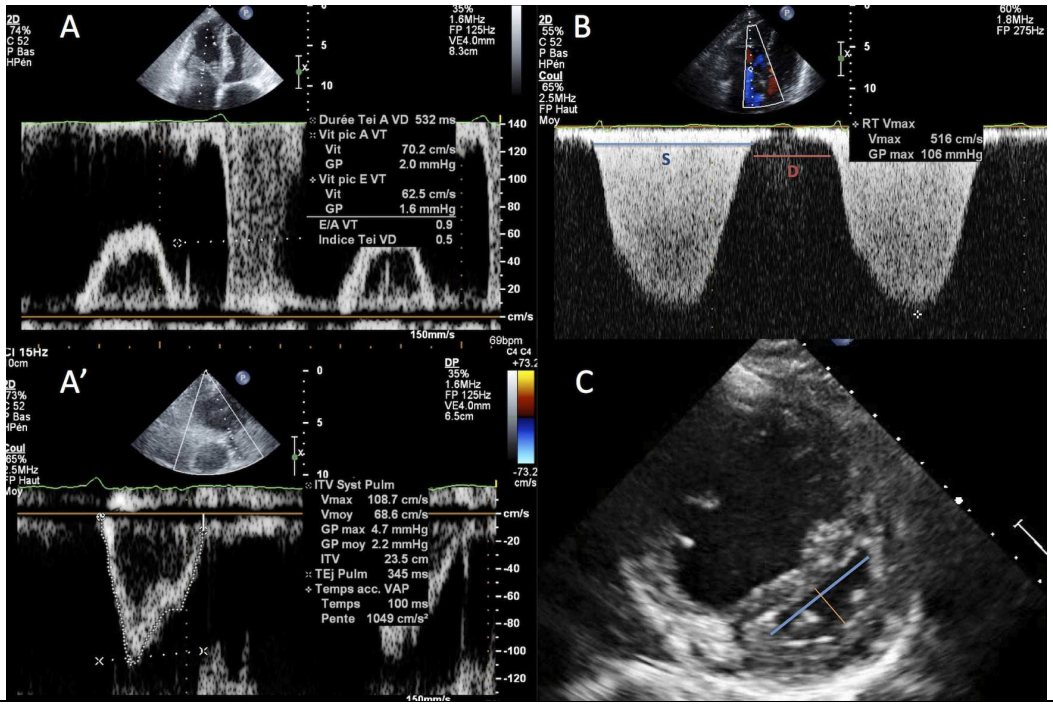

Figure 2: Assessment of RV adaptation and RV/LV interaction. (A) Trans-tricuspid flow with pulsed Doppler, measurement of tricuspid valve E and 'Tei a'. (A') Pulmonary flow with tracing of velocity-time integral (VTI) and measurement of pulmonary ejection time 'Tei b'; Tei index (or RV MPI) can be calculated using the formula (a—b)/b. (B) Tricuspid regurgitation flow in pulmonary hypertension and an example of the S/D ratio calculation (S = duration of tricuspid regurgitation; D = interval between S and the next TR flow). (C) Short-axis view with determination of left ventricular eccentricity index (>1.4).

2D-myocardial motion and deformation

Speckle-tracking imaging can help identifying the early signs of RV dysfunction and following patients under therapy. RV systolic longitudinal strain is reduced in PAH (Figure 1C) and probably accounts for the RV global dysfunction, given the fibre arrangement; it also improves in conjunction with the 6-minute walking distance in responders to advanced therapy (65). An RV longitudinal strain <19% has been described as an independent predictor of all-cause mortality (66). Patients with Eisenmenger syndrome present an increase RV transverse strain as compared to patients with pulmonary hypertension from other causes and a relatively preserved apical longitudinal and radial strain (67). Patients with post-tricuspid shunt in the setting of Eisenmenger

syndrome presented increased RV transverse strain, compared to patients with pre-tricuspid shunt (68).

RV free wall longitudinal strain is also useful in congenital heart disease patients. In patients with volume overload, a correlation between right ventricular dilatation and right ventricular 2D longitudinal strain has been found, explaining lower longitudinal strain in atrial septal defect patients, normalized once corrected for the right ventricular size (69). Reduced right ventricular deformation has been observed after surgical correction of tetralogy of Fallot, in association with reduced exercise tolerance (70). In a Dutch cohort of adult Fallot patients, Menting, *et al*. (71) found that RV free wall strain was decreased in these patients, especially at the apex. Recommendations from the American society of Echocardiography reviewed the use of new imaging techniques in Fallot patients (72) and did not suggest right ventricular strain estimation given the lack of industry standard but find the technique promising, expecting further studies (statement from 2014).

3D echocardiography

Complex anatomy is usually best assessed using a three- dimensional (3D) technique, but besides being useful in terms of visualizing directly the anatomy (especially in congenital heart disease patients), 3D echocardiography can provide with an estimation of ventricular volume and deformation, even in children (73). Recently, a consensus document about the use of three-dimensional echocardiography in congenital heart disease has been published jointly by the American Society of Echocardiography and the European Association for Cardiovascular Imaging (74). It leads to lower underestimation of volumes and reduced variability compared with 2D-echocardiography and provides an accurate and reproducible RV ejection fraction that could help with serial measurements. The lower cut-off for 3D RV ejection fraction is 44% and 3D echocardiography correlates well with cardiac magnetic resonance in children (75) and adults (76, 77). The upper reference limits for 3D-indexed RV end-diastolic and end-systolic volumes are 89 mL/m2 and 45 mL/m2, respectively. 3D RV volumes can be obtained directly by 3D acquisition with a specific probe or, more

recently, by 3D modelling adapted from 2D acquisition (knowledge-based reconstruction) (78, 79). Recently an expert consensus statement has been issued on 3D echocardiography in congenital heart disease (80); it provides guidance on the added value of 3D in several situations. 3D assessment of volumes and ejection fraction is comparable to results from cardiac magnetic resonance in Fallot patients (81, 82). 3D strain has also been studied in this population: 3D dyssynchrony has been related to 3D deformation and area strain was related to ejection fraction as assessed by cardiac magnetic resonance (83).

The future of right ventricular echocardiography

Given its safety and technical progress, it is likely that the role of echocardiography in the management of patients with right heart disease will only increase in the future (84). However, in RV assessment, especially in PAH, one test should never be considered as a 'stand alone' test. The multivariable approach should be the rule, combining different echocardiographical variables to obtain an 'RV performance score' or even combining the results of different examinations (e.g. echocardiography and right heart catheterization or magnetic resonance). The multivariable approach already has its place in diagnosis: an echocardiographic rule accurately defines pulmonary hypertension haemodynamic (85). It also has an emerging role in prognosis, a score built on the strongest echocardiographic predictors of outcomes in Eisenmenger syndrome allows the identification of very high-risk patients (39). Current prognosis equations would benefit from the incorporation of echocardiographic variables; it would improve their predictive power and help to identify patients who would benefit from further interventions.

6. Strain estimation

Strain is a dimensionless parameter representing an object deformation as compared to its original shape. There is a growing body of evidence indicating that strain assessment, especially by speckle tracking techniques provides incremental information in many clinical situations.

Strain (ε) is defined from the deformation gradient (dø/dX) which represents the spatial variations of the transformation ø that describes the motion of the object between two instants. Several strain formulations are used, depending on the relationship chosen between the deformation gradient and the dimensionality of the calculations (1D, or 2D/3D). The main strain formulations are the Green strain, the Engineering strain and the Natural strain:

1D Elasticity		3D Elasticity	
Deformation Gradient	$\frac{d\phi}{dX}$	Deformation Gradient	$\nabla\phi(X)$
Square Stretch Ratio	$s^2 = \left(\frac{d\phi}{dX}\right)^2$	Right Cauchy Green Deformation Tensor	$C = \nabla\phi^T \nabla\phi$
Green Strain	$\varepsilon(s) = \frac{1}{2}(s^2 - 1)$	Green Strain Tensor	$E = \frac{1}{2}(\nabla\phi^T \nabla\phi - Id)$
Engineering Strain	$\varepsilon(s) = (s - 1)$	Engineering or Biot Strain	$B = C^{1/2} - Id$
Natural Strain	$\varepsilon(s) = \ln(s)$	Natural or Henky Strain	$H = \frac{1}{2}\ln C$

1

One-dimensional (1D) strain estimation methods

In 1D, the deformation gradient is the local stretch ratio *s* which is defined by the following formula where L is the length of the object after deformation and L_0 the original length:

$$s = \frac{L}{Lo}$$

The Engineering strain ε and the natural strain ε_N have a fixed (non-linear) relationship:

$$\varepsilon_N(t) = \ln\big(1 + \varepsilon(t)\big) \text{ or } \varepsilon(t) = \exp(\varepsilon_N(t)) - 1$$

'ln' is the natural logarithm. If the extent of deformation is small (5–10%), Engineering and Natural strain values are close. However, for larger deformations (during cardiac ejection for example), the difference becomes significant. Thus, it is important to clearly state if the Natural or Engineering strains are studied.

Two-dimensional (2D) strain estimation methods

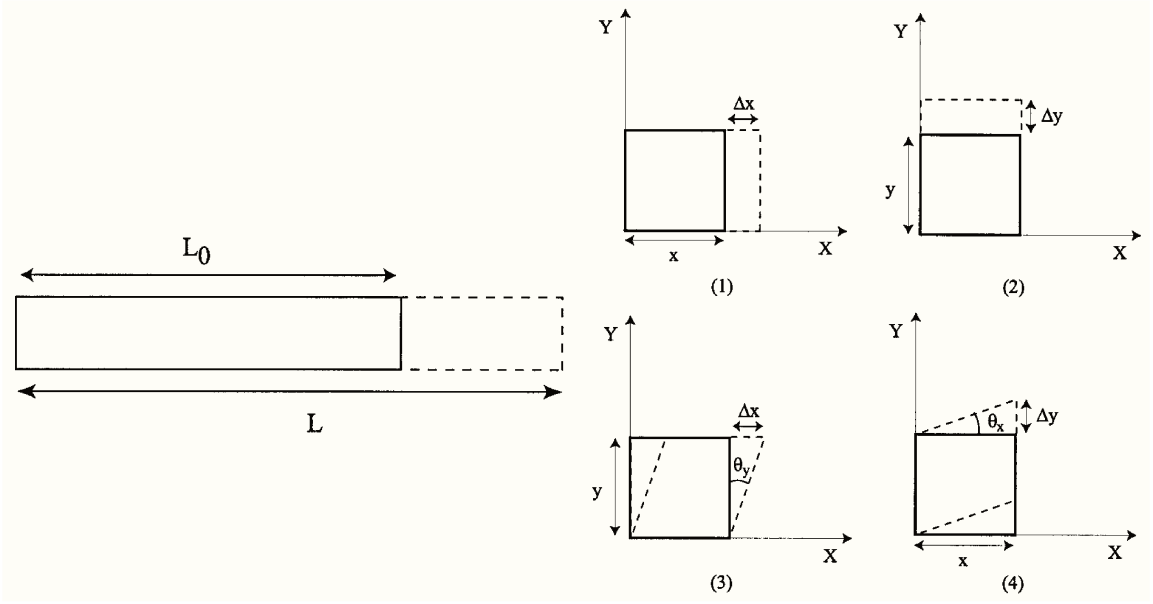

From D'hooge *et al.* (86): (a) Deformation (strain) of a one-dimensional object is limited to lengthening or shortening. Strain is the deformation of an object relative to its original shape. For a 2D object, deformation, i.e. strain, can be described by four strain components: two normal strains [(b1) and (b2)] and two shear strain components [(b3) and (b4)]. The shear strains are also completely characterized by the angles.

For a 2D object, the deformation is not limited to lengthening or shortening in one direction, but can also distort by the relative displacement of the upper to the lower border or the right to the left border. The first type of deformation (lengthening and shortening) is referred to as normal strain, while the latter deformation is called shear

strain (the associated motion is parallel to the border of the object). Thus, all four-strain components explain the overall deformation.

$$\begin{cases} \varepsilon_x = \dfrac{\Delta x}{x} \ \ and \ \varepsilon_y = \dfrac{\Delta y}{y} \\ \varepsilon_{xy} = \dfrac{\Delta x}{y} \ and \ \varepsilon_{yx} = \dfrac{\Delta y}{x} \end{cases} \qquad \begin{pmatrix} \varepsilon_x & \varepsilon_{xy} \\ \varepsilon_{yx} & \varepsilon_y \end{pmatrix}$$

This is referred as the strain tensor. Shear strain components (ε_{xy} and ε_{yx}) can also uniquely be determined by the angles θx and θy.

The components can be computed in longitudinal, circumferential and radial coordinates. The natural strain calculation is better suited for use with tissue Doppler imaging, since the reference length is different at each interrogation time point (each color tissue Doppler frame) and so will not be the same as at the reference time point (87). The logarithm in the formula enables to remove the reference length when computing strain rates.

However, speckle-tracking imaging is more subject to the calculation of Engineering strain, since the reference baseline length is always known.

Various echocardiographic techniques are available in order to calculate the strain.

Tissue Doppler Imaging (TDI): Strain and strain rate measurements can be obtained from data acquired by (TDI): strain rate is calculated from the instantaneous spatial velocity gradient in a small myocardial segment. Integrating these strain rate values allows calculation of strain. The advantage with TDI is the high temporal resolution. However, using TDI-based technique, the measurement axis is in only one dimension: parallel to the ultrasonic beam. The main limitations to this technique are inherent to the Doppler technique with its angle dependency and the low spatial resolution. Using the TDI-based technique, the longitudinal strain component is only measured toward or away from the transducer.

Non-Doppler based techniques: Speckle-tracking imaging

The speckles are acoustic markers in the 2D images (grey scale) distributed throughout the myocardium that can be followed during the cardiac cycle. Their size is 20 to 40 pixels (88). These markers are tracked by an algorithm calculating frame-to-frame changes using for instance a sum of absolute differences in image intensity or cross-correlation, and usually surrounding each pixel with a square of approximately 20x20 pixels. The change in the speckle position also allows determination of its velocity by time derivation. The advantage of this technique is that it will assess the whole myocardium without being angle-dependent. However, the temporal resolution is lower than the one of TDI and strain is estimated via an algorithm.

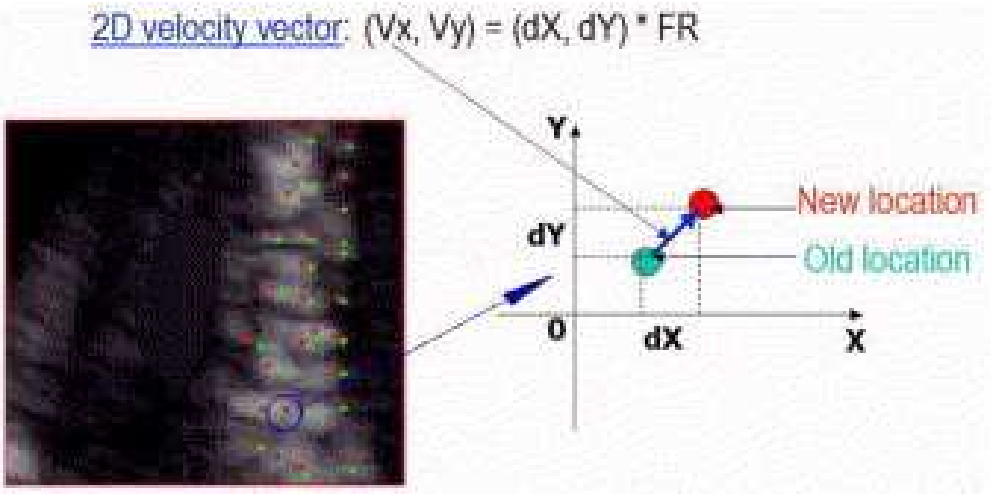

From Leitman, *et al*. (89).

From a practical point of view, 2D loops (with high resolution, usually > 50Hz) from the echocardiography are post-processed offline. Each speckle is followed for several consecutive frames forward and backward. The return to baseline coordinates is considered evidence for adequate tracking. The tracking can be rejected by the software if there are highly different velocities in adjacent speckles. A-posteriori drift compensation is often proposed to obtain cyclic curves. Drift generally highly depends

on the quality of the tracking and the images. Visual control of the tracking quality is required at the end of the tracking process.

3D strain estimation

Despite being obviously more informative than a simple visual assessment and more precise than an ejection fraction using the Simpson method (relying mostly on the observer), 2D strain techniques are limited to the 2D assessment in one plane of a 3D object, the heart. To obtain all strain components, many acquisitions are required. Some regions, especially in the right ventricle, cannot be studied using a standard 2D technique. This means that to estimate for example the global longitudinal left ventricular strain, we need to acquire at least 3 different left ventricular views and for the circumferential strain, 3 other views; of course at a different time. The timing of several acquisitions can have an impact on strain results, especially in situations such as rapid changing load conditions (haemodialysis for example) or when the heart rate is changing, especially in atrial fibrillation patients.

The estimation of 3D myocardial deformation, obtaining all strain components in one acquisition, may provide a better regional analysis of the left and right ventricle and eliminate the problem of out-of-plane motion observed in 2D myocardial tracking. However, even if the concept of 3D-tracking is very appealing, there might be some limitations, especially regarding the quality of 3D tracking and the image quality that we will discuss later.

3D strain estimation approaches can be divided in 3 main subgroups: block-matching, elastic registration and model-based approach:

Block-matching is the continuum of 2D-speckle-tracking. The displacement of a point is considered as the displacement of a region-of-interest around the point in the source frame resulting in the best match with a target frame. The displacement search is limited to a region around the point based on assumptions about the maximal tissue velocities (90). The main assumption of this technique is that the local speckle pattern between subsequent volumes is stable. It is the most popular approach given the "simplicity" and low computational complexity. Several commercial software using this

method are available: EchoPAC (4D Auto LVQ; GE Vingmed Ultrasound AS), TomTec 4D LV-Analysis (TomTec Imaging Systems, Germany), Siemens and 3D wall motion tracking software (Toshiba Medical Systems). Earlier studies using these methods in patients were published from 2009 to 2011/2012 (91-94). This technique might be affected by the lower temporal and spatial resolution of 3D probes as compared to 2D probes.

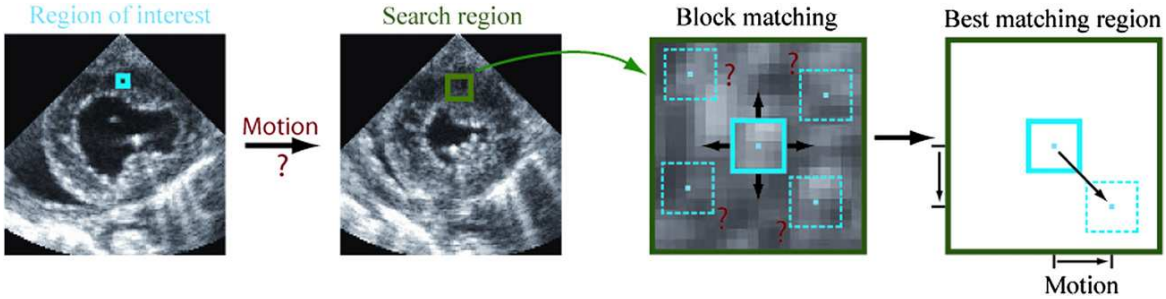

Illustration of Block-matching method. From Jasaityte *et al.* (95). *"A speckle pattern within a region of interest is identified in one frame and tracked within a search region of the successive frame. After comparing this block with all possible matching regions within this search region (dotted blocks), the position of the best matching block compared with the original block determines tissue motion. By repeating this process for multiple region-of-interest blocks, motion between two successive frames for the whole myocardium may be estimated."*

Elastic or non-rigid image registration uses image-warping method to estimate the cardiac motion (96, 97). It transforms a floating image to a reference image to determine corresponding image points (98). A full moving image is warped until it matches the target image: when the moving image and the target image are consecutive images during the cardiac cycle, the transformation matches the displacement between 2 consecutive frames. The computational time required for the analysis might be a limitation.

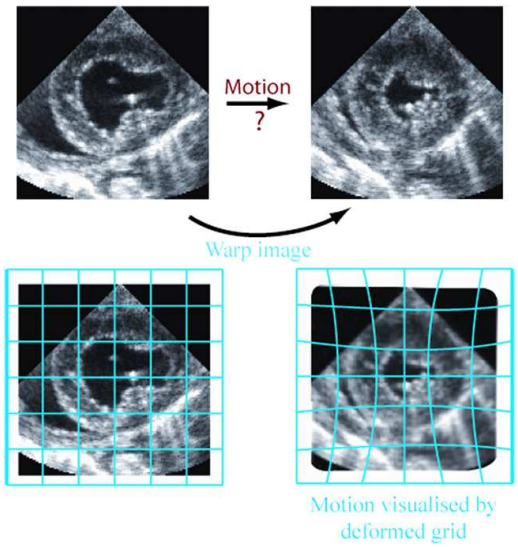

From (95): "*Principle of elastic registration*"

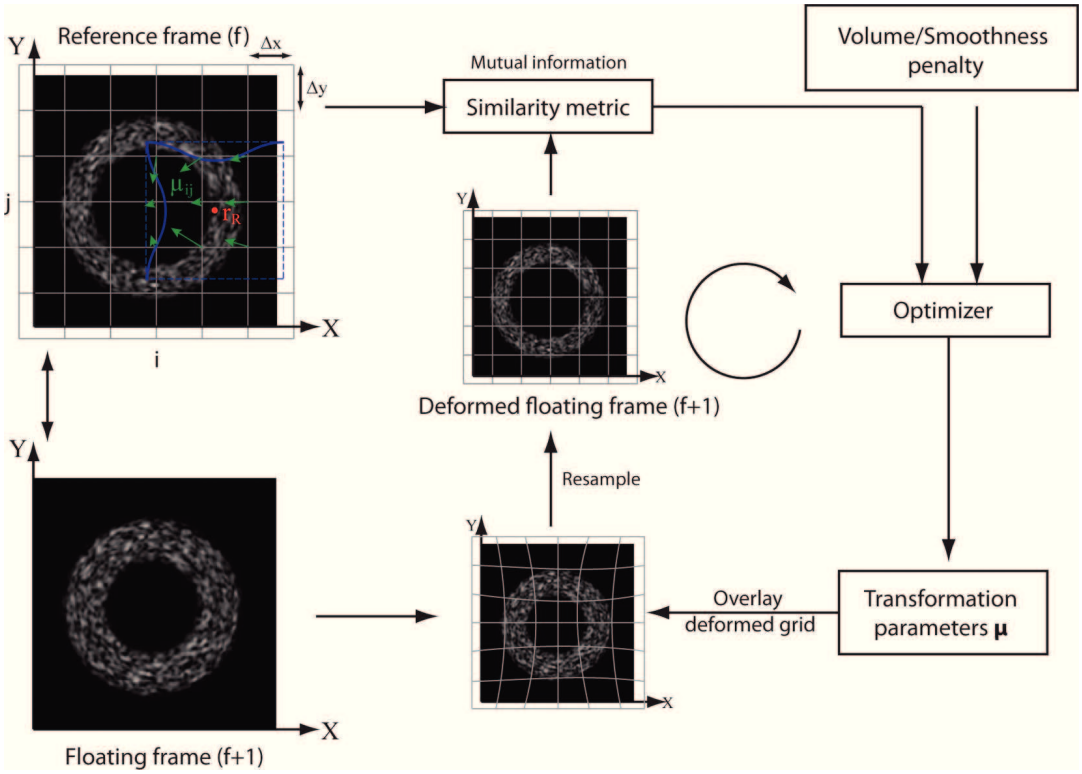

From (95): *"Principle of elastic registration. The whole image is deformed in multiple steps to look as similar as possible to the next image in the ultrasound sequence. This process can be visualized with a grid, which is attached to the underlying image. By manipulating this grid, the underlying image deforms. When both images match, the structure of the grid determines the motion for the whole myocardium at once."*

Model-based approach uses a prior knowledge to improve computational efficiency and guide 3D myocardial strain calculation. A model is first trained using normal and pathological hearts. Then in another data set, myocardial deformation is calculated by combining and comparing the image to the database (98). It seems to be the method supporting the software TomTec 4D RV Function (Tomtec Imaging Systems GMBH, Unterschleissheim, Germany).

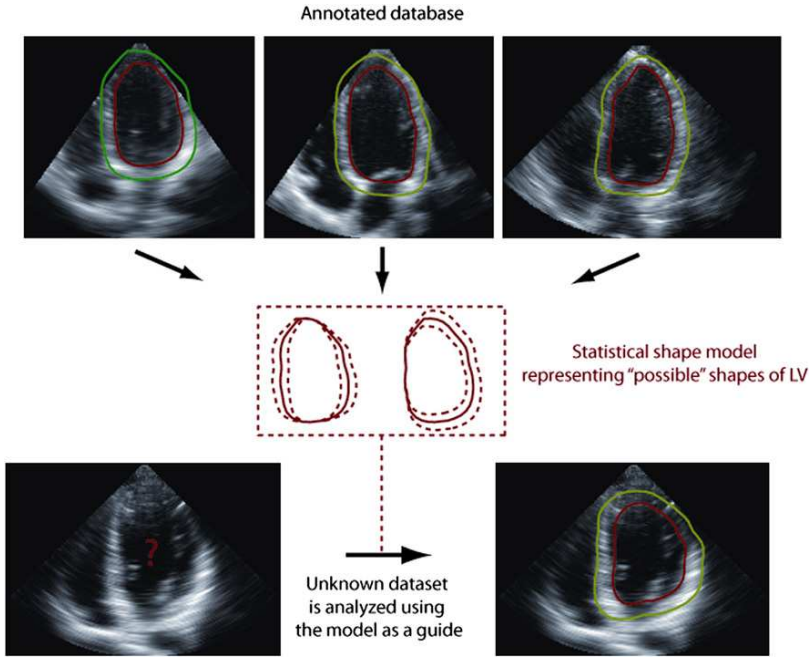

Principle of model-based strain estimation (96)

3D-strain techniques have been validated in simulated models: both block-matching (90) and elastic registration (98, 100) perform well. Both techniques were also validated in vitro using tissue-mimicking phantoms (96, 101) and in vivo with various results (97, 102-105). More generally, regarding the results of these techniques, moderate to good correlations were found for circumferential and longitudinal strain, whereas radial strain presented the worst agreement with sonomicrometry (106). So, to overcome this limitation, when assuming volume conservation, radial strain is the negative of area

strain, area strain being assimilated to the sum of longitudinal and circumferential strain. In detail : (LS longitudinal strain, CS circumferential strain, RS radial strain, AS area strain)

$$Area\ Strain = LS\,x\,CS + LS + CS \qquad and \qquad (LS+1)(CS+1)(RS+1) = 1$$

$$Radial\ strain = \frac{-AS}{AS + 1}$$

In clinical situations, 3D global area strain showed an overall good correlation with conventional LV systolic function parameters (91, 107, 108).

Normal values for LV global area strain and even more so for RV global area strain are still not defined. It will probably be very difficult to determine normal values, as normal values are changing according to the software used and according to the technique. It seems that 3D strain is lower than 2D strain estimation but higher than strain estimated by MRI tagging techniques (109). 3D strain estimation seems to overcome 2D strain analysis limitations, given the simplicity of the acquisition (one 3D-loop focused on the area of interest i.e. LV or RV), the good reproducibility (except for radial strain), the overall time required for the analysis as compared to 2D strain or cardiac magnetic resonance tagging and the analysis over only one cardiac cycle for the entire area of interest. However, several factors can affect the efficiency of 3D strain estimation: the high quality required for the volumetric analysis is challenging in some patients, especially when it is impossible, given their heart condition to hold their breath during 4 cycles (variable time according to the ultrasound machine) with respiration artefacts or when the acoustic window is not good enough with shadowing artefacts for example. The analysis of patients with high heart rate (for example sinus tachycardia related to heart failure) is also challenging as it poses the same problem as a study with normal heart rate but low frame rate (110).

Only few groups estimated 3D strain in the right ventricle. This will be discussed further in our second chapter. Despite the major interest yielded by 3D strain, the inter-vendor variability, the lack of homogeneity in the calculation of strain and even in the definition of strain limit (Engineering strain, Natural strain …) limit the widespread use of the technique. Furthermore, regarding RV analysis, there is only one software commercialised that is dedicated to the RV.

7. Ventricular shape study

Although, it is obvious that using 2D ultrasound, the observer will appreciate the shape of the ventricle and of the interventricular septum, only few parameters provide an objective estimation of the ventricular shape.

Left ventricular shape analysis

The left ventricle shape has been described first (111). The left ventrcicular shape carries prognostic information, independent from function and volume (112-114). Ventricular remodelling secondary to changing load conditions or ventricular failure leads to changes in volume, shape and function (115). Simple 2D parameters such as left ventricular sphericity index (figure) predict exercise capacity (114) and are related to left ventricular dysfunction. Cardiac magnetic resonance has also been used to determine the left ventricular shape. One of the most popular index of LV shape, LV sphericity volume index (SV = volume/(length^3 x π/6) equivalent to LV volume/volume of sphere with length of LV as the diameter) has been related to cardiovascular diseases for both low and extremely high sphericity (116).

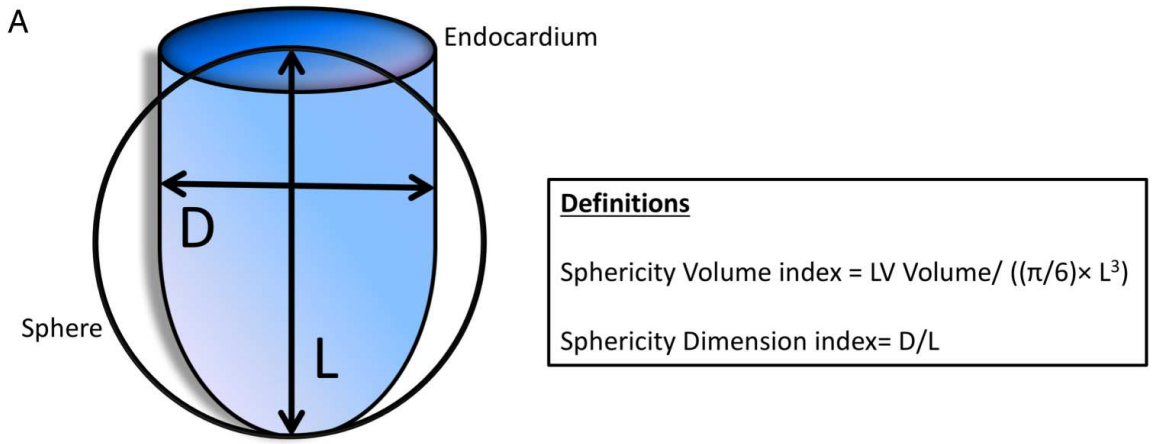

From (116). Calculation of the sphericity volume index.

Other methods to analyse the shape are also available, especially the shape description using a computational atlas (117, 118). The ability to detect shape changes

using standard geometrical characteristics and even sphericity index or local curvature is somehow limited. There is only a limited characterization of the variability in the heart 3D geometry. Anatomical variations can be described by means of a computational atlas which is a statistical representation of the anatomical variability (119). This atlas method can be applied the whole heart shape level, to the right ventricle (120, 121) but also at the fibre level (122) or pulmonary blood flow (123).

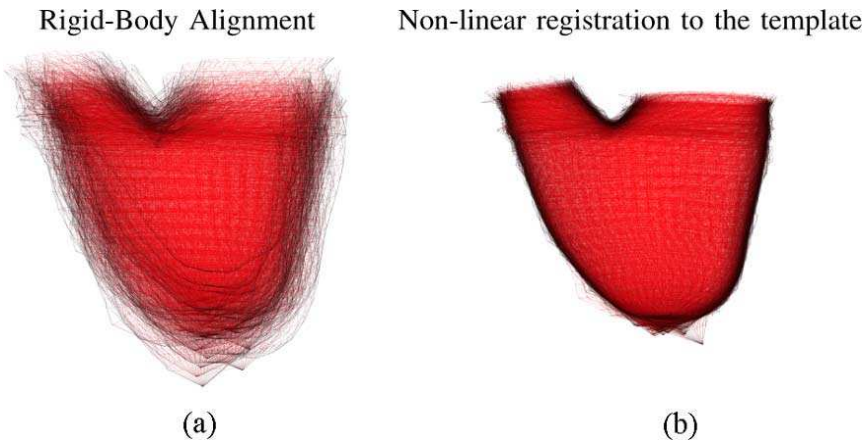

From (120). Example of shape study using a computational atlas. This figure illustrates on the left (a) the RV meshes of 49 patients with a large variability and on the right (b) the same meshes registered back to the template using the diffeomorphic nonlinear deformations. This template serves as reference atlas to determine the deformations towards each individual shape. This mean shape can be correlated to clinical parameters using principal components analysis and pathological shape features can be identified.

3D echocardiography has also been used to investigate left ventricular shape with success (124, 125). 3D left ventricular curvature has been shown to correlate with ventricular function: smaller curvature values thus rounder left ventricular shape was found predominantly in dilated cardiomyopathy patients (126). In this same study, regional analysis of LV shape showed some interesting features, especially the correlation between systolic apical mean curvature and LV ejection fraction, underlining the importance of a global but also regional analysis. The 2D sphericity index can be helpful, however, the following figure illustrates 2 common errors in 2D that 3D shape will correct:

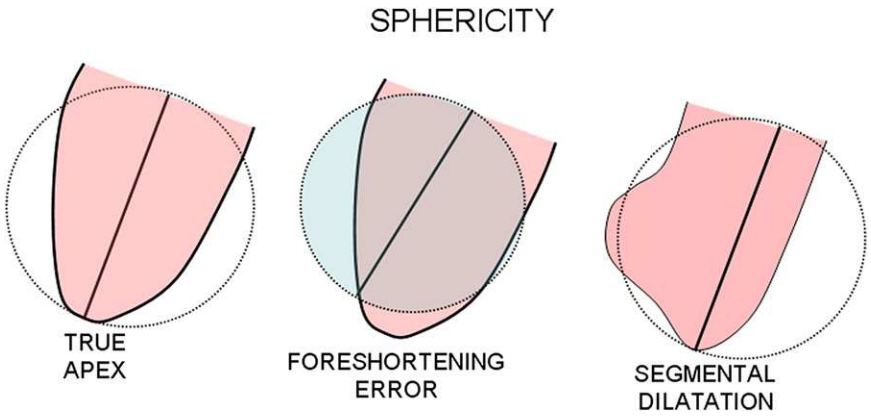

From (126). Limitations of 2D LV shape estimation; foreshortened apex and regional dilatation of the left ventricle

Right ventricular shape analysis

Paradoxically, the shape of the right ventricle is usually described in 2D, with the help of the left ventricle, by the left ventricular eccentricity index. There is a progressive systolic bowing of the interventricular septum occurring together with the increase in right ventricular pressure. High eccentricity index can predict pulmonary hypertension and the degree of eccentricity is related to myocardial fibrosis (7). In normal subjects, the eccentricity index at both end-systole and end-diastole is 1, as the left ventricular cavity is circular in the short-axis view. This index allows with time to differentiate between right ventricular volume or pressure overload: in atrial septal defect patients, the eccentricity index is above 1 at end-diastole but normal at end-systole, reflecting normal right ventricular systolic pressures. In patients with right ventricular pressure overload (pulmonary hypertension, significant pulmonary stenosis) the eccentricity index is greater than 1 at both end-systole and end-diastole (8). The septum curvature, reflected by the left ventricular shape, is thus a simple indicator of RV overload. However, this index has only a limited value and can overdiagnose pulmonary hypertension in patients with right ventricular volume overload (127).

Short axis view of the left ventricle: LV eccentricity index = D2/D1

In order to describe the right ventricular shape from the right ventricle "point of view" instead of the septum, cardiac magnetic resonance has been first used, especially in congenital heart disease patients. In Ebstein's anomaly, right ventricular shape analysis has been performed with the following method from magnetic resonance data (128): 20 evenly spaced planes were constructed orthogonal to the RV long axis from the RV apex to the most distant point on the tricuspid orifice. The intersection of the RV surface with these planes produced 20 cross sections whose areas and perimeters were measured (these areas were normalized by RV long axis length). Eccentricity was computed as $4\pi A/P^2$, where A is the area and P, the perimeter. Bulging of the RV lateral to the tricuspid valve was measured along the long axis as the distance from the centroid of the tricuspid orifice to the most basal point of the RV inlet (basal bulge), and normalized by body surface area. The tilt and shape of the tricuspid orifice were also computed. The following figure illustrates the wide variability in RV shape of Ebstein's patients.

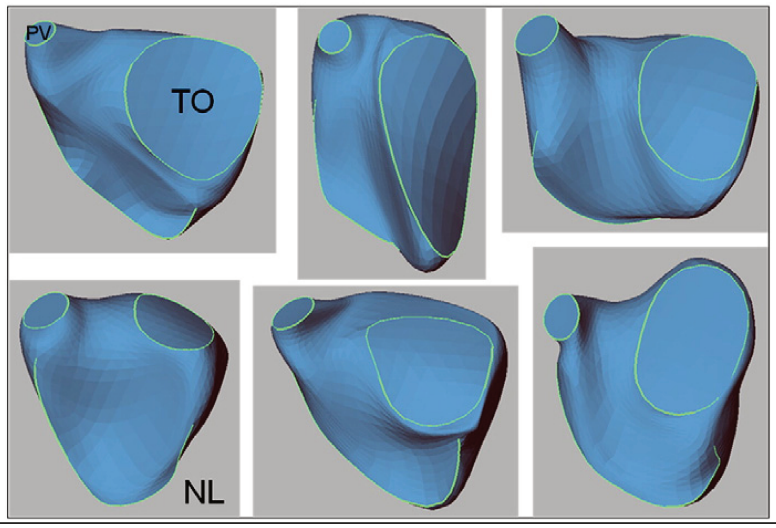

Various shape of the tricuspid orifice in Ebstein's anomaly (128)

In Fallot patients, RV shape presented a basal and apical bulging (129). Using principal components analysis, a multicentre study investigated differences in right ventricular shape in tetralogy of Fallot patients and correlated this shape to the degree of pulmonary regurgitation. The group identified first a mean RV shape, the template, and then compared individual right ventricles to this template. Severe pulmonary regurgitation was associated with a dilated apex and bulging of the right ventricular outflow tract (121). Zhong, *et al*. (130) studied the surface curvedness of the right ventricle of Fallot patients. 3-D surface shape descriptors were expressed in terms of local normal curvature and curvedness. To assess the shape on the meshes, a local surface geometry was fitted to the region and normal curvature (k) was computed:

$$k(\lambda) = \frac{L + 2M\lambda + N\lambda^2}{E + 2F\lambda + G\lambda^2}$$

The curvedness value (C) was calculated as :

$$C = \sqrt{\frac{\kappa_1^2 + \kappa_2^2}{2}}$$

They found decreased curvedness in the RV apex, suggesting that this region might be the first to dilate with RV volume overload.

Using echocardiography and knowledge based reconstruction in pulmonary arterial hypertension, the right ventricle presented more roundness in all segments, as well as

significant basal and apical bulging (130). Addetia, *et al*. (132), using 3D-echocardiography with Tomtec to export right ventricular meshes studied the right ventricular shape in pulmonary hypertension patients and normal controls.

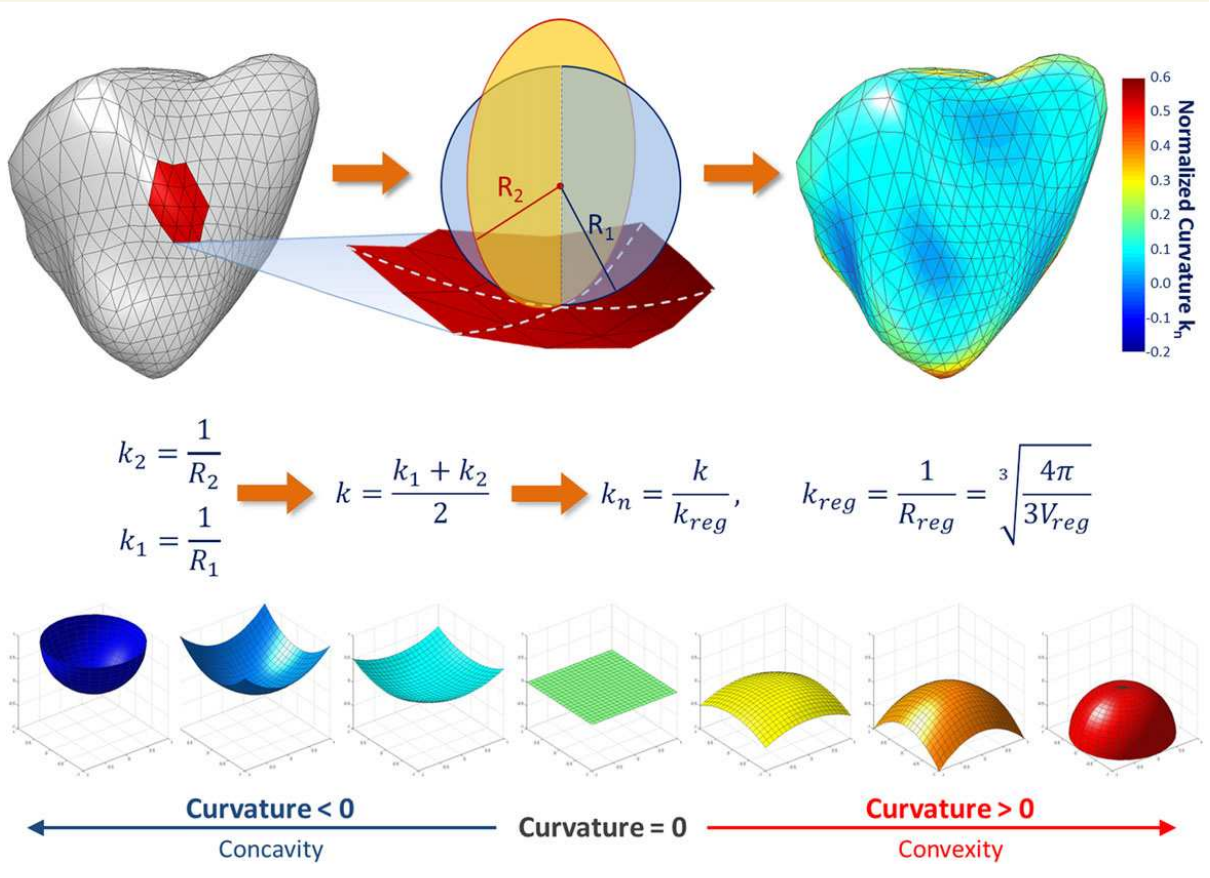

Calculation of 3D curvature according to Addetia, *et al*. Curvature is calculated for each vertex, considering a local neighbourhood. Then, the local surface surrounding the point of interest is fitted to calculate the maximum curvature, k_1 ($1/R_1$, R_1 being the radius of the smaller circle that would fit into the surface) and the curvature k_2 ($1/R_2$, R_2 being the radius of the circle fitting the surface in the perpendicular direction of R1). The indexed curvature K_n is calculated as the mean of k_1 and k_2, normalized by the regional curvature K_{reg}, calculated from the instantaneous regional RV volume, V_{reg}.

They found that in pulmonary hypertension, the septum remained convex throughout the cardiac cycle, bulging into the left ventricle, as described using 2D and the eccentricity index. They also pointed out that the free-wall segments remain equally

convex throughout the cycle, thus losing their contracting property; the “bellows- like action”.

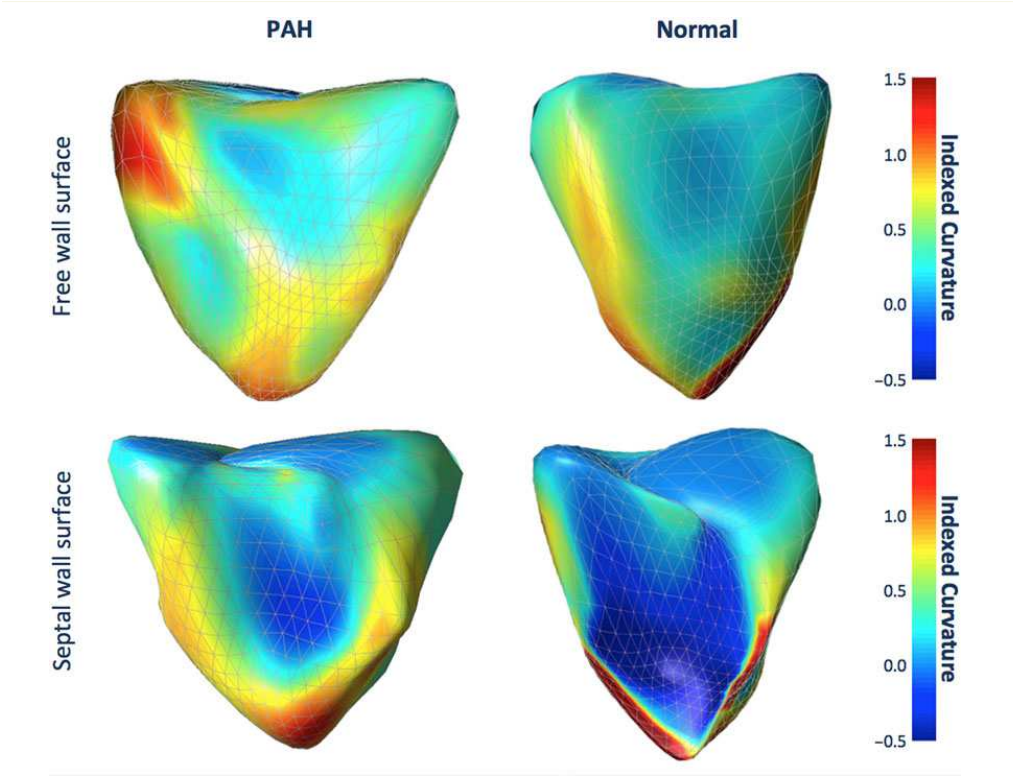

Illustration from Addetia, *et al*. comparing indexed curvature in pulmonary hypertension and controls.

These shape estimation techniques are accurate and provide important information that could lead to a better understanding of both left ventricular and right ventricular remodelling in many conditions affecting the heart (congenital or acquired). However, although giving explanations in the “Methods” sections, the authors fail to detail specifically their calculation method. For example, in the paper by Addetia, *et al*. despite detailed information, the notion of “local neighbourhood” of the point of interest on right ventricular meshes remains vague and limits the reproducibility of the technique. In the discussion section of Chapter 4, we provide an example of curvature analysis using different neighbourhoods, responsible for a huge variability.

The lack of available information detailing the different measurements and calculation techniques contributes to limiting the diffusion of the technique.

8. Objectives

In this thesis, we aimed to investigate right ventricular function according to different loading conditions, using various methods. Only few data exist on how different RV regions remodel according to different disease conditions. How remodelling differs in each region likely has significant influence on how the RV adjusts to different loading conditions and could provide insight into RV failure. Given the difficult imaging of RV shape and function by two-dimensional imaging, we chose to use three-dimensional echocardiography to describe RV remodelling in this work.

- The objective of the second chapter was to investigate the role of 3D global and regional RV deformation in healthy controls and in patients with RV pressure overload (pulmonary hypertension). We also aimed to assess the relationship between 3D RV strain and clinical outcomes.

- In the third chapter, we hypothesize that serial changes in RV deformation could improve the assessment of pulmonary hypertension patients. The aim of the study was to assess the role of a longitudinal evolution assessment of RV deformation parameters in comparison with a single assessment at baseline, in terms of clinical outcome.

- The fourth chapter aimed to investigate RV shape and deformation in volume overload patients (atrial septal defect and tetralogy of Fallot patients) in comparison with healthy controls.

- Finally, in the fifth chapter, we aimed to evaluate the personalised circulatory model parameters added value in characterising pulmonary arterial hypertension and predicting the response to advanced specific therapy.

9. Manuscript organization and contributions

Strain study in pulmonary hypertension patients

Three-dimensional right-ventricular regional deformation and survival in pulmonary hypertension

In this prospective study, we studied the role of 3D global and regional right ventricular (RV) shape and deformation in healthy controls and pulmonary hypertension (PH) patients and assessed their relationship with clinical outcome. 3D transthoracic RV echocardiographic sequences were acquired in 104 adult PH patients and 34 healthy controls. Output RV meshes; obtained after myocardial tracking by a RV dedicated software; were post-processed to extract area strain and temporally aligned. RV shape and strain patterns were gradually deteriorated in PH patients according to the WHO class. Global RV area strain also provided independent prognostic information in this population.

This contribution led to an article published in *European Heart Journal: Cardiovascular Imaging* (133):

- **Moceri P**, Duchateau N, Baudouy D, Schouver E, Leroy S, Squara F, et al. Three-dimensional right-ventricular regional deformation and survival in pulmonary hypertension. *Eur Heart J Cardiovasc Imaging*. 2017. doi:10.1093/ehjci/jex163

The study was presented during the *ESC congress 2016* (Rome, IT) (Session - Novelty in cardiovascular imaging – Rapid Fire Abstract) and the *French society of Cardiology congress 2017* (poster presentation) and preliminary data were presented as a moderated poster during *EuroEcho congress 2015* (Seville, ES)

- **Moceri P**, Duchateau N, Baudouy D, Leroy S, Bouvier P, Schouver D, Sermesant M, Ferrari E. *European Heart Journal* (2016) 37 (Abstract Supplement), 994

- Duchateau N, Sermesant M, Gibelin P, Ferrari E, **Moceri P**. 3D regional right ventricular function in pulmonary hypertension. *Eur Heart J Cardiovasc Imaging Abstracts Supplement* (2015) 16 (Supplement 2), ii69

Longitudinal study of strain evolution in pulmonary hypertension patients

Prognostic value of changes in 3D right ventricular function in pulmonary hypertension

We hypothesized that serial changes in RV deformation could improve the assessment of pulmonary hypertension patients. Our study demonstrates the incremental prognostic value of following changes in RV function as assessed by 3D echocardiography. The most significant changes occur in septal segments. A composite score including changes in WHO functional class, BNP, 3D RV global AS identifies a high-risk population with increased mortality. This simple score could be helpful to guide advanced therapy uptitration or escalation.

The manuscript was submitted for the 1st time in September 2017. The abstract will be submitted to the *French Society of Cardiology* and *AHA congress* in 2018.

- **Moceri P**, Duchateau N, Baudouy D, Sanfiorenzo C, Squara F, Ferrari E, Sermesant M. Incremental prognostic value of changes in 3D right ventricular function in pulmonary hypertension.

Shape and strain study in congenital heart disease patients

Comparative Analysis of shape and strain in Tetralogy of Fallot and Atrial Septal Defect

Right ventricular (RV) function assessment is crucial in congenital heart disease (CHD) patients with volume overload: atrial septal defect (ASD) and tetralogy of Fallot (TOF) patients. We thus aimed to study 3D RV shape and deformation in these patients as compared to a control population in a prospective study. Volume overload in ASD patients seems to impact RV shape but preserves the strain. In contrast, TOF patients present with lower area and longitudinal strain as well as a different shape. This may be explained by the difference in RV volume overload as well as history of previous pressure overload in TOF patients and myocardial damage related to surgery. A larger cohort of

patients could help understand the insight of RV remodelling in CHD with 3D echo images.

These data were accepted for poster presentation during *EuroEcho Imaging 2017* (6th of December, Lisbonne PT) and an article has been written and will be submitted.

Modelling study in pulmonary hypertension patients

Personalised 0D modelling of cardiovascular circulation: disease characterisation and drug effect

0D models of the circulation are powerful tools to integrate flow and pressure information and estimate mechanical parameters, like compliance. Once personalised, new simulations can be launched to predict the cardiac behaviour in several conditions. In this last chapter, we focused on the personalisation of a 0D model of the circulation. The aim of this study was to evaluate the added value of such personalised model parameters to characterise pulmonary arterial hypertension (PAH) and predict the response to PAH therapy. The model was personalised to 11 PAH patients' data before and after advanced PAH therapy. The model parameters reflected with accuracy the expected changes with therapy.

CHAPTER 2.

STRAIN STUDY IN PULMONARY HYPERTENSION

Three-dimensional right-ventricular regional deformation and survival in pulmonary hypertension

CONTENTS

This manuscript was published in the European Heart Journal: Cardiovascular Imaging (133).

ABSTRACT

Background: Survival in pulmonary hypertension (PH) relates to right ventricular (RV) function. However, the RV unique anatomy and structure limit 2D analysis and its regional 3D function has not been studied yet. The aim of this study was to assess the implications of global and regional 3D RV deformation on clinical condition and survival in adults with PH and healthy controls.

Methods and Results: We collected a prospective longitudinal cohort of 104 consecutive PH patients and 34 healthy controls between September 2014 and December 2015. Acquired 3D transthoracic RV echocardiographic sequences were analysed by semi-automatic software (TomTec 4D RV-Function 2.0). Output meshes were post-processed to extract regional motion and deformation. Global and regional statistics provided deformation patterns for each subgroup of subjects.

RV lateral and inferior regions showed the highest deformation. In PH patients, RV global and regional motion and deformation (both circumferential, longitudinal and area strain) were affected in all segments ($p<0.001$ against healthy controls). Deformation patterns gradually worsened with the clinical condition. Over 6.7 [5.8-7.2] months follow-up, 16 (15.4%) patients died from cardio-pulmonary causes. Right atrial pressure, global RV area strain, TAPSE, 3D RV ejection fraction and end-diastolic volume were independent predictors of survival. Global RV area strain >-18% was the most powerful RV function parameter, identifying patients with a 48%-increased risk of death (AUC 0.83 [0.74-0.90], $p<0.001$).

Conclusions: RV strain patterns gradually worsen in PH patients and provide independent prognostic information in this population.

INTRODUCTION

Pulmonary hypertension (PH) is a severe condition, responsible for symptoms and premature death related to right ventricular (RV) function and remodelling (37, 39, 84, 134). In clinical practice, two-dimensional (2D) echocardiography is the most common RV imaging modality, especially in the setting of PH. Transthoracic 2D ultrasound provides a number of descriptors for evaluating right heart haemodynamic but is limited by the anterior position of the tripartite RV and the 2D one-slice plane.

Strain estimation using speckle-tracking on 3D echocardiographic sequences has been suggested as a better means of assessing RV function (26, 135), due to the singular anatomy and structure of the RV, and the inherent 3D nature of cardiac deformation. However, little is known about the deterioration of 3D RV function and deformation with disease, and their relation with survival. Descriptors of shape, sphericity (111, 113) and curvature (132,136,137) have been proposed, but overall regional RV strain changes have not been studied yet. RV free wall peak longitudinal strain and transverse strain have previously been shown to relate to cardiovascular events and mortality in pulmonary hypertension (68, 138-142), but finer markers and analyses are required (143, 144). We hypothesized that the analysis of regional 3D RV strain spatiotemporal patterns, which has not been performed yet, could provide additional insights into the deterioration of RV function and survival.

To do so, we extracted both global and regional 3D RV deformation, and we adapted efficient computational tools to these new types of RV data. Based on these descriptors, we assessed whether statistical differences exist between patients with PH and healthy controls, and related them with clinical outcome.

METHODS

Study design and patients

We performed a prospective longitudinal study on PH patients followed up at our centre (Pasteur University Hospital, Nice, FR) between September 2014 and December 2015. Consecutive clinically stable PH patients were enrolled into a standardized echocardiographic protocol. Healthy controls were enrolled to help determining normal values of 3D RV deformation imaging with our software. Our local research Ethics committees approved this study protocol, which conforms to the ethical guidelines of the 1975 Declaration of Helsinki.

Adult PH patients who consented to the study were included. Pre-capillary PH was considered according to right heart catheterization data, when mean pulmonary artery pressure at rest was ≥25 mmHg with pulmonary capillary wedge pressure ≤15 mmHg. Patients with significant left heart disease, arrhythmias or poor acoustic windows were excluded. Patients with chronic thromboembolic pulmonary hypertension were excluded if they had been scheduled for either endarterectomy or pulmonary angioplasty. Patients with PH due to lung diseases and/or hypoxemia were included only if they were considered as stable (regarding the respiratory status) for at least 3 months and already under oxygen if needed. Asymptomatic healthy volunteers were recruited from the community to serve as controls and included if they had a normal trans-thoracic echocardiography, and if they were in sinus rhythm.

Demographics, clinical data (age, gender, diagnosis, baseline WHO class, PH-targeted advanced therapy), BNP plasma levels (Beckman Access 2, Triage BNP assay (Biosite Diagnostics Inc, San Diego, CA)) and 6-minute walk test distance were collected at baseline. The time of echocardiography was considered as the start date for the study enrolment (the ultrasound qualifying the patient for inclusion). Follow-up was considered from the date of echocardiography and continued until patients either died or reached the end of the study (December 2015). Clinical outcome was defined by mortality related to PH.

2D-echocardiographic acquisitions and measurements

Echocardiographic examination was performed using an IE-33 or EPIQ-7 ultrasound system and a S5 or X5-1 transducer (Philips Medical system, Andover, MA). Doppler echocardiography was performed according to the recommendations of the American Society of Echocardiography (ASE) / European Association for Cardiovascular Imaging (EACVI) (44, 145, 146).

Two different staff cardiologists, with advanced training in echocardiography, performed the cine-loops acquisitions and interpreted 2D-echo datasets. The measured parameters were averaged over three consecutive cycles. The following parameters were measured: left ventricular ejection fraction, right atrial area, tricuspid annular peak systolic velocity (s'), myocardial acceleration during isovolumic contraction (IVA) (49), tricuspid annular plane systolic excursion (TAPSE), systolic pulmonary artery pressure (derived from the tricuspid valve regurgitation), right ventricular outflow tract (RVOT) velocity-time integral (VTI) and right atrial pressure estimated on the basis of IVC diameter and collapse.

3D Trans-thoracic Echocardiography

At least four 3D cine-loops of the RV were acquired from an apical 4-chamber view focused on the RV, using an IE-33 or EPIQ-7 ultrasound system and a matrix-array X5-1 transducer (Philips Medical system, Andover, MA). Full-volume acquisition over 2 heartbeats (for loop storage) was performed using ECG-gating over 4-to-6 cardiac cycles, during a quiet breath-hold. Frame rate was maximized to allow the use of the RV-dedicated quantification software. Care was taken to include the entire RV within the images. Digital 3D data sets were stored and analysed using commercial software dedicated to the RV (4D RV Function 2.0, TomTec Imaging Systems GmbH, DE) (Figure 1). This software allowed tracking the RV endocardium along the cardiac cycle using 3D speckle-tracking. It directly estimated the RV end-diastolic and end-systolic volumes, ejection fraction, and wall-specific peak strain. Test-retest variability (intra-operator, inter-loop and inter-operator variability) was also assessed in a randomly selected group of 10 patients and 10 healthy controls.

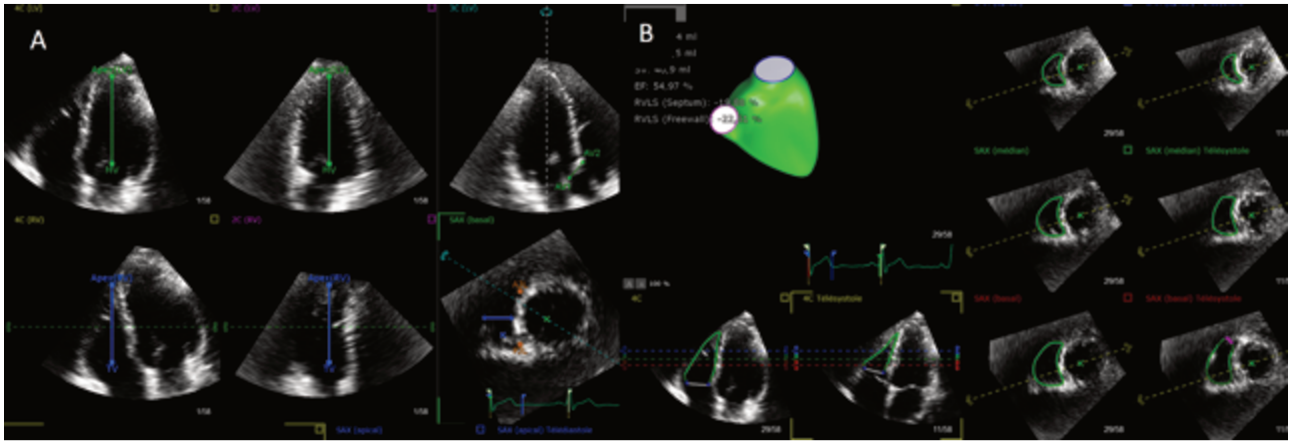

Figure 1: Example of RV 3D analysis using TomTec 4D RV function 4.0. (A) Initial alignment of 3D dataset and identification of landmarks. (B) End-systolic verification and editing of endocardial RV borders.

Displacement and deformation analysis

Motion and deformation were analysed at each point of the RV endocardium and at each instant of the cycle. Motion (3D displacement) was projected along the radial, circumferential and longitudinal directions. Circumferential and longitudinal strains were computed as the *engineering strain* ---the relative change of length--- along these directions, within a 5 mm neighborhood. Area strain was computed as the area change of each mesh triangle. Due to the availability of endocardial surfaces only, radial strain was not computed. We used the mesh correspondences provided by the commercial software to label the RV regions according to *Haddad et al*. (13) (Figure 2).

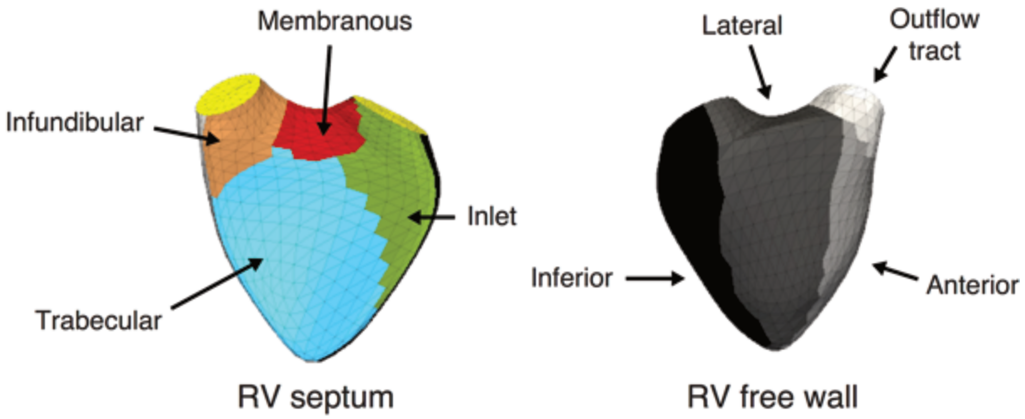

Figure 2 : RV regions used in our study, according to Haddad et al.

These computations were done using VTK (v 7.10, Kitware, New York, US), and Matlab (v.R2011a, MathWorks, Natick, US), as previously validated in (147).

Right heart catheterization

Right heart catheterization was performed on 67 patients within 2 months from the ultrasound examination and in the same day on 29 patients as part of their standard treatment plan and follow-up.

Statistical analysis

Data were summarized as mean ± standard deviation for continuous variables with normal distribution; median [95% confidence interval] for other continuous variables and number of subjects (%) for categorical variables. The variables were tested by the Student t-test for normally distributed variables otherwise, Mann-Whitney U-test was performed. Categorical variables were compared using Fisher's exact test. Bonferroni correction was used for multiple comparisons. Right heart catheterization data were correlated to global area strain using the Pearson test. The relationship between echocardiographic parameters and survival was assessed through univariate and multivariate Cox proportional hazard regression, starting at the date of echocardiography. Multivariate survival analysis included all variables with a p-value <0.10 in the univariate analysis as well as previously described prognostic parameters: WHO functional class, BNP, 6-minute walking distance and PH-targeted advanced therapy. Receiver operating characteristics curves were constructed to derive the optimal cut-off values to predict survival (Youden's index method). Test-retest variability consisted of intra- and inter-operator comparisons as well as inter-loop strain comparisons, and included intra-class correlation coefficients. For all analyses, statistical significance was defined as a p-value <0.05. Statistical analyses were performed using MedCalc 16.1 (MedCalc Software, Mariakerke, BE).

RESULTS

Baseline characteristics

One hundred four consecutive adult PH patients and 34 healthy controls were included in the study. One hundred seventeen patients were initially screened, 13 were excluded because of atrial fibrillation in 4 of them and poor acoustic window in the other 9. Table 1 summarizes baseline characteristics for patients and healthy controls.

Our patients' population included 65 (62.5%) group 1 pulmonary arterial hypertension (PAH) patients (detailed below), 26 (25.0%) group 3 PH patients, 11 (10.6%) group 4 PH patients and 2 (1.9%) group 5 PH patients according to the most

Table 1 **Baseline characteristics of the population, including three-dimensional and RV deformation data**

	Pulmonary hypertension *n* = 104	Healthy controls *n* = 34	*P*-value
Age (years)	65.9 [62.0–68.8]	45.5 [33.7–50.4]	<0.001
Female sex, *n* (%)	58 (55.8%)	15 (44.1%)	0.3
Body surface area (m^2)	1.72 ± 0.2	1.75 ± 0.1	0.3
WHO functional class ≥ III	66 (63.4%)		
BNP (ng/mL)	126 [94.0–182.0]		
6MWD (m)	359.5 ± 106		
AT at baseline, *n* (%)	87 (83.7%)		
Death, *n* (%)	16 (15.4%)		
2D echocardiographic data			
LVEF (%)	69.1 ± 8.5		
Right atrial pressure (mmHg)	10.0 [10.0–10.0]		
Right atrial surface (cm^2)	24.0 [22.4–25.0]		
Pulmonary VTI (cm)	15.0 ± 4.7		
Systolic PAP (mmHg)	75.2 ± 24.9		
TAPSE (mm)	20.4 ± 5.2		
Tricuspid s′ (cm/s)	11.6 ± 3.0		
IVA (m/s^2)	2.0 [1.9–2.2]		
RHC data			
PVR (Wood U)	6.6[5.9–7.6]		
Mean PAP (mmHg)	43.3 ± 12.6Min–max [25–70]		
Right atrial pressure (mmHg)	9.0 [7.0–10.0]		
Cardiac index ($L/min/m^2$)	2.7 [2.4–2.8]		
3D echocardiographic data			
RV EF (%)	35.6 ± 9.7	55.9 ± 5.8	<0.001
RV EDV (mL)	91.0 ± 40.6	51.4 ± 21.9	<0.001
Global area strain (%)	-18.8 ± 5.4	-29.5 ± 4.4	<0.001
Global circumferential strain (%)	-11.6 ± 3.6	-17.3 ± 3.2	<0.001
Global Longitudinal strain (%)	-8.4 ± 3.6	-14.1 ± 3.6	<0.001
Frame rate (Hz)	17.7 [16.6–18.7]	18.0 [17–19]	0.1

6MWD, 6-minute walk test distance; AT, advanced therapy; BNP, brain natriuretic peptide; EDV, end-diastolic volume; EF, ejection fraction; IVA, myocardial acceleration during isovolumic contraction; LVEF, left ventricular ejection fraction; PAP, pulmonary artery pressure; PVR, pulmonary vascular resistance; RHC, right heart catheterization; RV, right ventricular; TAPSE, tricuspid annular plane systolic excursion; VTI, velocity-time integral.

recent PH classification (148). PAH aetiology was idiopathic PAH in 17 patients (26.2% of group 1 PAH patients), heritable PAH in 1 patient (1.5%), 4 drug- and toxin-induced PAH (6.2%), PAH associated with connective tissue disease in 16 patients (24.6%), associated with congenital heart disease in 13 patients (20%) (including 4 ventricular septal defects, 4 atrial septal defects, 1 complete atrio-ventricular septal defect and 4 closed left-to-right shunts), associated with portal hypertension in 12 (18.5%) patients, and HIV-associated PAH in 2 patients (3.1%). All group 1, 4 and 5 patients as well as 9 patients from group 3 PH were treated with advanced targeted PAH therapy at baseline.

Eighty-six PH patients (82.7%) had a reduced RV ejection fraction <45%, 43 of them (41.3%) had a TAPSE below 20 mm and 52 (50%) a BNP level above 100 ng/mL.

The full 3D RV analysis using TomTec software required an average of 185±42 seconds including image alignment and manual correction of the detected endocardial RV borders.

Table 2 RV regional deformation data in healthy and PH subjects

	Pulmonary hypertension *n* = 104	Healthy controls *n* = 34	*P*-value
Area strain (%)			
Anterior wall	-17.8 ± 7.0	-29.5 ± 6.6	<0.001
Inferior wall	-24.4 ± 8.8	-37.9 ± 7.4	<0.001
Lateral wall	-28.5 ± 9.1	-43.4 ± 6.6	<0.001
RVOT anterior	-14.7 ± 6.0	-22.2 ± 5.9	<0.001
Infundibular septum	-17.8 ± 7.0	-27.2 ± 7.1	<0.001
Membranous septum	-14.7 ± 7.6	-23.3 ± 8.1	<0.001
Inlet septum	-16.7 ± 8.2	-27.8 ± 9.4	<0.001
Trabeculated septum	-15.9 ± 6.3	-24.8 ± 7.1	<0.001
Circumferential strain, %			
Anterior wall	-12.9 ± 6.2	-20.8 ± 7.4	<0.001
Inferior wall	-13.4 ± 6.3	-20.4 ± 6.0	<0.001
Lateral wall	-19.0 ± 6.2	-29.5 ± 6.2	<0.001
RVOT anterior	-7.8 ± 3.7	-11.6 ± 4.6	<0.001
Infundibular septum	-12.1 ± 3.8	-16.7 ± 3.9	<0.001
Membranous septum	-8.4 ± 4.0	-11.7 ± 3.5	<0.001
Inlet septum	-10.3 ± 6.1	-14.6 ± 6.5	0.001
Trabeculated septum	-8.7 ± 4.4	-13.1 ± 4.7	<0.001
Longitudinal strain (%)			
Anterior wall	-6.5 ± 3.6	-10.8 ± 4.3	<0.001
Inferior wall	-12.2 ± 4.9	-20.3 ± 5.8	<0.001
Lateral wall	-10.5 ± 4.6	-16.0 ± 3.8	<0.001
RVOT anterior	-8.3 ± 5.1	-12.5 ± 5.9	<0.001
Infundibular septum	-7.1 ± 6.1	-11.2 ± 5.8	0.001
Membranous septum	-7.3 ± 6.0	-13.2 ± 6.7	<0.001
Inlet septum	-7.4 ± 5.6	-14.9 ± 7.3	<0.001
Trabeculated septum	-7.8 ± 3.8	-13.4 ± 5.0	<0.001

RV, right ventricular; RVOT, right ventricular outflow tract; PH, pulmonary hypertension.

RV segmental and global strain

Global and regional RV strain comparisons between patients and healthy controls are summarized in

Tables 1 and 2. In healthy controls, area strain predominated at the lateral and inferior wall. Circumferential and longitudinal RV strain predominated at the lateral and inferior wall, respectively. The septal component of the RV also contributed to the global RV deformation. As compared to healthy controls, PH patients had significantly reduced global and regional RV area strain (in all RV segments, p<0.001). Similar observations were made for the RV longitudinal and circumferential strain in all segments.

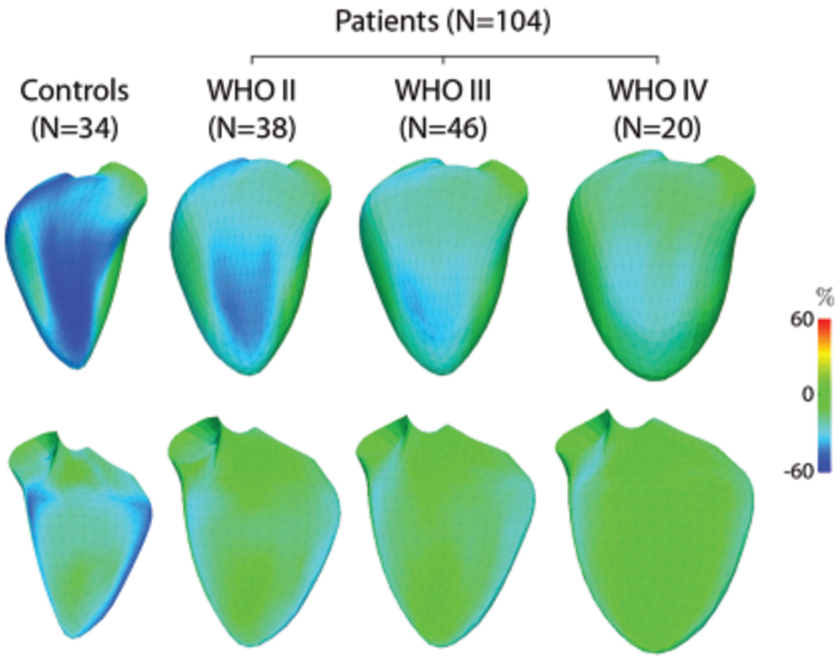

Figure 3: End-systolic strain patterns according to baseline WHO class: the median pattern over each WHO subgroup is represented on the subgroup average shape.

Table 3 **Three-dimensional and RV deformation data according to baseline WHO functional class in PH patients**

	WHO II *n* = 38	WHO III *n* = 46	WHO IV *n* = 20	*P*-value II vs. III	*P*-value II vs. IV	*P*-value III vs. IV
RV EF (%)	38.9 ± 8.7	35.5 ± 8.8	29.4 ± 10.9	0.27	<0.001	0.04
RV EDV (mL)	78.1 ± 29.6	90.6 ± 43.0	116.6 ± 42.7	0.43	0.001	0.04
Global area strain (%)	-20.4 ± 5.4	-18.9 ± 4.4	-15.6 ± 6.1	0.61	0.003	0.05
Global circumferential strain (%)	-12.5 ± 3.4	-11.5 ± 3.2	-10.0 ± 4.3	0.5	0.04	0.4
Global longitudinal strain (%)	-9.3 ± 3.9	-8.6 ± 3.0	-6.3 ± 3.3	0.99	0.007	0.05

EDV, end-diastolic volume; EF, ejection fraction; PH, pulmonary hypertension; RV, right ventricular.

Link with the severity of the disease

A gradient in RV area strain was observed according to the severity of the disease (assessed by baseline WHO functional class, Figure 3 and 4). It was accompanied by a gradual dilatation of the RV (Table 3).

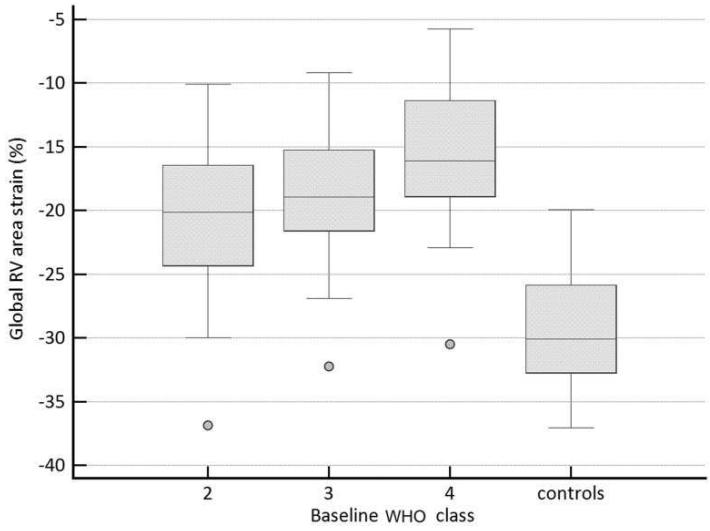

Figure 4: End-systolic global AS according to baseline WHO class.

Apart from this gradual decrease in the peak deformation, a slight but gradual delay in the contraction was also associated with the WHO class, as visible in all the strain components at the segments with higher contraction (RV lateral, Figure 5). We tested the correlation between global RV area strain and invasive parameters collected the same day in a subset of 29 patients. None of the invasive parameters were significantly associated with global RV area strain: pulmonary vascular resistance ($r=0.10$; $p=0.4$); mean pulmonary artery pressure ($r=0.20$; $p=0.3$); cardiac index ($r=-0.16$; $p=0.4$); right atrial pressure ($r=-0.12$; $p=0.6$). On the opposite, RV ejection fraction was closely associated to RV global area strain ($r=-0.90$, $p<0.0001$).

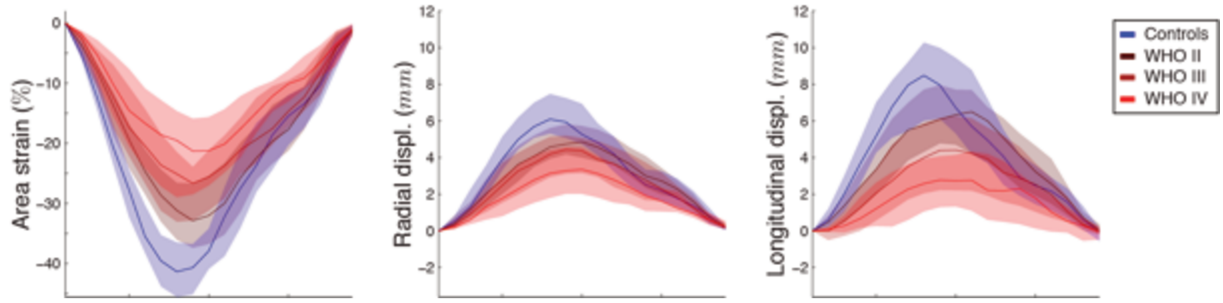

Figure 5: Motion and deformation along the cycle according to the functional capacity (median and first/third quartiles over each subgroup, at the RV lateral segment).

Survival analysis

Over a median follow-up of 6.7 months [5.8–7.2], 16 patients (15.4%) died from cardio-pulmonary causes. On univariate survival analysis, baseline WHO functional class IV (HR 2.89 [1.08-7.72]; p=0.03), 6-minute walking distance (HR 0.98 [0.97-1.00]; p=0.05), PH-targeted advanced therapy (HR 0.24 [0.09-0.67]; p=0.006), BNP (HR 1.002 [1.001-1.003]; p<0.001), invasive mean PA pressure (HR 1.06 [1.01-1.11]; p=0.02) were predictors of survival. Echocardiographic predictors of survival on univariate analysis included 3D RV ejection fraction (HR 0.87 [0.81-0.93]; p<0.001), 3D RV end-diastolic volume (HR 1.02 [1.01-1.03]; p<0.001), moderate or severe tricuspid regurgitation (HR 8.45 [3.08-23.15]; p<0.001), systolic PA pressure (HR 1.03 [1.01–1.05]; p=0.009), right atrial pressure (HR 1.41[1.24-1.61]; p<0.001), right atrial area (HR 1.08 [1.05-1.12]; p<0.001), pulmonary VTI (HR 0.86 [0.75-0.98]; p=0.02), tricuspid s' (HR 0.82 [0.69-0.97]; p=0.02), TAPSE (HR 0.8 [0.72-0.90]; p<0.001), global RV area strain (HR 1.34 [1.18-1.52]; p<0.001), global RV circumferential strain (HR 1.53 [1.24-1.88]; p<0.001) and global RV longitudinal strain (HR 1.31 [1.10-1.56]; p=0.002).

On multivariate analysis including baseline WHO functional class, BNP, 6-minute walking distance and PH-targeted advanced therapy as covariates, global area strain (HR 1.72 [1.07-2.78]; p=0.03), 3D RV ejection fraction (HR 0.80 [0.64-0.99], 3D RV end-diastolic volume (HR 1.03 [1.00-1.05]; p=0.02), TAPSE (HR 0.72 [0.52-0.99]; p=0.04) and right atrial pressure (HR 1.61 [1.09-2.36]; p=0.02) were independent predictors of survival.

On receiver operating curve analysis, the average area under the curve for the global RV area strain was 0.83 [0.74-0.90], p<0.001 compared to 0.81 [0.72-0.88], p<0.001 for TAPSE and 0.80 [0.71-0.87], p<0.001 for 3D RV ejection fraction (Figure 6). Global RV area strain >-18% identified patients at high risk of mortality with a sensitivity of 94% and a specificity of 62%.

Figure 6: Kaplan–Meier and ROC curves for prediction of survival.

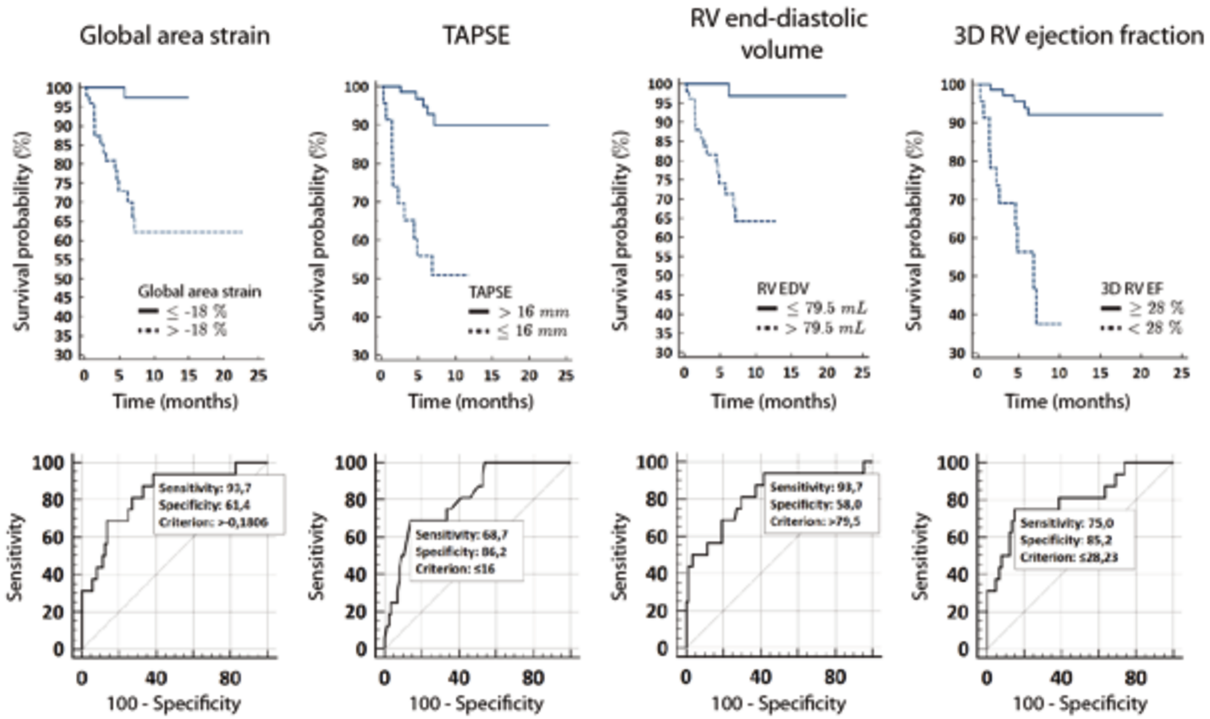

Reproducibility

Intra-class correlation coefficients for inter-observer variability were 0.90 [0.77-0.96] for RV EF and 0.94 [0.86-0.98] for RV EDV. Intra-class correlation coefficients for intra-observer variability (same cine loop analysed) were 0.95 [0.88-0.98] for RV EF, 0.98 [0.96-0.99] for RV EDV and 0.93 [0.83-0.97] for RV global area strain, respectively. Intra-class correlation coefficients for inter-loop variability (intra-observer variability using a second dataset acquired at a different time) were 0.94 [0.86-0.98] for RV EF, 0.94 [0.86-0.98] for RV EDV and 0.94 [0.86-0.98] for RV global area strain.

DISCUSSION

Studying the RV function is challenging but of critical importance, especially in a devastating disease such as pulmonary hypertension. Our study analysed for the first time RV 3D deformation patterns in healthy controls and pulmonary hypertension patients using dedicated RV software. Our results highlight the role of regional deformation analysis, which reveal the dominant RV regions (inferior and lateral wall) and subtle pattern changes with disease severity. This study also demonstrates the prognostic role of RV area strain in PH patients.

2D vs 3D RV analysis and regional function

Standard evaluation of the RV usually requires 2D assessment. Despite being correlated with MRI RV EF, widely used parameters such as TAPSE and TV s' (to assess RV function in routine clinical practice) only assess the lateral tricuspid annulus. 2D speckle-tracking echocardiography has been used to quantify RV myocardial deformation, but mainly focuses on longitudinal strain. Indeed, given the complex anatomy of the RV, circumferential strain cannot be fully assessed by 2D techniques. Actually, MRI studies have highlighted the value of considering RV circumferential strain for some pathologies such as arrhythmogenic RV cardiomyopathy (149) or RV afterload changes (150, 151). Besides, going beyond global measurements and assessing regional RV function is determinant in the evaluation of Tetralogy of Fallot patients (152-154) and pulmonary embolism (155, 156), but is usually assessed with MRI. In this study, we demonstrate using dedicated software the feasibility and high value of 3D echocardiographic analysis to estimate RV ejection fraction, volumes (157), and regional RV function (45) in healthy volunteers and PH patients. We also believe that adding circumferential strain to the longitudinal RV strain analysis, which allows computing RV area strain, provides additional prognostic information.

The tracking accuracy and therefore the relevance of motion and deformation values were fully conditioned by the Tomtec commercial software, whose use has been validated in (158). Our post-processing software only uses standard mathematical

formulations to compute *local* motion and deformation from already existing mesh data, and corresponds to the validated tools (147).

Our study provides a new statistical characterization of 3D RV deformation patterns. It first illustrates the normal contraction pattern over the whole RV: the lateral wall is predominant in terms of area strain, but the inferior wall, the anterior wall as well as the inlet septum are also significant contributors to the RV global area change. Longitudinal deformation predominates at the inferior wall, whereas the lateral wall provides more circumferential deformation. Then, this statistical characterization is extended to the comparison of PH against healthy deformation patterns, and confirms that RV dysfunction predominates in these regions.

RV remodelling and outcome

Our method provided a reliable full analysis of the right ventricle, including regional analysis. Using left ventricle-dedicated software, previous studies already reported that RV global area strain is associated with outcomes in PH (142, 159, 160). Our results confirm the prognostic role of RV area strain. The use of dedicated RV software allowed studying the entire RV structure and refining observations at the regional level. Despite playing a "minor" role as compared to the lateral, anterior and inferior wall, the RVOT and infundibular septum significantly contribute to RV area strain. This opens the door to complementary analyses of the RV function in PAH, such as the timing alteration of RV segments.

RV adverse remodelling, RV dilatation and reduction in RVEF and/or area strain are associated with mortality in our cohort of PH patients. Cardiac index, a known but debated invasive indicator of prognosis reflecting RV contractility (161), did not reach statistical significance in our cohort, probably because of the low number of patients with right heart catheterization data. RV area strain is independently and strongly associated with survival, illustrating the initial role of decreasing strain before reducing RV EF and dilating the cavity. Indeed, our echocardiographic parameter could be interpreted as a consequence of the RV-PA unit, a marker of RV-PA coupling (162), which among other parameters has been recently related to prognosis in PH (163). Finer markers of RV

function like area strain are therefore useful to detect early changes in PAH patients and could help improving the follow-up and prognosis of such patients.

Limitations

3D RV analysis was feasible in 88.9% of patients, the main limitation being the imaging quality. Given the expected intra-individual variability, patients with atrial fibrillation were excluded from this preliminary study. This could represent a selection bias. Patients with post-capillary PH were not studied and the conclusions made in this paper are consequently not extendable to this population. Indeed, left heart disease could influence RV deformation.

Classically, 3D RV assessment was limited by its feasibility. In our study, thanks to RV dedicated software, intra- and inter-operator and inter-loop reproducibility were acceptable, as previously described (158). Furthermore, the duration of the 3D quantification analysis was acceptable and could be applicable in routine clinical practice.

Our cohort of control patients was relatively small, as compared to the PH group. Indeed, identifying patients in the Echo Lab, without any structural heart disease (potentially influencing RV remodelling) has been very difficult. Furthermore, this issue prevents us from age-matching our control population to the PH population. Indeed, this could represent another limitation given that age could influence 3D RV quantification (164).

The lack of correlation between haemodynamic parameters and RV area strain can be confusing. However, this could be expected, as the number of patients with invasive data was relatively low compared to the overall number of patients. Right atrial pressure, a strong marker of risk in PH patients was also a predictor of mortality in our population, but not related to RV area strain. This might be explained by the evolution of PH itself as right atrial pressure increases gradually with RV dysfunction, while RV area strain might be an earlier marker of RV dysfunction, explaining the relative independence of both markers.

The prognostic importance of decreased RV area strain is obvious in our cohort, however as our patients suffer from multiple PH aetiologies, a larger multicentre study could help verifying and generalizing our conclusions in a larger population. Given the relatively small cohort of patients, no etiological subgroup analysis was performed. A larger study would allow describing RV shape and deformation patterns in a finer way for each PH aetiology, especially in group 1 patients.

CONCLUSIONS

We examined the implications of a finer analysis of 3D RV deformation on clinical condition and survival in a cohort of adults with PH and 34 healthy controls. We quantitatively demonstrated that RV strain patterns gradually worsen in PH patients and provide independent prognostic information. This new technique could help better stratifying the risk in PH patients.

SUPPLEMENTARY MATERIAL

SUPPLEMENTARY METHODS

Non-commercial software used in our study: The implementation of the shape and deformation analysis software was realized using Matlab v.R2011a (MathWorks, Natick, MA), and corresponds to an upgrade of the left ventricle- and Echopac-specific analysis software, publicly available online at: http://nicolasduchateau.wordpress.com/downloads/ .

SUPPLEMENTARY RESULTS

Supplementary Table 1: Bland-Altman data for repeated measures in 10 healthy controls and 10 patients

Variability		Mean			SD		
		Global	Patients	Controls	Global	Patients	Controls
RV EF (%)	*Intra-operator*	0.2	-0.7	0.6	3.1	2.4	3.5
	Inter-loop	-1.6	-1.5	-1.7	3.4	1.9	4.5
	Inter-operator	-0.4	-2.1	1.4	4.2	3.4	4.3
RV EDV (mL)	*Intra-operator*	-2.3	-2.3	-2.8	4.3	4.3	6.5
	Inter-loop	0	-1.8	1.9	11.5	13.7	9.2
	Inter-operator	6.2	8.8	3.7	10.9	11.7	9.8
RV AS (%)	*Intra-operator*	-0.3	-0.6	-0.5	10.2	6.5	11.6
	Inter-loop	-0.3	1.7	-2.7	9.1	6.0	12.6

AS, area strain; EDV, end-diastolic volume; EF, ejection fraction; ICC intra-class correlation coefficient; SD, standard deviation; RV, right ventricle

Figure SM 1: Validation of the semi-automated software for RV quantification (3D RV ejection fraction and end-diastolic volume) and of the post-processing of 3D RV meshes (RV area strain).

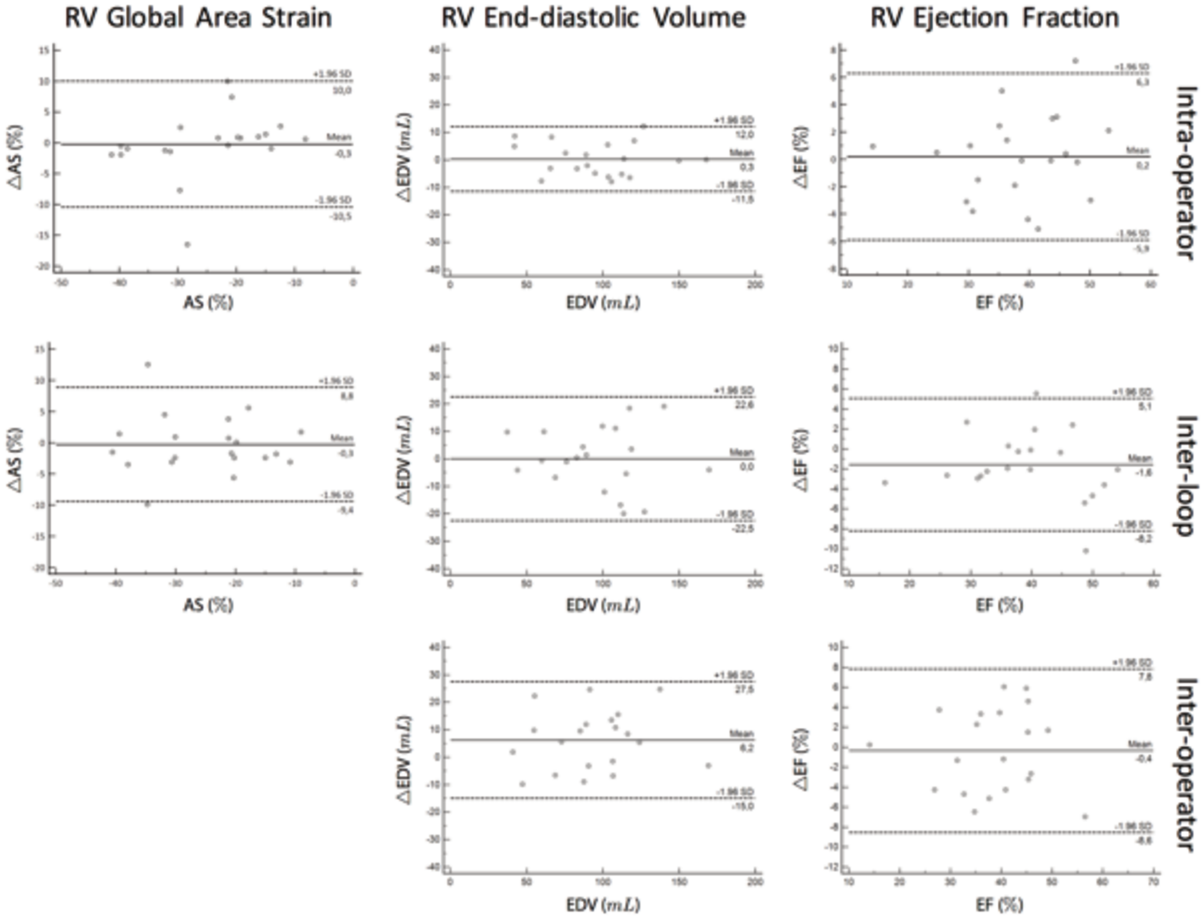

Bland-Altman analysis of 3D right ventricular end-diastolic volume, ejection fraction and area strain. Intra-operator variability was assessed comparing data obtained from the same loop with the same operator but at a different time (one week later). Inter-loop variability compared data obtained from the same operator but using 2 different cine-loops. Inter-operator variability compared data from different cine-loops and different operators (blinded to each other results).

CHAPTER 3.

LONGITUDINAL STUDY OF STRAIN EVOLUTION IN PULMONARY HYPERTENSION PATIENTS

Prognostic value of changes in 3D right ventricular function in pulmonary hypertension

CONTENTS

ABSTRACT

Background: Outcomes in PH are related to RV function and remodelling. We hypothesized that changes in RV function, especially area strain (AS), could provide incremental prognostic data. In this study, we aimed to assess global and regional 3D right ventricular (RV) function changes between baseline and 6-months visit and evaluate their prognostic value in pulmonary hypertension (PH).

Methods and results: 65 PH patients were prospectively included. All patients underwent 2D and 3D transthoracic echocardiography at baseline and at a 6-month follow-up. They underwent regular follow-up at 3- to 6-month intervals, per clinical status. 3D RV echocardiographic sequences were analysed by semi-automatic software and output meshes were post-processed to extract regional deformation. Most of our population consisted in group 1 PH (74%) and female patients (61.5%). At baseline, there was no significant difference in RV AS between patients' clinical subgroups. Patients who were considered clinically stable or improving were more likely to present at 6-months a significant increase in 3D RV EF (p=0.04) and a decrease in RV global AS (p=0.001). Most significant regional changes occurred within the septum. Over a median follow-up of 24.8 months [22.1-25.7], 1 patient was transplanted and 15 patients died from PH. On multivariate COX analysis, 6-month changes in WHO class (HR 17.4[5.2-58.5]), BNP (HR 1.003[1.001-1.004]) and RV global AS (HR 1.12[1.03-1.21]) were independent predictors of survival. A composite score including 6-months changes in WHO class, increase in BNP and decrease in ≥24% RV AS could identify patients with a 9.1-fold increased risk of death or lung transplant.

Conclusions: Our study demonstrates the additional prognostic value of following changes in RV deformation using 3D echocardiography. A composite score including changes in WHO function class, BNP and 3D RV AS could help stratifying the patients' risk.

INTRODUCTION

Pulmonary hypertension (PH) is a severe cardiopulmonary disorder, which gradually leads to symptoms and premature death. Outcomes are mostly related to right ventricular (RV) function and remodelling (26, 37, 39, 84, 134, 141). Volume and strain analysis from 3D speckle-tracking are now feasible on the RV (142, 158, 165, 166) and provides valuable information about its regional function and relation with prognosis (132, 133).

Nonetheless, baseline information may still be limited for the patients' evaluation and risk stratification, in the presence of both incident and prevalent cases. Data that may help refine the patients' risk between treatment-naïve incident patients and prevalent cohorts of PH patients are lacking. The ESC/ERC guidelines for the management of PH (148) recommend the goal-oriented therapy, which implies considering improvements in both clinical and echocardiographic parameters and BNP levels. Despite this, only few studies (167, 168) investigate such changes in relation with the patient outcome, from the perspective of generic parameters. Instead of baseline only, a dynamic assessment of the PH patient can reflect both PH evolution and therapy effect and might offer a more reliable risk assessment.

In this study, we hypothesized that changes in 3D RV function, especially area strain, can provide incremental insights into the prognosis of PH patients. For this purpose, we performed a comprehensive examination of both global and regional 3D RV deformation changes between baseline and follow-up, and evaluated their added value to characterize the patients' outcome.

METHODS

Study design and patients

The study was prospective and longitudinal. We included consecutive clinically stable adult PH patients followed up at our centre (Hôpital Pasteur, CHU de Nice, FR) between September 2014 and June 2017 who were enrolled into a standardized echocardiographic protocol. All participants consented and provided written informed consent. The study was approved by the research Ethics committees at our institution, and complied with the ethical guidelines of the Helsinki Declaration.

Pre-capillary PH was considered when mean pulmonary artery pressure at rest was ≥25 mmHg with pulmonary capillary wedge pressure ≤15 mmHg (using right heart catheterization data). We excluded patients with significant left heart disease, arrhythmias or poor acoustic windows, and patients with chronic thromboembolic pulmonary hypertension if they had been scheduled for either endarterectomy or pulmonary angioplasty. No patient had severe tricuspid regurgitation. We included patients with PH due to lung diseases and/or hypoxemia only if they were considered stable (regarding the respiratory status) for at least 3 months, already under oxygen if needed and if their mean PA pressure was ≥35mmHg.

Demographics and clinical evaluation (age, gender, diagnosis, baseline WHO class, PH targeted advanced therapy), determination of BNP plasma levels (Beckman Access 2, Triage BNP assay (Biosite Diagnostics Inc, San Diego, CA)) and 6-minute walk test were performed at baseline and follow-up. The first echocardiography qualified the patient for inclusion and was taken as the start date for the study enrolment. Follow-up was considered from this date until the patient's death or the end of the study (June 2017). Clinical outcome was defined by either mortality related to PH, lung transplantation, hospitalization for heart failure related to PH, need to start therapies targeting the PGI2 pathway.

The flow chart of the study summarizes this information in Figure 1.

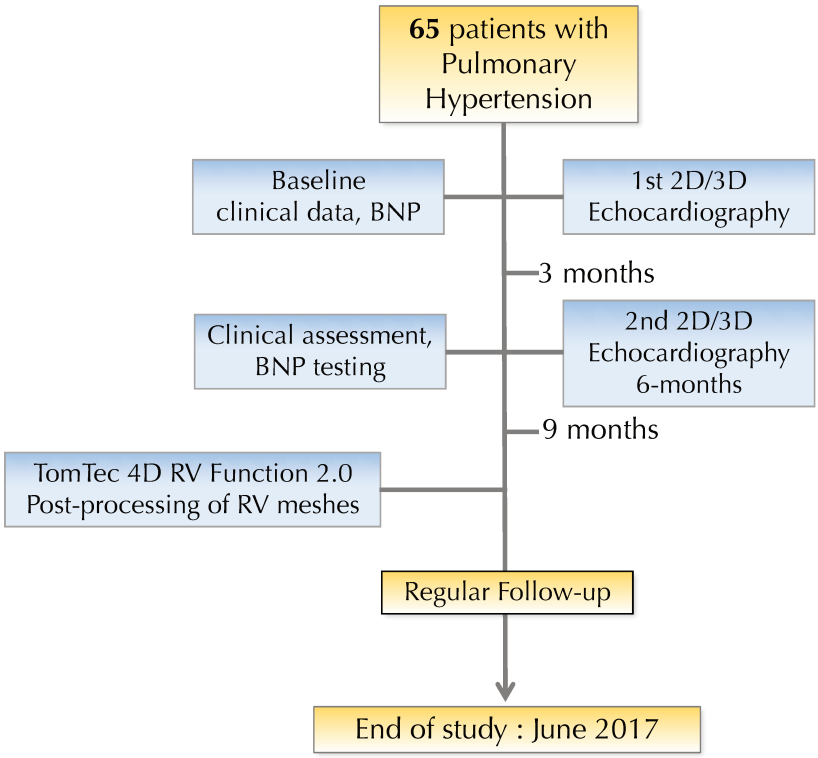

Figure 1: Study flowchart: Patients underwent regular follow-up with two different 3D ultrasound assessments: baseline and at 6 months (between 3 et 9 months from baseline)

Data collection during follow-up

Patient follow-up consisted of consecutive evaluations on a regular time basis of at least 6 months. At every visit, clinical and biochemical characteristics were evaluated. The second assessment with transthoracic 2D and 3D echocardiography was scheduled after 6 months. The most recent evaluation was taken as the final visit.

2D-echocardiographic acquisitions and measurements

We performed a 2D echocardiographic examination using an IE-33 or EPIQ-7 ultrasound system and an X5-1 transducer (Philips Medical system, Andover, MA). It included Doppler echocardiography complying with the recommendations of the American Society of Echocardiography (ASE) / European Association for Cardiovascular Imaging (EACVI) (169, 170). The following parameters were measured and averaged over three consecutive cycles: left ventricular ejection fraction, right atrial area, tricuspid annular peak systolic velocity (s'), myocardial acceleration during isovolumic contraction

(IVA)(49), tricuspid annular plane systolic excursion (TAPSE), systolic pulmonary artery pressure (derived from the tricuspid valve regurgitation), right ventricular outflow tract (RVOT) velocity-time integral (VTI) and right atrial pressure estimated on the basis of IVC diameter and collapse (170).

3D trans-thoracic echocardiography

We also performed a 3D trans-thoracic echocardiographic examination using an IE-33 or EPIQ-7 ultrasound system and a matrix-array X5-1 transducer (Philips Medical system, Andover, MA). At least four 3D cine-loops of the RV were acquired from an apical 4-chamber view focused on the RV. This focused view was not a classic 4-chamber view as the probe was tilted anteriorly to focus on the entire right ventricle. Loops were stored from full-volume acquisition over 2 heart beats, which required ECG-gating over 4 cardiac cycles during a quiet breath-hold. To allow post-processing with dedicated software, care was taken to maximize the frame rate ($\geq$ 20 frames per second) and to include the entire RV within the images.

3D deformation analysis

Offline analysis was performed via commercial software dedicated to the RV (4D RV Function 2.0, TomTec Imaging Systems GmbH, DE). This software tracked the RV endocardial surface along the cardiac cycle using 3D speckle-tracking, which can be exported for post-processing. It also directly estimated the RV end-diastolic, end-systolic volumes and ejection fraction (157, 164). Trabeculations and papillary muscles were included as part of the RV cavity, as recommended (169). Examples of RV cavity delineation with the dedicated software are available in our previously published article (132).

The exported meshes were analysed at each point of the RV endocardium and at each instant of the cycle using VTK (v 7.10, Kitware, New York, US), and Matlab (v.R2011a, MathWorks, Natick, US), as previously validated in an electromechanical model and in a large series of patients (147). Deformation was computed as the *engineering strain* ---the relative change of length--- within a 5mm neighbourhood along

the circumferential and longitudinal directions, and as the *area strain* ---the area change of each mesh triangle. Due to the availability of endocardial surfaces only, radial strain was not computed. Mesh correspondences were obtained from the commercial software. They were used to compare the data from different subjects and acquisitions both globally and regionally according to conventional RV regions definition (13). For the purpose of this study, peak systolic strain was analysed.

Statistical analysis

Continuous variables are shown as mean ± standard deviation in case of normal distribution or median [95% confidence interval] if not. Categorical variables are shown as number of subjects (%). Changes between baseline and the 2nd assessment were expressed as a percentage of baseline value. Inter-group differences (paired data) between continuous variables were assessed by the Student's t-test or the Wilcoxon test depending if the variables were normally distributed or not, and the Fisher's exact test for categorical variables. Bonferroni correction was used for multiple comparisons. Multiple regression and the associated variance inflation factor were used to test multicollinearity between several variables. The relationship between echocardiographic parameters and survival was assessed through univariate and multivariate Cox proportional hazard regression, starting at the date of echocardiography. The date of the second assessment was used as starting date for Cox analysis when analysing the association between changes in the patients' status and clinical outcomes. Multivariate survival analysis included all variables with a p-value <0.10 in the univariate analysis and the previously described prognostic parameters (WHO functional class, BNP, 6-minute walking distance and PH-targeted advanced therapy). Patients were labelled as "*worsening*" if they presented one of the following outcomes: need to start advanced therapy targeting the PGI2 pathway, hospitalization related to PH complication during the follow-up, lung transplant or death. They were labelled as "*improving*" if they experienced on the last follow-up visit a decrease in the WHO class and either showed a >10% increase of their 6-minute walking distance or a >10% decrease in their BNP level (171, 172). Other patients were labelled as "*stable*". The optimal cut-off values to predict survival were

obtained from receiver operating characteristics curves. ROC curves were compared using the DeLong, *et al*. (173) method. Test–retest variability consisted of intra- and inter-operator comparisons as well as inter-loop strain comparisons, and included intra-class correlation coefficients. For all analyses, a p-value of <0.05 was considered statistically significant. Statistical analyses were performed using MedCalc 17.5.5 (MedCalc Software, Mariakerke, BE).

RESULTS

Overall, 116 patients with pulmonary hypertension were screened for this study. Over those, 31 were excluded because the study clinical outcome occurred before the second assessment; 18 because their second 3D ultrasound assessment fell outside the allowed study period (<3months or >9 months) and 2 because of lost to follow-up. Finally, 65 patients with pulmonary hypertension were included in our study and followed over a median of 24.8 [22.1-25.7] months.

General characteristics of the population

The main characteristics of our population are presented in Table 1. Mean age at inclusion was 57.8 ± 18.7 years old, 40 of them were female (61.5%). It consisted of 48 patients (74%) suffering from group 1 PAH: 13 had PAH associated with connective tissue disease, 12 had idiopathic PAH, 10 had PAH associated with congenital heart disease, 7 had PAH associated with portal hypertension, 4 had drug-induced PAH and 2 had HIV-associated PAH. Among the remaining 17 patients (26%), 10 patients had group 3 PH and 7 had group 4 PH. Sixty patients (92.3%) were treated with advanced PH therapy at baseline: 8 with triple combination therapy (endothelin receptor antagonist + PDE5 inhibitor + prostacyclin), 19 with dual combination therapy (endothelin receptor antagonist + PDE5 inhibitor) and 33 with single oral PH therapy (18 patients were treated with endothelin receptor antagonists, 13 with PDE5 inhibitors and 2 patients with riociguat). Multiple regression indicates that baseline area strain is significantly related to RV EF ($p<0.001$). The variance inflation factor is 1 between those 2 variables, excluding high multicollinearity. Variability was previously assessed using intra-class correlation coefficients (132) : inter-observer variability was 0.90 [0.77–0.96] for RV EF; intra-observer variability was 0.95 [0.88–0.98] for RV EF and 0.93 [0.83–0.97] for RV global AS; inter-loop variability was 0.94 [0.86–0.98] for RV EF and 0.94 [0.86–0.98] for RV global AS.

	Baseline	Second assessment	p-value
WHO class ≥ III, n(%)	39 (60%)	34 (52%)	0.50
BNP, pg/mL	148.0[96.4-231.6]	111.5[91.4-148.1]	0.26
6MWD, m	374.7±92.9	363.8±118.9	0.83
3D RV EF, %	34.6±8.7	36.3±10.7	0.13
RV EDV, mL	88.3[72.1-106.0]	95.2[85.1-109.9]	**0.01**
Global RV area strain, %	-13.2±6.1	-14.0±7.1	0.27
Global RV circumferential strain, %	-11.5[-13.2- -10.6]	-12.5[-13.5- -10.8]	0.38
Global RV longitudinal strain, %	-8.1[-9.4- -7.0]	-9.1[-10.4- -7.8]	0.11
TAPSE, mm	20.4±5.1	18.9±4.9	0.08
TV s', cm/s	11.2±2.9	11.3±2.8	0.38
IVA, m/s²	2.0[1.7-2.3]	2.1[1.8-2.3]	0.86
RA pressure, mmHg	10.3±3.8	10.5±4.9	0.80
RA surface, cm²	23.5[21.1-24.8]	23.3[21.1-27.0]	0.39
RVOT VTI, cm	15.0±4.8	15.5±4.5	0.18
LV EF, %	67.4±8.3	67.1±7.9	0.85
RV-RA gradient, mmHg	76.0[70.0-90.2]	74.0[67.2-83.2]	0.11
Pericardial effusion, n (%)	10 (15%)	11 (17%)	0.93

6MWD, 6-minute walking distance; WHO, world health organization; BNP, brain natriuretic peptide; EDV, end-diastolic volume; EF, ejection fraction; IVA, myocardial acceleration during isovolumic contraction; LV, left ventricular; RA, right atrial; RV, right ventricular; RVOT, right ventricular outflow tract; TV, tricuspid valve; VTI, velocity-time integral

Table 1: Main characteristics of our population at baseline and at 6 months (second assessment)

Patients' evolution

At follow-up, 15 patients died from PH and 1 patient underwent lung transplant. Compared to baseline, 28 patients were considered *stable*, 10 patients had *improved* their clinical condition and 27 patients had *worsened* and were hospitalized because of right heart failure or needed to start therapies targeting the PGI2 pathway. Twenty-three patients (35.4%) required an uptitration or escalation of their oral advanced therapy. Median delay between baseline (first 3D echocardiography) and the second 3D assessment was 6 [5.6-6.3] months. Patients who were considered stable or improving

were more likely to present at 6-months a significant increase in 3D RVEF (p=0.04) and a decrease in RV global area strain as well as circumferential and longitudinal strain (p=0.001, 0.01 and 0.001, respectively). In contrast, no significant change in TAPSE or RA surface was observed (p=0.85 and 0.35, respectively).

Table 2. Changes in patients' characteristics at 6-months according to the vital status of the patient

6-months change in	Survivors without transplant n=49	Death or Transplant n=16	p-value
BNP, pg/mL	-80.2± 223.5	+166.4±398.2	**0.006**
3D RV EF, %	+3.9±7.2	-4.8±11.2	**0.02**
% from E1	+13.0±26.0	-10.0±29.3	**0.04**
3D RV EDV, mL	+8.3±31.6	+19.3±48.6	**0.03**
Global RV area strain, %	-2.6±5.4	4.1±8.2	**0.03**
% from E1	+15.3±30.6	-16.2±36.5	**0.001**
Global RV circumferential strain, %	-0.97±3.2	+2.6±5.9	**0.003**
% from E1	+12.1±36.8	-9.7±50.0	0.07
Global RV longitudinal strain, %	-1.7±3.8	+1.7±4.2	**0.004**
% from E1	+29.4±61.3	-14.6±52.1	**0.01**
TAPSE, mm	-1.2±7.2	-1.9±4.9	0.72
RA surface	-0.74±7.8	-0.49±8.8	0.92

BNP, brain natriuretic peptide; E1, 1st echocardiographic assessment at baseline; EDV, end-diastolic volume; EF, ejection fraction; RV, right ventricular

Figure 2 illustrates the evolution of RV global area strain in each patients' group.

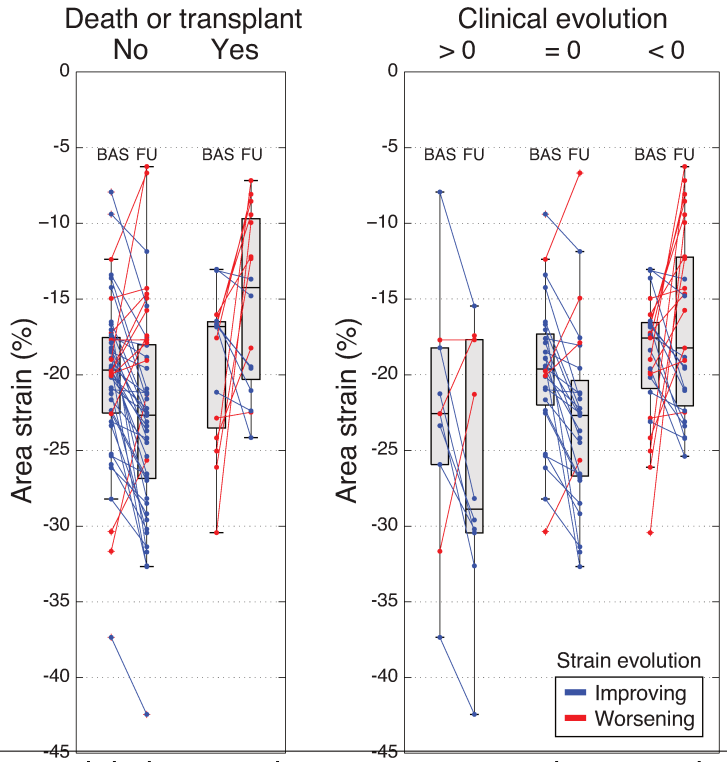

Figure 2 : RV global AS evolution over 6 months, according to the clinical evolution (improving >0, stable =0 or worsening <0). Red and blue colors stand for patients with worsening and stable or improving RV global AS. BAS, baseline; FU follow-up.

Improvements in the global area strain were associated with stable or improving clinical condition as well as survival. Differences in the spatial distribution of strain patterns were also observed between groups. These may be hard to assess at a single stage (baseline, for example no significant difference in baseline global RV AS, p=0.27 according to the survival groups) but are emphasized when displaying evolutions from baseline to follow-up (Figure 3). The highest changes occurred within the inlet (p=0.001), the trabecular septum (p<0.001), and the RV inferior wall (p=0.001). Patients who will survive free from transplant present no significant difference in baseline global AS, as compared with others (p=0.27), but clearly better AS on follow-up (-22.7[-24.4- -21.2] vs -14.2[-20.1 - -9.8], p=0.0004). The same pattern is observed when studying patients who will remain stable or clinically improve: no significant difference in baseline AS was observed (p=0.12) but they have significant better AS on follow-up (-23.2[-26.7 - -21.4] vs -18.2[-20.9 - -13.6]; p=0.0001).

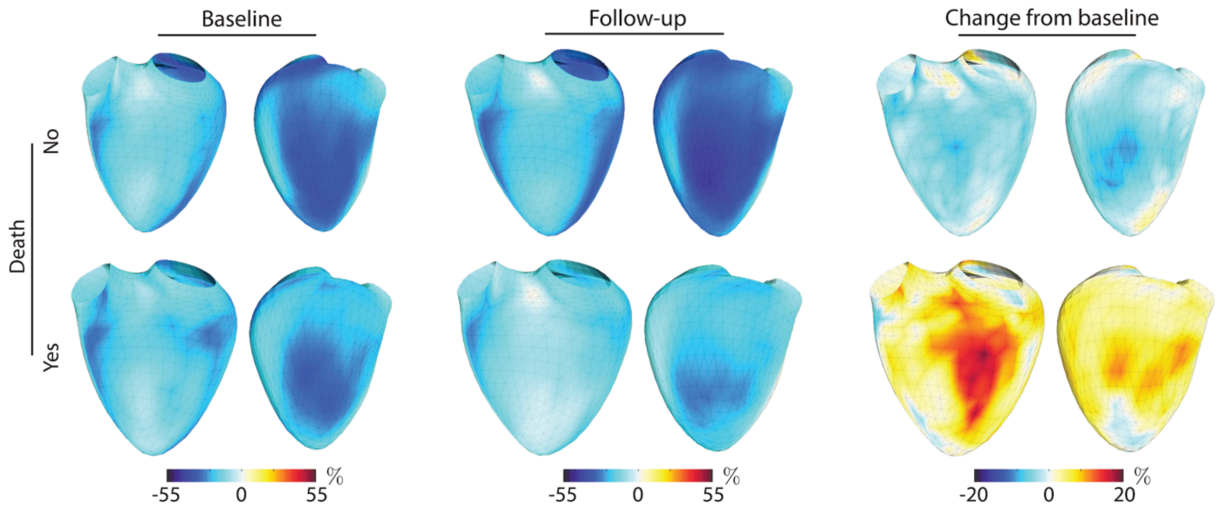

Figure 3: Mean pattern of RV AS at baseline and 6-months follow-up represented over the mean RV shape of the subgroups (according to the vital status). On the RV patterns represented in "Change from baseline", yellow to red represent an increase (deterioration) in AS, whereas blue indicates a decrease in AS (improvement). Red pattern (the most severe) is only observed in deceased patients. Important changes predominate in the septal area.

Outcome analysis

At baseline, right atrial pressure (HR 1.22[1.06-1.40], p=0.005), Class IV WHO (HR 3.0[1.0-8.7], p=0.05), LVEF (HR 1.08[1.02-1.14], p=0.01) and RVOT VTI (HR 0.87[0.77-0.97], p=0.03) were univariate predictors of survival free from transplant. On univariate survival COX analysis, global RV area strain at baseline was not a predictor of survival or transplant, unlike the inlet septum area strain (HR 0.93[0.86-0.99], p=0.04). Using follow-up data, regional changes in the area strain were predictors of survival, as observed for the inlet septum (HR 1.07[1.03-1.12], p=0.002), the RV inferior wall (HR 1.13[1.06-1.20], p=0.0002) and the trabecular septum (HR 1.10[1.04-1.17], p=0.001). Global changes were also predictors of survival, as observed for the area strain (HR 1.13[1.06-1.20], p=0.0003), the circumferential (HR 1.19[1.06-1.34], p=0.003) and longitudinal strain (HR 1.19[1.07-1.33], p=0.002) and the 3D RVEF (HR 0.97 [0.96-0.99], p=0.005), WHO class (HR 3.5[1.6-7.6], p=0.002) and BNP (HR 1.003[1.001-1.004], p=0.001. Changes in RV global area strain over 6 months were also predictor of

clinical worsening (HR 1.11[1.05-1.17], p=0.0002), unlike RV global area strain at baseline.

On multivariate COX analysis, changes in WHO class (HR 17.4[5.2-58.5]), BNP (HR 1.003[1.001-1.004]), RV global area strain (HR 1.12[1.03-1.21]) and RV septal area strain (HR 1.14 [1.03-1.25]) were independent predictors of survival.

ROC curves identified that a decrease in 24% or more of the initial RV global area strain predicted poor outcome (death or transplant) and corresponded to 50% sensitivity and 92% specificity (AUC 0.733[0.609 to 0.836]). A decrease <0.8% or an increase in RV septum area strain identified high risk patients (AUC 0.810[0.694-0.897]).

Composite score

Based on these observations, we built a composite score from the predictors of outcomes identified on the multivariate Cox analysis. One point was attributed to each of the following parameter changes over the initial 6 months' period: increase in WHO functional class; increase in BNP plasmatic levels (≥100 ng/mL) and decrease in ≥24% RV area strain. Changes in RV global area strain over 6-months significantly increase the predictive value as compared to the changes in WHO from baseline (AUC 0.781[0.661-0.874] compared with 0.657[0.529-0.770]; p=0.04). Changes in BNP also tend to increase the predictive value of changes in WHO alone (AUC 0.739[0.615-0.840], p=0.14). The predictive value of the composite score including changes in WHO class, changes in RV global area strain and BNP (AUC 0.816[0.700-0.901]) increases significantly compared to changes in functional class alone (p=0.01) and also increases the predictive value over changes in WHO class and BNP (AUC 0.739[0.615-0.840], p=0.10) (Figure 4).

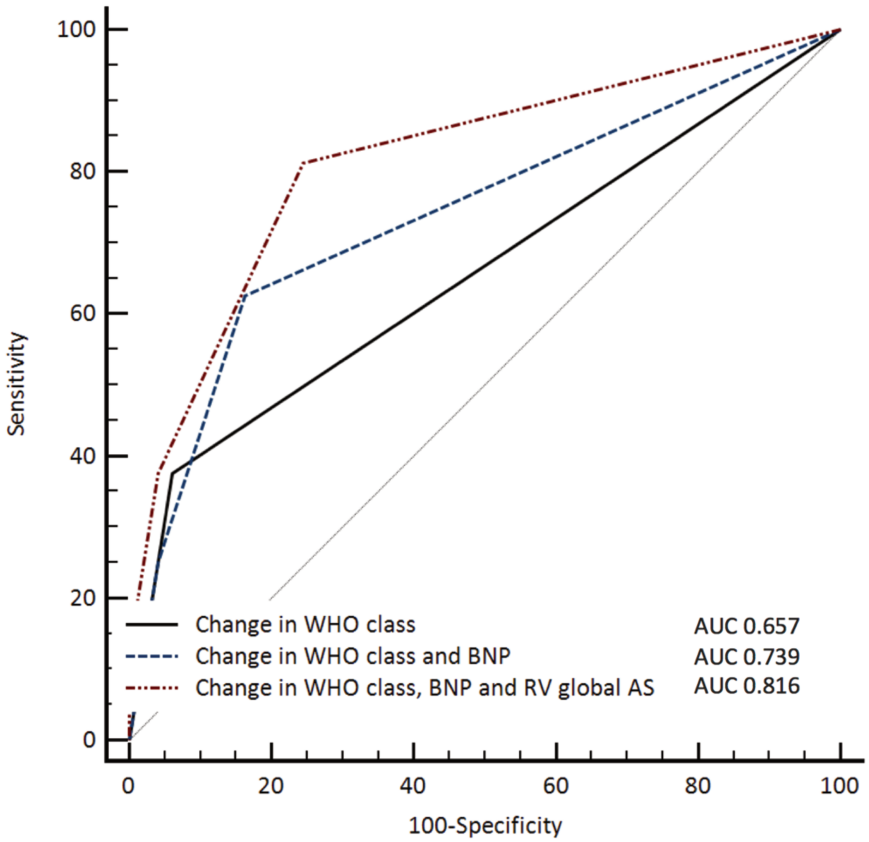

Figure 4: ROC curves for survival free from transplant in PH. AUC of different scores are presented: changes in WHO class, WHO class + BNP or WHO class + BNP + RV global AS are presented. The addition of echocardiographic data increases the AUC.

A score ≥1 identifies a very high-risk population with a 9-fold increased risk of death or transplantation (HR 9.1[2.6-32.2]) (Figure 5). As the AUC of the score including septal AS was similar to the one with RV global AS, we choose to present the results with RV global AS (AUC (0.816[0.700-0.901] vs 0.823[0.709-0.907]; p=0.82).

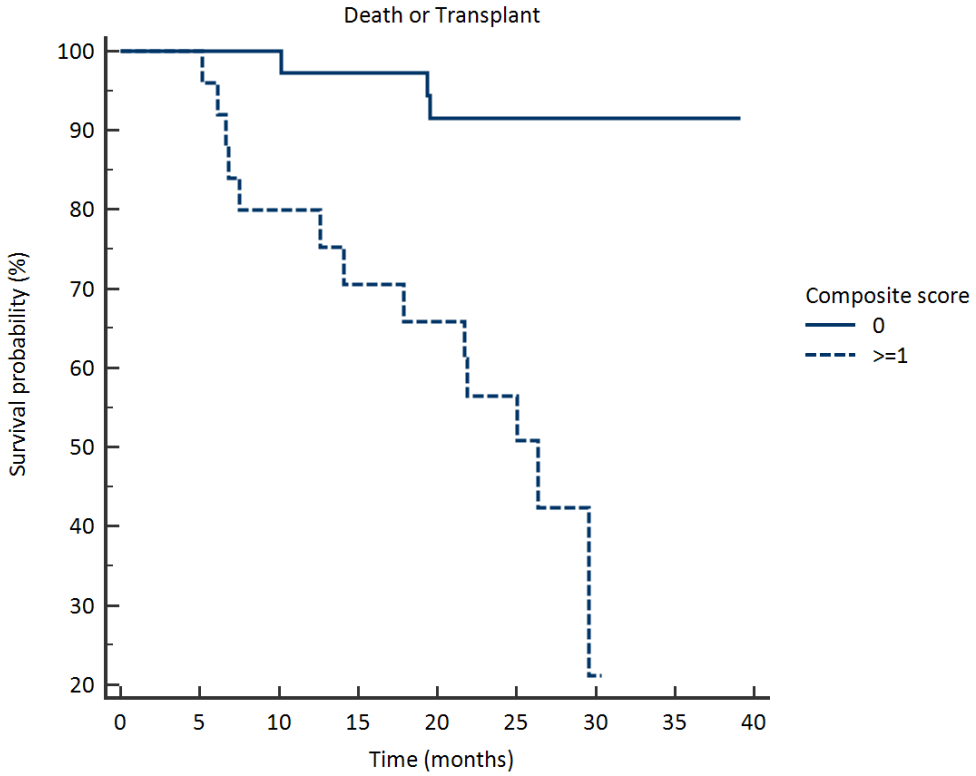

Figure 5: Kaplan-Meier curves illustrating the difference between patients with a score =0 or a score ≥1 with a 9-fold increased mortality risk.

DISCUSSION

To our knowledge, this is the first study designed to interpret the prognosis value of changes in functional class, BNP and RV deformation and function in PH patients. Individual and regional changes in RV deformation are highly related with clinical outcome. Our study also proposes a simple composite score including dynamic changes in WHO function class, BNP and 3D RV AS to identify very high-risk patients with a 9-fold increased risk of death or transplantation. Echocardiographic changes in RV deformation provide independent prognostic information and add a significant positive value to changes in WHO functional class and in BNP levels.

Dynamic parameters instead of baseline assessment

Baseline RV deformation and function in our cohort were not significant predictors of outcomes unlike AS changes over 6-months. This result underlines the importance of dynamic assessment combined with baseline data. Nonetheless, we previously identified in a larger population, baseline RV AS as a predictor of outcome, meaning that 6-months AS changes provides an even more significant information regarding RV changes with pressure overload. In our study, no significant difference in baseline AS was found between our patients' groups (survival or clinical evolution), whereas we found significant differences in follow-up global AS. In order to increase the comparability of our population and better assess the risk, in our view, an assessment of RV function evolution is preferable over a single assessment. Previous studies already underlined the need for a dynamic assessment in PH patients. A worsening saturation in exercise capacity predicted clinical deterioration in patients with Eisenmenger syndrome (174). Recently a post-hoc analysis of PATENT-2 found that changes in WHO functional class and NT-pro BNP at 12 weeks were associated with clinical worsening-free survival, but not with survival (175). Our study differs in terms of rate of events (24.6%) and population, as patients with various PH aetiologies without any age limitation were included. An increase in pulmonary arterial capacitance over time (assessed by right heart catheterization) has been associated with decreased mortality (176). Changes in

pulmonary arterial capacitance and RV deformation (affected by PA compliance and capacitance) could represent, in association with changes in WHO and BNP, a more advanced evaluation strategy for PAH therapies.

Risk assessment

Currently, guidelines recommend in the "goal-oriented therapy" approach to assess patients for the presence of pericardial effusion and to monitor the right atrial area. In our study, given the relatively low number of patients, baseline pericardial effusion and changes in the right atrial area were not predictors of outcomes (HR 2.7 [0.95-7.9]; p=0.06 and 0.98 [0.91-1.06]; p=0.68, respectively). In fact, RA remodelling in terms of size reduction probably occurs at a slower rate compared to changes in RV deformation. This could therefore be expected at 6-months follow-up. The faster rate of changes in RV deformation may come from the higher sensitivity of the RV to advanced PH therapies-induced modifications. We therefore believe on the potential of RV area strain changes to assess the response to therapy in PH.

Beyond underlining the importance of RV functional assessment in PH patients, our study also suggests the importance of multi-modality assessment. Even if the prognostic value of baseline WHO class and changes in WHO class are important, their predictive value is only improved when adding change in BNP and change in RV deformation to the prognostic score. Simple cut-offs have been used: the reduction of >24% in RV global AS and the increase in BNP. Such factors could allow physicians to improve disease severity classification and identify whether a patient is deteriorating on treatment and escalate therapy if needed.

Three-dimensional RV assessment

Substantial changes in patients with poor outcomes occur in the inferior wall and mostly in the septum, in particular the inlet and trabecular septum. These regions are actually associated to subgroup differences in RV deformation. They undergo pressure overload and the septum deformation is affected by RV-LV interactions. We already know that LV parameters such as eccentricity index and LV strain (134, 177, 178) are of

prognostic importance in PAH. Given the LV-RV interactions, the observations along the RV septum AS are therefore not surprising in our cohort of PH patients. A recent study investigating rat models of RV pressure overload concluded that altered geometry and wall stress lead to adverse RV-LV interactions through the septal hinge-points and fibrosis (179). This fibrosis might explain the sensitivity of changes in RV septal AS for the detection of high-risk patients. RV septum AS and more generally global RV AS might be earlier markers of severity. Changes in these factors seem to be even more determinant than baseline parameters, allowing personalized patients' assessment.

Limitations

This was a single centre prospective study with a relatively limited number of patients. Mean RV end-diastolic volume in our population can be considered normal, however, from previous studies, we know that 3D echo tends to underestimate volumes as compared to cardiac magnetic resonance (180). This limited number of patients prevented us from confirming the prognostic role of global RV AS at baseline, however it was sufficient to confirm our hypothesis regarding the role of RV deformation changes over time. The mortality or transplant rate in our study was 24.6%, which is quite high and can be explained by the mean age and severity of our population, 60% of patients being class III WHO or more at baseline. We have chosen to divide our patients' population in three different subgroups according to the clinical evolution. This can be criticized, but whether a stable patient who is not improving despite advanced PH therapy can be classified as improving or deteriorating is a challenging question. Complementary insights are given in the Supplementary Material using clinical evolution subgroups. Given our results, the clinical subgroups "improving" and "stable" are quite similar compared to the "worsening" group.

In summary, our study demonstrates the incremental prognosis value of following changes in RV function as assessed by 3D echocardiography. The most significant changes occur in septal segments. A composite score including changes in WHO function class, BNP and RV global AS identifies a high-risk population with increased mortality. This simple score could be helpful to guide advanced therapy uptitration or escalation.

DATA SUPPLEMENTS

Expanded results:

Additional Figure: RV area strain evolution according to the patients' clinical evolution

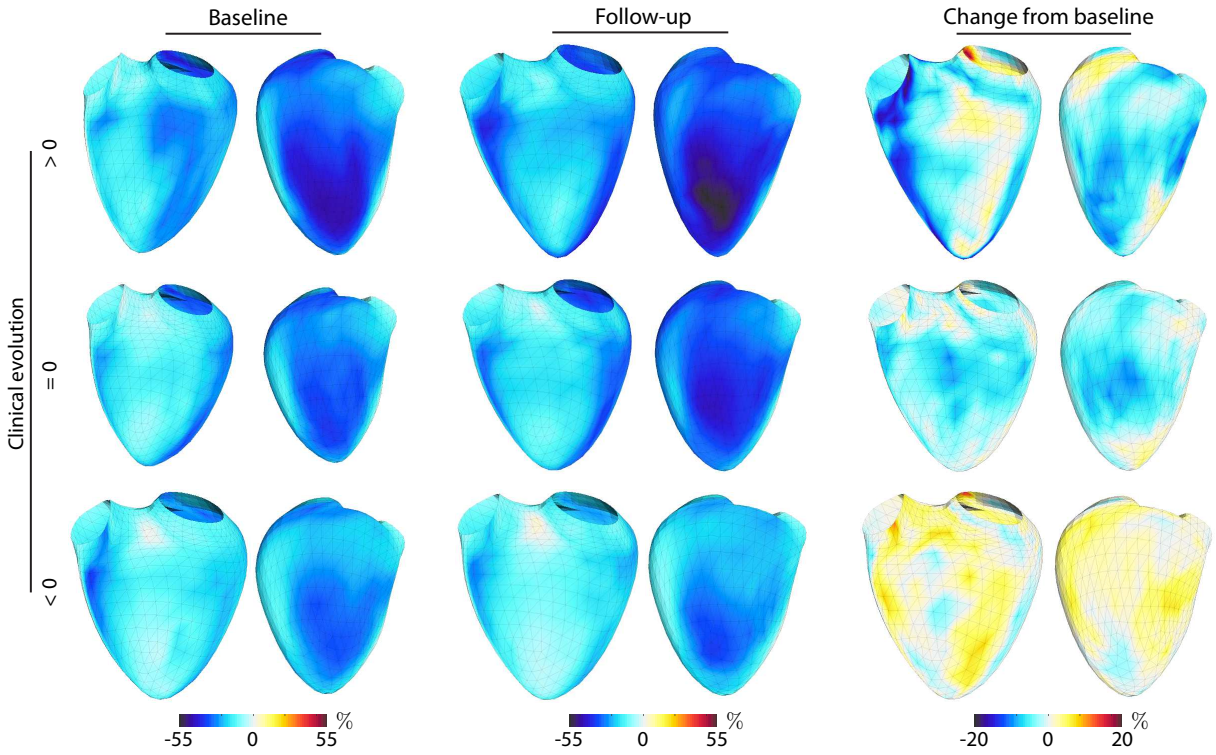

Mean pattern of RV area strain (AS) at baseline and 6-months follow-up represented over the subgroup average shape (subgroups according to the clinical evolution, improving >0, stable =0 or worsening <0). Yellow and red represent an increase (deterioration) in AS, whereas blue indicates a decrease in AS (improvement).

Additional Table: Changes in patients' characteristics at 6-months according to the patients' clinical evolution

	Clinical Evolution			p-value
6-months Change in	**Worsening**	**Stable**	**Improvement**	
BNP, pg/mL	+91.4±337.9	-47.3±146.6	-228.6±367.1	**0.02**
3D RV EF, %	-1.7±10.7	+4.11±6.4	+4.3±8.7	**0.04**
% from E1	-1.4±30.7%	+12.7±24.4%	+15.8±29.1%	0.1
3D RV EDV, mL	+10.7±46.1	+16.4±25.0	-3.3±32.9	0.35
Global RV area strain, %	+2.4±7.4	-3.1±4.6	-3.7±6.9	**0.003**
% from E1	-8.6±35.2	+17.3±26.9	+23.8±37.9	**0.004**
Global RV circumferential strain, %	+1.5±5.1	-1.1±2.8	-1.5±4.3	**0.04**
% from E1	-4.9±42.5	+11.3±26.6	+25.4±61.9	0.10
Global RV longitudinal strain, %	+1.1±3.9	-2.2±3.7	-2.2±4.4	**0.005**
% from E1	-9.0±48.8	+39.6±63.8	+34.3±64.6	**0.008**
TAPSE, mm	-1.4±5.1	-1.0±6.8	-2.5±10.7	0.85
RA surface	-0.5±7.5	+0.3±6.9	-4.4±12.1	0.35

CHAPTER 4.
SHAPE AND STRAIN STUDY IN CONGENITAL HEART DISEASE PATIENTS

Comparative Analysis of shape and strain in Tetralogy of Fallot and Atrial Septal Defect

CONTENTS

ABSTRACT

Background: Right ventricular (RV) function assessment is crucial in congenital heart disease (CHD) patients, especially in atrial septal defect (ASD) and Tetralogy of Fallot (TOF) patients. Indeed, prognosis substantially differs between TOF and ASD patients and only little is known about 3D deformation and shape changes in RV overload. The aim of our study was to assess RV remodeling differences between ASD, TOF patients and controls.

Methods: We prospectively included 55 patients into this prospective case-control study. We included 19 patients with an ASD (4 of them had PAH, 10 had large defects and 5 had small defects), 15 with TOF (8 had severe pulmonary regurgitation) who were older than 16 years old and 21 subjects who were free from any cardiovascular disease into a control group. 3D transthoracic RV echocardiographic sequences were acquired. Myocardial tracking was performed by a semi-automatic software. Output RV meshes included spatial correspondences. They were post-processed to align the data temporally and extract local deformation. Global and local statistics provided deformation and shape patterns for each subgroup of subjects.

Results: No difference was found between ASD patients and controls in terms of RV area strain, longitudinal or circumferential strain. There was a trend toward increased longitudinal strain in patients with small ASD whereas patients with PAH associated with ASD had lower longitudinal strain. TOF patients had lower RV area and longitudinal strain, especially in the inferior, lateral wall and in the trabecular septum. There was almost no difference in circumferential strain, except that it was lower in the lateral wall and the trabecular septum. TOF patients had predominant circumferential over longitudinal strain. Using curvature indices, differences in RV shape are highlighted between controls and RV volume overload patients whereas there was almost no difference between ASD and TOF patients regarding RV shape, except at the septum. In the whole population, QRS duration has been significantly correlated with RV end-diastolic volume and RV area strain. In TOF patients, a strong correlation exists between the RV inferior wall curvature and QRS duration ($r=0.85$, $p=0.0001$).

Conclusion: Volume overload alters RV shape to the same extent in ASD and TOF whereas it has differential effects on strain. In ASD patients the strain is relatively preserved whereas TOF patients had particularly impaired longitudinal strain. These data could help understanding RV remodeling in congenital heart disease.

INTRODUCTION

Right ventricular (RV) function evaluation is of utmost importance in congenital heart disease (CHD) (74, 135). Indeed, volume overload; frequently observed in CHD; leads to right ventricular (RV) remodeling in terms of RV shape and function (69). RV remodeling affects the patient's prognosis, especially in congenital heart disease patients (181). Knowledge about the left ventricular adaptation to afterload stress is already available, however, the RV is very different from the left ventricle, even from an embryologic point of view (182). Differences begin early during the fetal stage and right heart failure differs from left heart failure (183), even in terms of response to therapy (beta-blockers for example might not be as beneficial in patients with right heart failure as it is in left ventricular systolic dysfunction (184)). While only little is known about RV response to afterload changes, it is a crucial problem in CHD. Atrial septal defect (ASD) with left to right shunting is an example of long standing RV volume overload, generally well tolerated for years. On another hand, tetralogy of Fallot (TOF) patients usually develop RV dilatation and dysfunction earlier because of chronic pulmonary regurgitation, a classic and likely systematic complication after surgical correction of TOF.

Hence, in this study, we aimed to investigate the differential effects of RV volume overload on myocardial mechanics in ASD and TOF patients as compared to a control group and give an insight into RV remodeling in these 2 models of chronic RV volume overload.

Pathophysiology of ASD and TOF

ASD are the third most common type of congenital heart disease (185). Anatomic positions of the different atrial septal defects are presented on the following figure. Secundum ASD represents the most frequent form of ASDs (Figure 1).

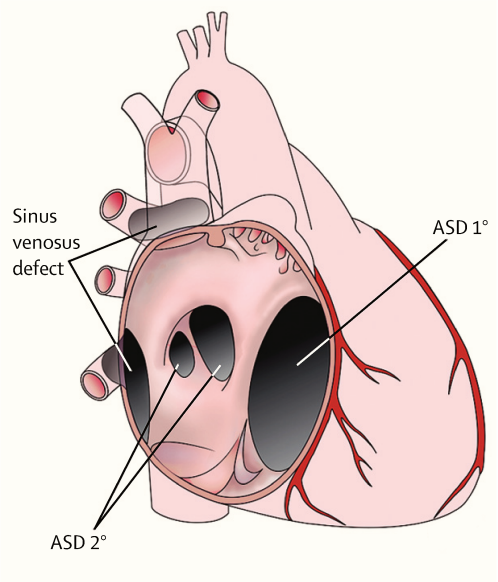

Figure 1 : Anatomy of ASD (186)

Most ASD are sporadic but some have been linked to genetic mutations or have been encountered in genetic syndromes (187, 188). ASD is responsible for a left-to-right shunt at the atrial level. Therefore, if the shunt is significant, it will lead to volume overload of the right heart with dilated right atrium, RV and pulmonary arteries. Usually symptoms will occur in the second decade of life (186). The most frequent symptoms are shortness of breath with exertion, palpitations, fatigue, exercise intolerance. Paradoxical embolism can also be a discovery mode. Hemodynamically significant ASD should be closed (189, 190).

Tetralogy of Fallot is the most frequent cyanotic congenital heart disease. It is a cono-truncal defect, the main underlying pathophysiology being an anterior malalignment of the infundibular septum. This malalignment is responsible for a tetrad of abnormalities : ventricular septal defect, dextroposition of the aorta, right ventricular outflow tract obstruction) and RV hypertrophy (191). Figure 2 illustrates the classic form of Tetralogy of Fallot (adapted from Medscape https://emedicine.medscape.com/article/2035949).

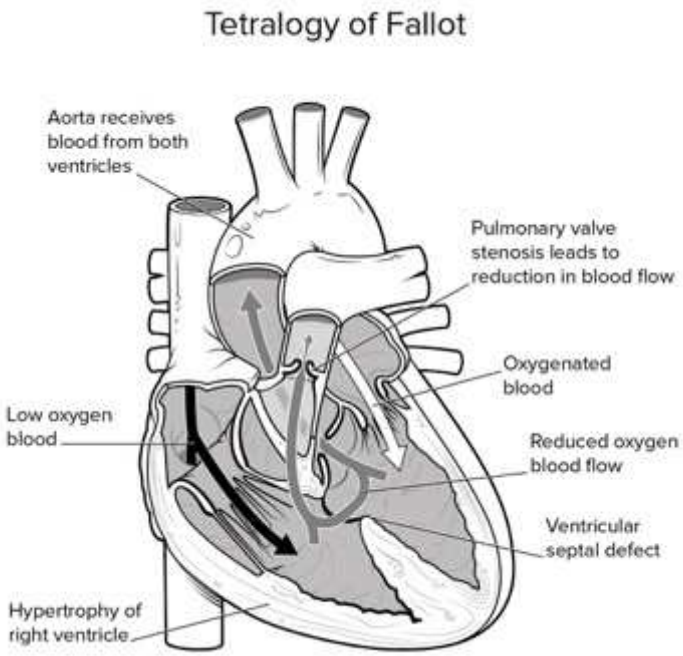

Figure 2:

Description of TOF

The mortality is very low in the present era, with excellent long-term survival and quality of life. Given the excellent prognosis, there is currently more adults than children with tetralogy of Fallot (192, 193). Tetralogy of Fallot is a cyanotic disease, because there is a right-to-left shunt at the level of the ventricular septal defect given the increased right ventricular pressure (secondary to right ventricular outflow and pulmonary stenosis). First, before the advent of complete correction, Helen Taussig and Alfred Blalock performed the first palliative shunt in a TOF child in 1944. They created the Blalock-Taussig shunt between the subclavian artery and the pulmonary artery in order to increase the pulmonary blood flow. The first open heart surgical correction has been performed in 1954 by Scott (194). Nowadays, the ideal treatment plan is to wait a few months (for growth) to realize the complete corrective surgery or, in case it's needed before corrective surgery is feasible (mostly very low weight for example, abnormal coronary artery, multiples ventricular septal defects, very small pulmonary arteries), to perform first a palliative shunt (to correct partially cyanosis and improve the pulmonary blood flow) then to perform the total repair. The surgeon will close the ventricular septal

defect with a patch and resect the infundibulum to relieve the right ventricular outflow tract obstruction. In the late 60's, the surgery consisted, after the age of 5 years old, in a ventricular septal defect repair with a large right ventriculotomy and extensive resection of the outflow tract and pulmonary valve that consistently led to pulmonary regurgitation, RV dilatation and dysfunction. From the 80's, repair was performed earlier in order to avoid prolonged exposure to low pulmonary blood flow and pressure and chronic cyanosis. The "optimization" of TOF repair (195) has been introduced, to preserve the right ventricle by avoiding or limiting the extent of the right ventriculotomy and trying to preserve the pulmonary valve, usually after the age of 3 months (196). The transatrial approach can be used, isolated or in combination with the trans-pulmonary approach to perform pulmonary valve commissurotomy or pulmonary artery enlargement when needed (197, 198). However, despite this approach, if there is a residual right ventricular outflow tract obstruction with RV pressure > 75% of LV pressures, usually a trans-annular patch is necessary (Figure 3), illustrating the limits of pulmonary valve sparing. The trans-annular patch technique relieves the right heart obstruction but usually leads to a free pulmonary regurgitation. This pulmonary regurgitation can cause RV volume overload.

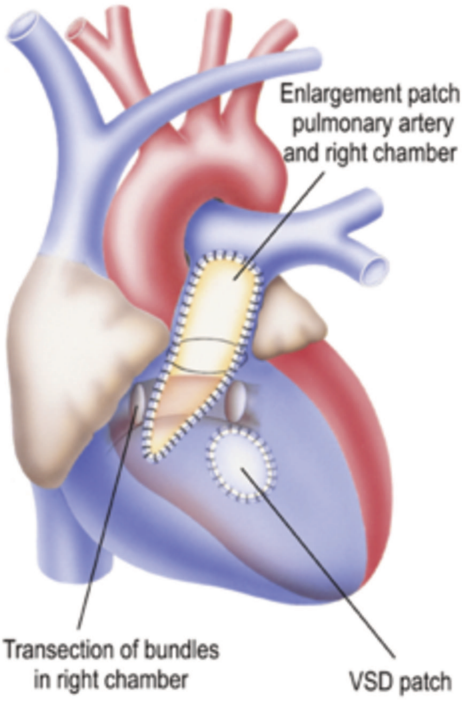

Figure 3 from http://www.dhzb.de illustrating a transannular pulmonary patch in TOF repair.

METHODS

Study design and patients

We performed a case control study on patients (adult and children > 16 years old) with ASD and TOF followed up at our centre (Pasteur University Hospital, Nice, FR) between September 2016 and September 2017. Stable patients were enrolled into a standardized echocardiographic protocol including two-dimensional (2D) and three-dimensional (3D) echocardiography. Healthy controls were enrolled to help determining normal values of 3D RV deformation imaging with our software. Our study protocol was approved by the local research Ethics committees. Personal and parental or guardian's consent were obtained and we obtained the child's assent in patients < 18 years old.

Asymptomatic healthy volunteers were recruited from the community to serve as controls and included if they had a normal trans-thoracic echocardiography, and if they were in sinus rhythm. They were matched to the study population for age and sex.

ASD patients were included if they had an open shunt. Patients were classified into 3 groups: small shunt (defect without any haemodynamic consequence according to 2D echocardiographic criteria: basal RV diameter < 41mm (199)), large shunt (significant left to right shunt) and pulmonary arterial hypertension associated with atrial septal defect (defined by a mean pulmonary artery pressure > 25mmHg according to right heart catheterization data and pulmonary vascular resistance > 8 Wood Unit/m^2).

TOF patients with significant pulmonary stenosis were excluded (max gradient across the pulmonary valve > 40mmHg). They were classified according to the presence of severe pulmonary regurgitation (PR) which was defined by a PR jet width on colour Doppler > 50% of the pulmonary annulus, a PR index < 0.77 (duration of PR/diastolic duration ratio) and / or diastolic flow Doppler reversal (72, 200, 201).

Demographics, clinical data (age, gender, diagnosis, baseline WHO class, PH-targeted advanced therapy) and BNP plasma levels (Beckman Access 2, Triage BNP assay (Biosite Diagnostics Inc, San Diego, CA)) were collected on inclusion.

2D-echocardiographic acquisitions and measurements

Echocardiographic examination was performed using an EPIQ-7 ultrasound system and an X5-1 transducer (Philips Medical system, Andover, MA). Doppler echocardiography was performed according to the recommendations of the American Society of Echocardiography (ASE) / European Association for Cardiovascular Imaging (EACVI) (44, 145, 146).

A single staff cardiologist, with advanced training in echocardiography, performed the cine-loops acquisitions and interpreted 2D-echo datasets. The measured parameters were averaged over three consecutive cycles. The following parameters were measured: left ventricular ejection fraction, right atrial area, tricuspid annular peak systolic velocity (s'), tricuspid annular plane systolic excursion (TAPSE), RV basal diameter and RV wall thickness.

3D Trans-thoracic Echocardiography

At least four 3D cine-loops of the RV were acquired from an apical 4-chamber view focused on the RV, using an IE-33 or EPIQ-7 ultrasound system and a matrix-array X5-1 transducer (Philips Medical system, Andover, MA). Full-volume acquisition over 2 heartbeats (for loop storage) was performed using ECG-gating over 4 cardiac cycles, during a quiet breath-hold if possible. Frame rate was maximized to allow the use of the RV-dedicated quantification software and follow the current quantification guidelines (frame rate > 20 Hz)(146). Care was taken to include the entire RV within the images. Digital 3D data sets were stored and analysed using commercial software dedicated to the RV (4D RV Function 2.0, TomTec Imaging Systems GmbH, DE). This software allowed tracking the RV endocardium along the cardiac cycle using 3D speckle-tracking. It directly estimated the RV end-diastolic and end-systolic volumes, ejection fraction, and wall-specific peak strain. An example of adequate RV tracking is presented below in a patient with a primum atrial septal defect.

Figure 4: Upper panel: Identification of LV/RV landmarks; Middle panel: RV endocardial tracking; final step: measured values: RV volumes and ejection fraction – export of RV meshes.

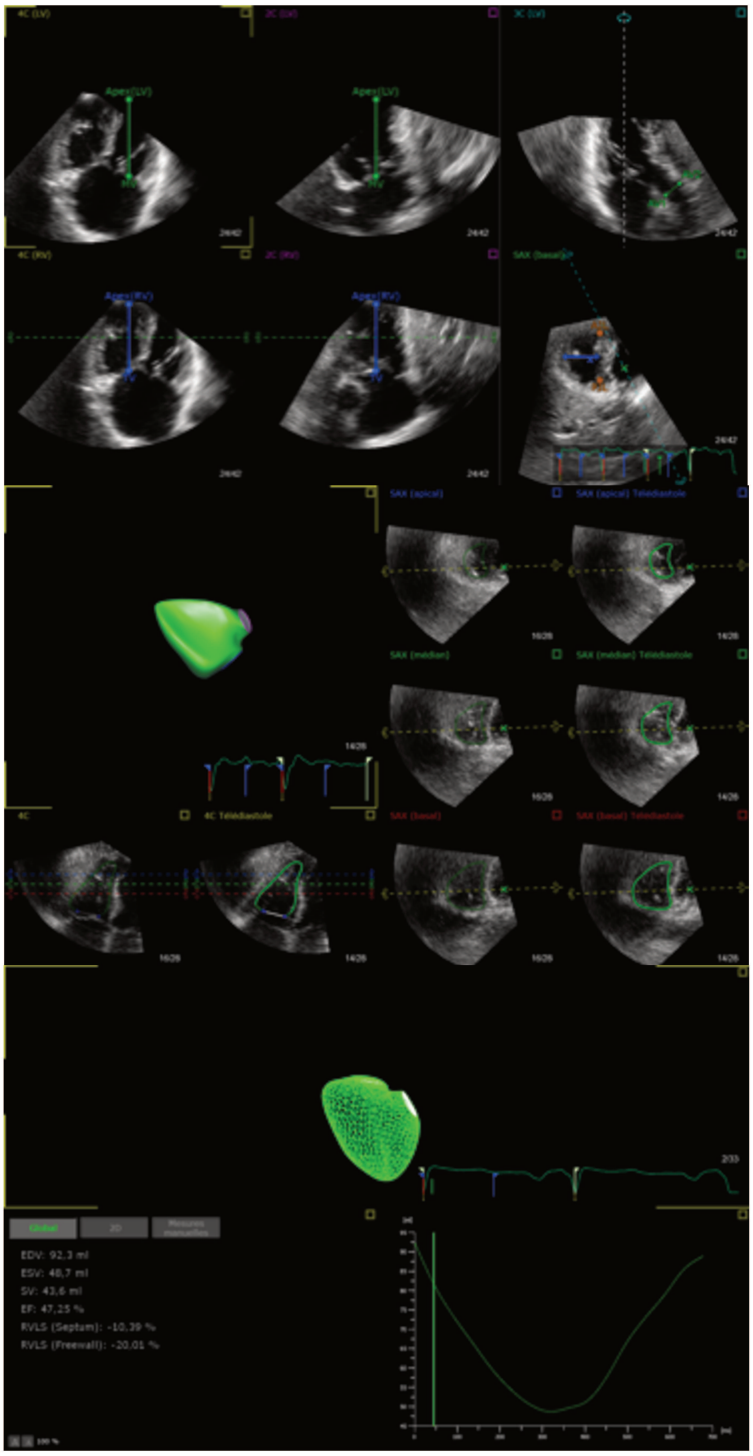

Displacement and deformation analysis

Motion and deformation were analysed at each point of the RV endocardium and at each instant of the cycle. Motion (3D displacement) was projected along the radial, circumferential and longitudinal directions. Circumferential and longitudinal strains were computed as the *engineering strain* ---the relative change of length--- along these directions, within a 5mm neighbourhood. Area strain was computed as the area change of each mesh triangle. Due to the availability of endocardial surfaces only, radial strain was not computed. We used the mesh correspondences provided by the commercial software to label the RV regions according to Haddad *et al*. (13) (Figure 5).

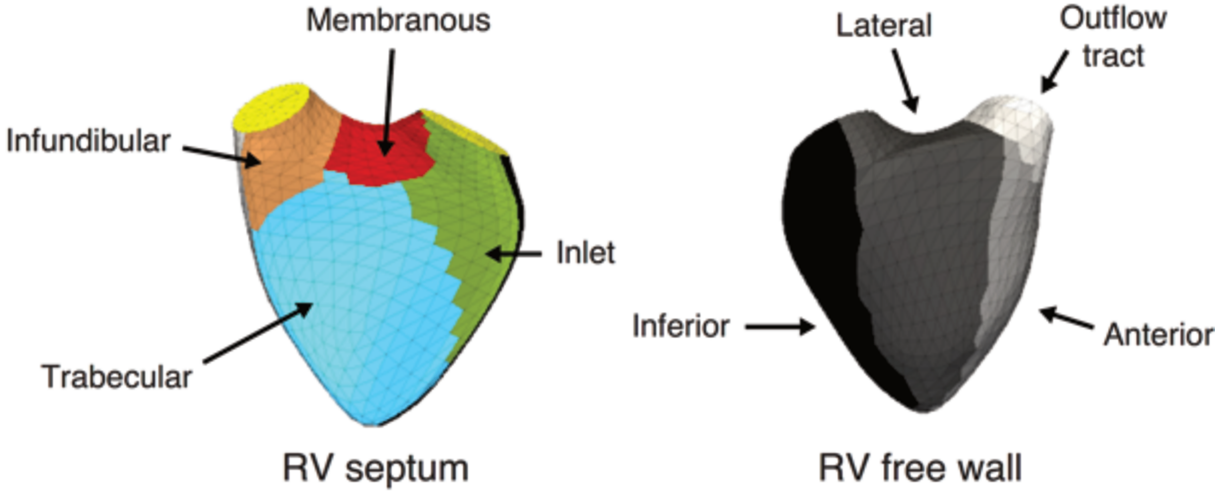

Figure 5 : RV segmentation according to (13)

These computations were done using VTK (v 7.10, Kitware, New York, US), and Matlab (v.R2011a, MathWorks, Natick, US), as previously validated in (147).

Shape analysis

After meshes were obtained, we carried out shape modelling for each RV from the database. The curvature was computed at end-diastole (given the strong interaction of contraction with the shape at end-systole). The mean curvature was obtained using the Computational Geometry Algorithms Library (CGAL 4.11, Inria, FR) (202-204). We chose a neighbourhood of 2 rings around the point of interest on the mesh at which the curvature is computed (an example of curvature using different rings is

presented in Figure 15). This method relies on smooth differential geometry calculations by approximating the local surface with a quadric (Figure 6).

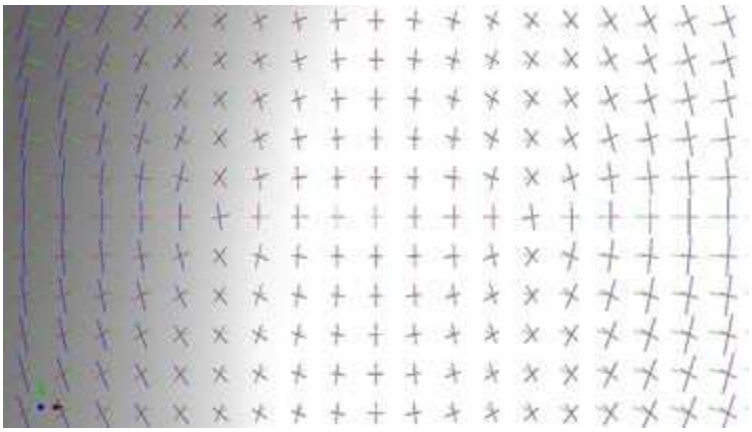

Figure 6: This figure illustrates the principal directions of curvature and normals at vertices of a mesh of the graph of the function $f(x,y)=2x^2+y^{2.}$

In each population, mean RV shape has been presented according to its mean curvature index.

Statistical analysis

Data were summarized as mean ± standard deviation for continuous variables with normal distribution; median [95% confidence interval] for other continuous variables and number of subjects (%) for categorical variables. The variables were tested by the Student t-test for normally distributed variables. Otherwise, the Mann-Whitney U-test was performed. Categorical variables were compared using Fisher's exact test. Bonferroni correction was used for multiple comparisons (ANOVA). Differences between patient group and controls have been tested regularly (considering the Euclidean distance) and using the Hotelling's T-Square test statistic (205) under Matlab (v.R2011a, MathWorks, Natick, US). This computation returned a p-value pattern at every location of the RV shape, low p-value indicating high degree of differences. Patterns were displayed in a logarithmic scale to highlight differences, multiplied by the sign of the differences between the populations (206, 207). For other analyses, statistical significance was defined as a p-value <0.05. Statistical analyses were performed using MedCalc 17.5.5 (MedCalc Software, Mariakerke, BE).

RESULTS

General characteristics of the population

We included 15 patients with TOF; 15 patients with an ASD and left to right shunt; 4 patients with an ASD and severe pulmonary hypertension. We then matched 21 controls to this population. General characteristics of the population are presented in table 1. Among TOF patients, all but one had a trans annular patch during the original surgery. Eight of them presented severe pulmonary regurgitation, 3 already had pulmonary valve replacement at the time of the study. Among ASD patients, 5 had small defects whereas 10 had large defects with significant hemodynamic consequence and evidence on 2D ultrasound of RV volume overload. Among ASD patients with large shunt, all had secundum ASD except one patient with a sinus venosus defect and 1 with a primum ASD, 2 patients suffered from embolic ischemic stroke and 3 of them presented paroxysmal supra-ventricular tachycardia.

Table 1: Main characteristics of our population

	Controls n=21	**ASD (without PAH) n=15**	**Tetralogy of Fallot n=15**	**p-value**
Age, years	36.0[28.0-46.0]	31.0[17.3-58.5]	34.0[24.1-36.5]	0.051
Female sex, n (%)	10 (47.6%)	11 (73.3%)	9 (60%)	0.46
Height, cm	168.6±8.4	168.3±11.4	165.5±12.0	0.66
Weight, kg	65.1±10.0	67.5±18.1	64.1±19.1	0.83
NYHA class III or IV, n(%)	-	2 (33.3%)	2 (33.3%)	1
Heart rate, bpm	58.3±12.6	76.2±13.2	78.1±16.0	0.73
BNP, ng/mL	-	66.0[43.8-80.7]	49.0[30.4-96.8]	0.49
QRS duration, ms	-	104.0[87.1-108.9]	140.0[121.3-167.2]	**0.0006**
Frame rate, Hz	19.0[18.0-22.3]	22.0[21.3-26.0]	24.0[20.3-26.0]	0.09

ASD, atrial septal defect; BNP, brain natriuretic peptide; NYHA, New York Heart Association; PAH, pulmonary arterial hypertension

Differences between TOF, ASD (excluding pulmonary hypertension) and controls

Two-dimensional echocardiographic results are presented in Table 2. Patients with RV volume overload presented an overall dilated right ventricle. No difference in RV diameter was found between ASD and TOF patients. Patients with TOF had a more hypertrophic right ventricle (p=0.03) but reduced systolic function as assessed by RV fractional area change (p=0.02), TAPSE (p<0.001) and tricuspid valve s' (p 0.004) as compared with ASD.

Table 2: Echocardiographic characteristics of our population

	ASD (without PAH) n=15	Tetralogy of Fallot n=15	p
RV diameter, mm	40.0[38.3-51.0]	45.0[39.9-51.1]	0.53
RV wall thickness, mm	5.0[4.0-7.0]	7.0[6.0-9.9]	**0.03**
RV fractional area change, %	53.1±4.3	47.4±6.7	**0.02**
TAPSE, mm	30.9±6.0	18.3±3.8	**<0.001**
TV s', cm/s	15.6±3.5	10.8±3.3	**0.004**
LV EF, %	61.0±6.2	62.9±9.4	0.51

Results from 3D analysis are presented in Table 3. Three-dimensional RV volumes confirm the larger volumes in ASD and TOF patients as compared to controls, as well as the reduced RV EF in TOF patients. No difference was found between ASD patients and controls in terms of RV area strain, longitudinal or circumferential strain, either at the global RV level or the regional level.

Between TOF patients and controls, many differences have been observed: RV area strain was generally lower, especially in the inferior, lateral wall and in the trabecular septum. There was almost no difference in circumferential strain, except that it was lower in the lateral wall and the trabecular septum. Substantial differences appear between TOF and other patients regarding the longitudinal strain where all segments but the septum (except the trabecular septum) present a decrease in longitudinal strain. The

ratio Circumferential / Longitudinal strain (CS/LS) was significantly higher in TOF patients as compared to ASD and controls, confirming that in TOF patients, circumferential strain is predominant over longitudinal strain. Figure 7 represents, over the mean RV shape for each subgroup, area strain as well as differences in area strain using different methods. The fourth column represents TOF differences with ASD patients.

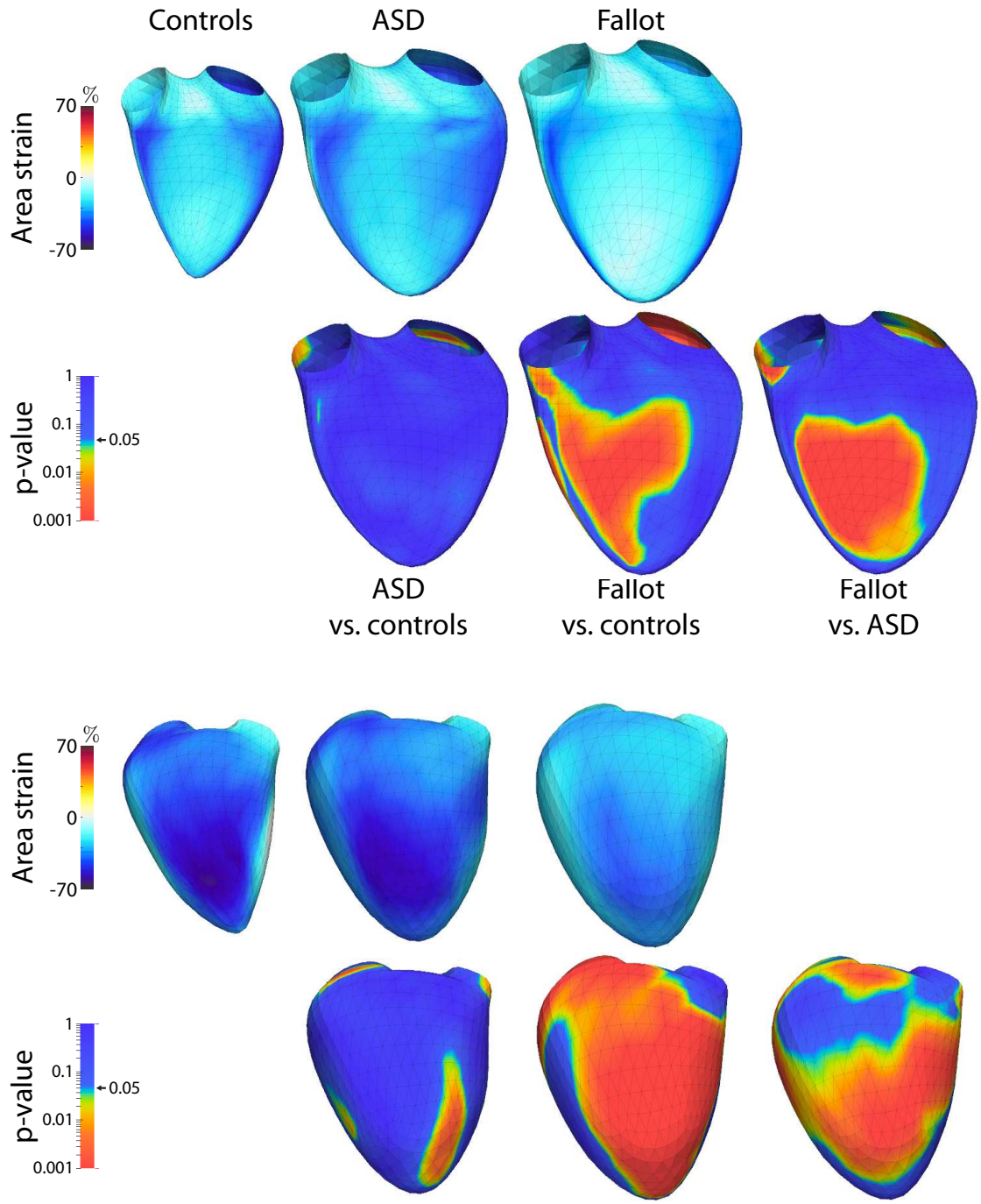

Figure 7: The first 2 lines represent the septum, the 3rd and 4th, the RV free wall. The first line for each RV image presents the patients data. The 2nd line presents differences between controls and ASD, controls and TOF in the last column differences between ASD and TOF. Significant differences are presented according to the p-values gradient: p values <0.05 are green – yellow – orange and red, whereas the blue pattern indicate that there is no significant difference between the studied groups. This figure illustrates differences in area strain especially in TOF patients either versus controls or ASDs.

Table 3: 3D echocardiographic data

	Controls n=21	ASD (without PAH) n=15	Tetralogy of Fallot n=15	p-value
RV EDV, mL	54.8±18.4	139.1±87.6	144.4±71.2	**<0.001**
RV EF, %	55.3±5.8	51.5±9.8	46.0±9.8	**0.008**
RV Area strain, %				
global AS	-29.5±4.5	-29.9±6.1	-24.6±6.3	**0.02**
Anterior wall	-28.5±6.7	-29.6±6.8	-24.3±7.4	0.09
Inferior wall	-38.3±6.3	-37.8±7.3	-30.1±9.6	**0.006**
Lateral wall	-41.7±5.5	-38.5±8.6	-29.7±7.7	**<0.001**
RVOT anterior	-22.2±5.3	-25.6±5.7	-21.3±7.1	0.13
Infundibular septum	-27.8±7.1	-29.3±6.6	-26.5±6.8	0.54
Membranous septum	-22.9±7.8	-22.2±8.3	-20.9±7.9	0.76
Inlet septum	-29.3±9.9	-28.9±10.7	-25.7±7.9	0.51
Trabecular septum	-25.6±6.2	-27.1±5.3	-18.7±6.1	**<0.001**
RV Circumferential strain, %				
Global CS	-16.2±2.8	-17.1±3.9	-15.2±4.0	0.34
Anterior wall	-17.5±7.2	-19.1±4.9	-16.4±7.5	0.53
Inferior wall	-19.6±5.5	-20.7±5.8	-17.1±6.8	0.26
Lateral wall	-27.8±5.7	-26.2±7.1	-20.1±5.4	**0.002**
RVOT anterior	-9.6±3.5	-12.4±5.0	-13.2±5.6	0.054
Infundibular septum	-16.4±3.5	-17.2±5.4	-19.0±5.3	0.27
Membranous septum	-11.0±4.0	-12.5±4.8	-11.8±4.1	0.57
Inlet septum	-15.0±5.3	-15.4±6.7	-14.3±4.6	0.87
Trabecular septum	-12.5±3.7	-13.2±4.6	-9.3±4.1	**0.03**
RV Longitudinal strain, %				
Global LS	-14.8±3.7	-13.9±5.1	-10.1±3.3	**0.004**
Anterior wall	-12.6±4.5	-11.7±4.9	-8.7±2.7	**0.02**
Inferior wall	-21.7±4.9	-20.0±4.5	-14.3±4.8	**<0.001**
Lateral wall	-16.4±4.1	-14.8±4.0	-10.7±3.6	**<0.001**
RVOT anterior	-13.6±4.9	-13.9±7.5	-9.0±3.5	**0.02**
Infundibular septum	-12.2±5.0	-11.7±8.9	-7.8±4.8	0.11
Membranous septum	-12.2±7.2	-10.1±6.7	-9.3±5.3	0.41
Inlet septum	-15.1±8.0	-14.1±9.0	-11.6±5.4	0.41
Trabecular septum	-14.3±5.7	-14.8±3.0	-9.6±3.8	**0.004**

EDV, end-diastolic volume; EF, ejection fraction; PH, pulmonary hypertension; RV, right ventricular; RVOT, right ventricular outflow tract.

Differences in circumferential strain represented over the mean RV shape for each group are presented on the following figure 8.

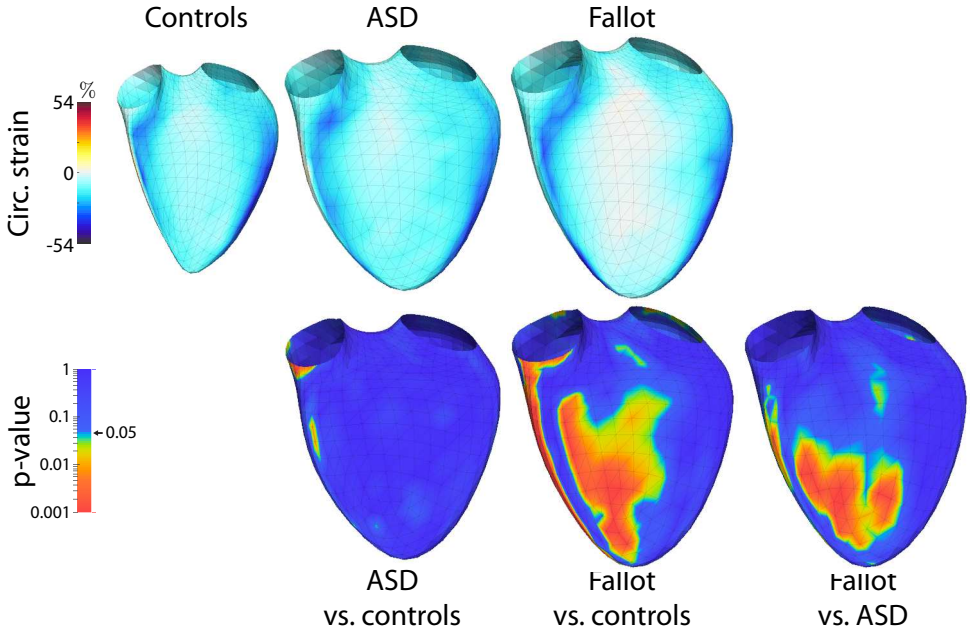

Figure 8

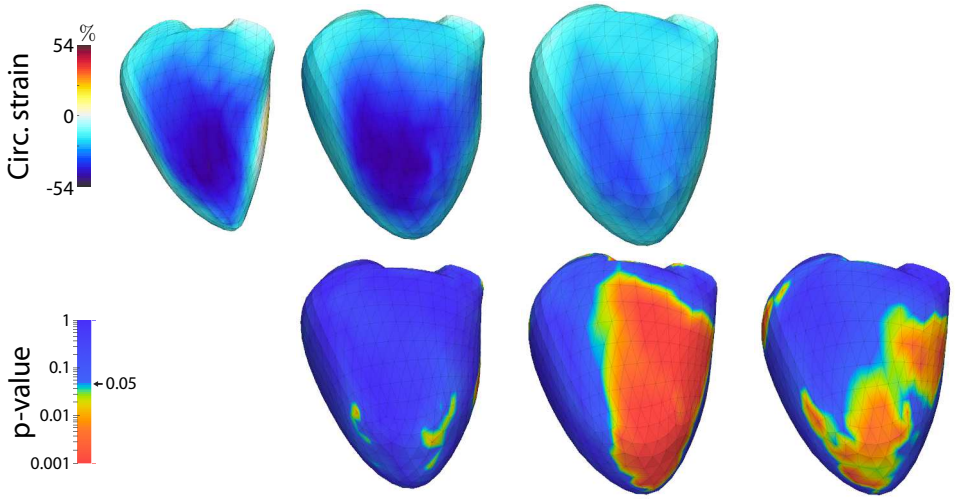

Figure 8: Despite no statistically significant differences when studying entire regions, this figure illustrates a lower circumferential strain in TOF patients as compared to controls, especially at the lateral, anterior wall and the apex (which could have been diluted in our previous regional analysis (Table 3) as the apex has not defined as an entire region according to our definition).

Differences in longitudinal strain are presented here (Figure 9):

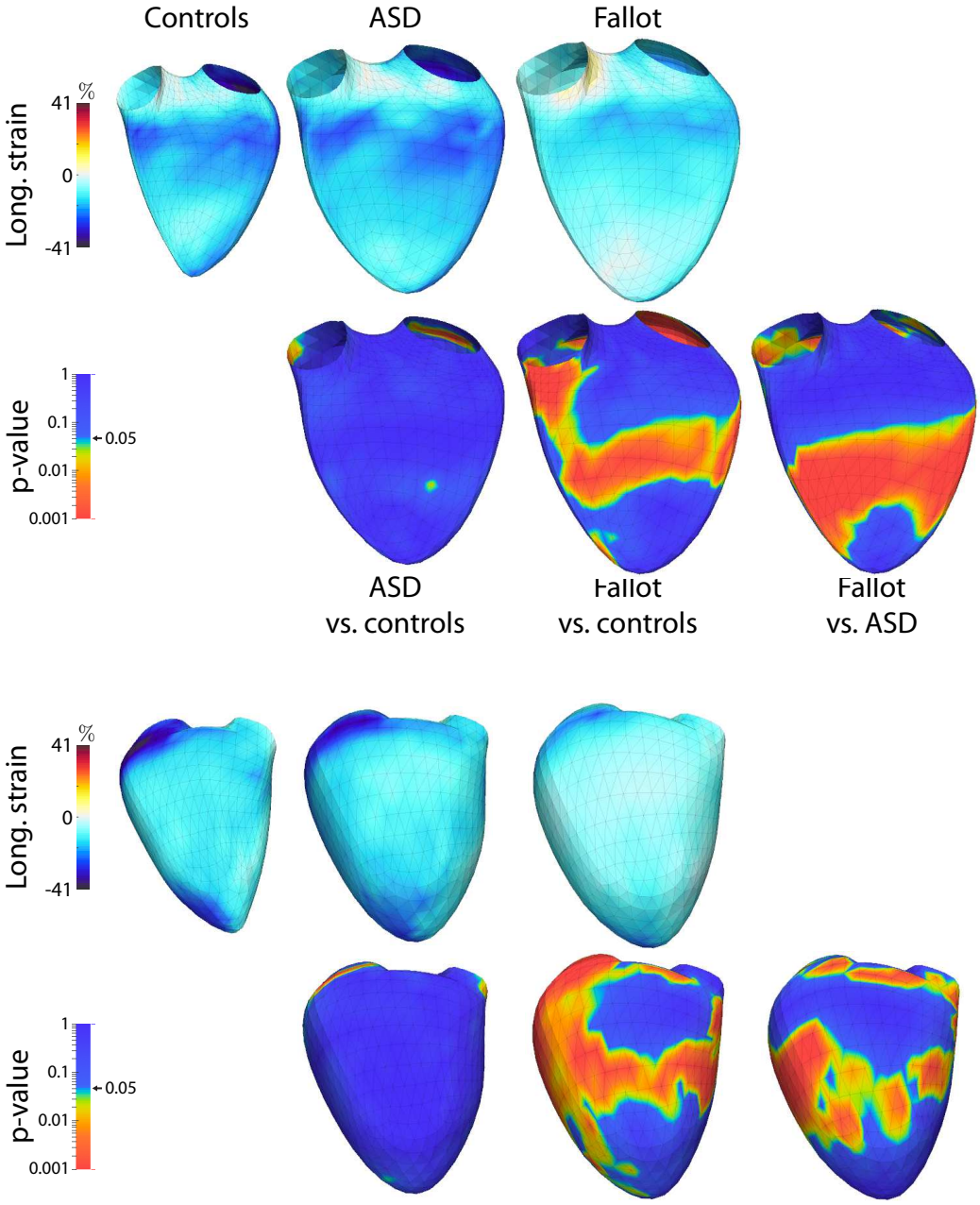

Figure 9: This figure illustrates major differences in longitudinal strain within the trabecular septum as well as in the inferior and lateral wall.

This kind of representation is particularly interesting in terms of regional analysis.

Following the same methodology, the RV shape has been analyzed:

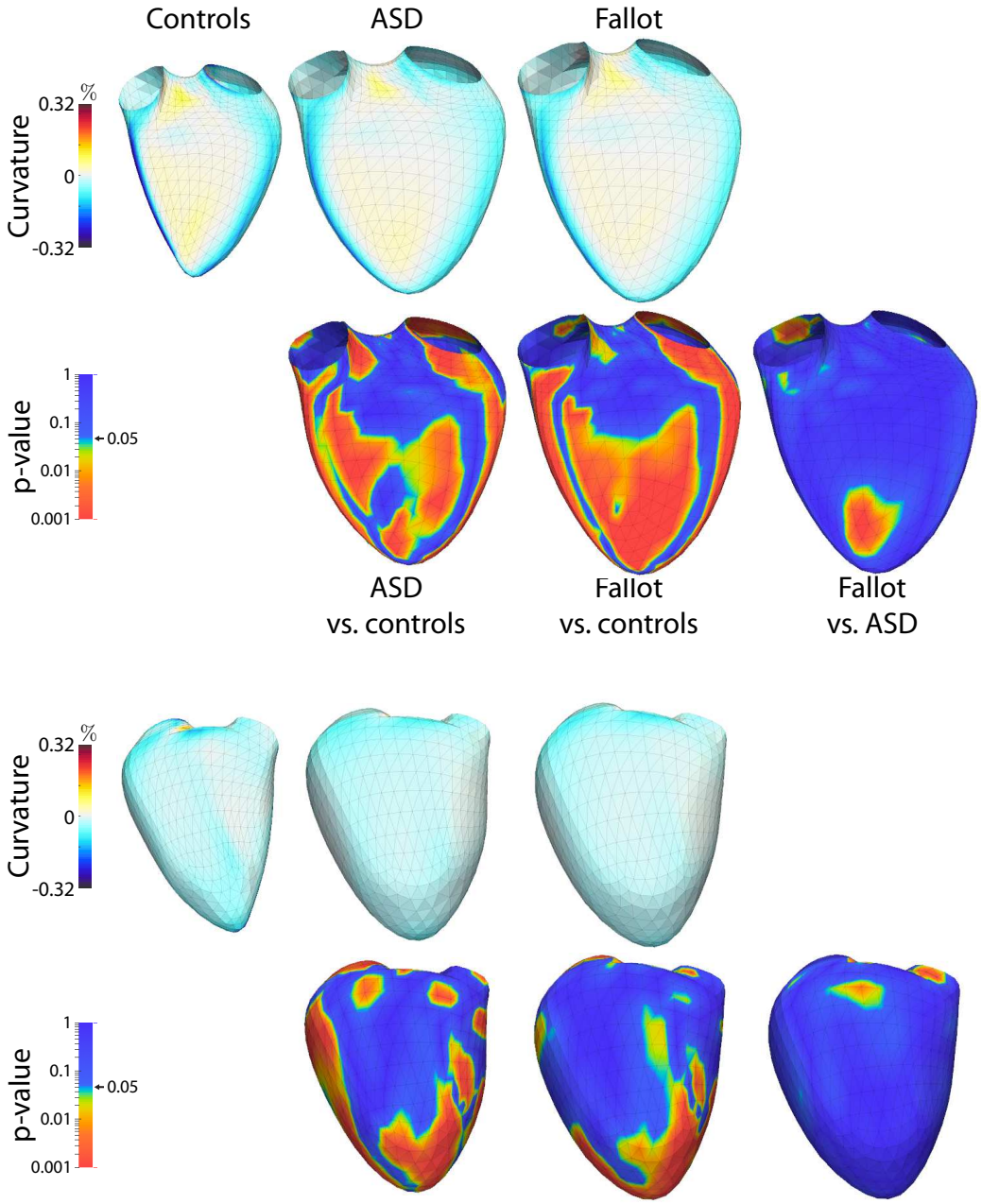

Figure 10: RV shape in controls and patients as well as differences between the 3 groups. Important differences are observed within the septum between volume overload patients and controls, whereas almost no difference is recorded between TOF and ASD patients, except in the right ventricular outflow tract.

While no significant difference in strain was observed between ASD patients and controls, this figure illustrates shape differences between those 2 populations. Differences are also highlighted between TOF and controls but are less obvious between TOF and ASD patients, except in the RV outflow tract. Differences seems to occur preferentially at the septum level as well as at the lateral and inferior wall. Table 4 presents curvature indices classified by RV regions.

Table 4: 3D regional curvature results for normal controls, ASD and tetralogy of Fallot patients

Curvature	Controls n=21	ASD (without PAH) n=15	Tetralogy of Fallot n=15	p
Anterior wall	-0.034±0.007	-0.027±0.007	-0.025±0.005	**<0.001**
Inferior wall	-0.051±0.005	-0.040±0.008	-0.040±0.007	**<0.001**
Lateral wall	-0.036±0.006	-0.029±0.006	-0.029±0.004	**<0.001**
RVOT anterior	-0.050±0.010	-0.036±0.010	-0.038±0.010	**<0.001**
Infundibular septum	-0.062±0.009	-0.051±0.010	-0.043±0.009	**<0.001**
Membranous septum	-0.047±0.014	-0.036±0.009	-0.035±0.009	**0.003**
Inlet septum	-0.050±0.008	-0.042±0.008	-0.038±0.008	**<0.001**
Trabecular septum	-0.031±0.010	-0.025±0.008	-0.027±0.007	0.12

P-values were provided by an ANOVA with Bonferroni correction. All p-values < 0.05 indicate a statistically significant difference between controls and either ASD or TOF patients but not any statistically significant difference between TOF and ASD patients.

Observations within the group of ASD patients

Two-dimensional echocardiography allowed us to demonstrate that patients with ASD without PAH had better systolic RV function as assessed by TAPSE (p=0.02), tricuspid valve s' (0.05) and fractional area change (p=0.02) and compared to TOF patients. Main results are presented in Table 5. All patients with ASD had higher RV volumes using 3D echocardiography (p<0.001). Controls and patients with small ASD had higher RV ejection fraction as compared to ASD with PAH patients (p=0.001), but not compared to large defects. RV global area strain is lower in ASD-PAH in comparison with small ASD and controls.

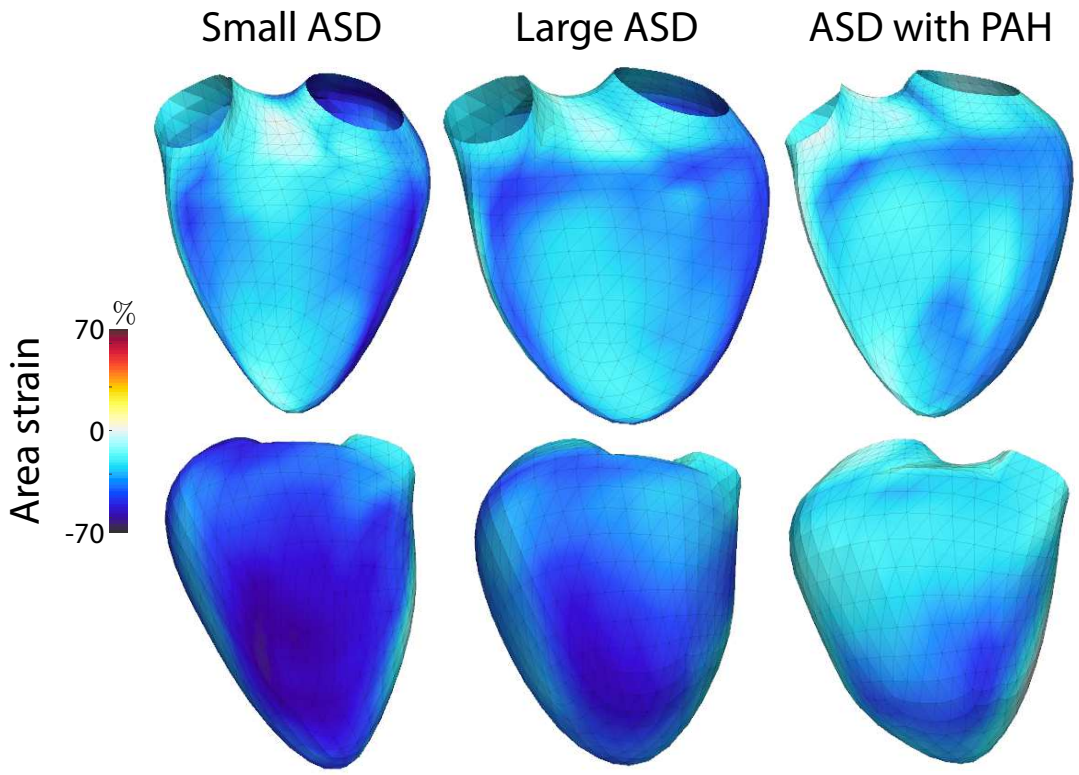

Figure 11: Area strain represented over the mean RV shape in each group of ASD A gradient in area strain is observed according to the ASD natural history.

Table 5: Comparison between ASD patients

	ASD Small defect n=5	ASD Large defect n=10	ASD PAH n=4	p-value
RV EDV, mL	94.2±44.7	161.6±96.7	126.0±41.4	**<0.001**
RV EF, %	56.6±7.1	49.0±10.2	37.8±11.7	**0.001**
RV Area strain, %				
global AS	-31.8±3.1	-28.9±7.1	-21.6±6.6	**0.04**
Anterior wall	-33.4±6.7	-27.6±6.2	-21.1±10.2	0.09
Inferior wall	-40.6±5.8	-36.4±7.9	-26.4±5.5	**0.01**
Lateral wall	-45.9±8.9	-34.8±5.9	-26.0±10.8	**<0.001**
RVOT anterior	-26.4±3.0	-25.1±6.8	-18.3±7.7	0.13
Infundibular septum	-30.4±4.7	-28.7±7.6	-19.0±11.5	0.12
Membranous septum	-20.4±6.6	-23.1±9.2	-18.1±8.1	0.68
Inlet septum	-29.7±5.6	-28.5±12.8	-22.8±7.1	0.69
Trabecular septum	-27.7±2.1	-26.8±6.4	-21.1±11.7	0.47
RV Circumferential strain,%				
Global CS	-19.6±2.7	-15.8±4.0	-11.7±5.5	**0.02**
Anterior wall	-22.0±5.9	-17.7±3.9	-14.4±6.9	0.35
Inferior wall	-23.8±4.5	-19.1±5.9	-13.6±3.5	0.06
Lateral wall	-32.1±8.1	-23.2±4.5	-16.5±8.7	**0.002**
RVOT anterior	-14.6±6.9	-11.3±3.7	-9.7±7.9	0.17
Infundibular septum	-18.5±6.1	-16.6±5.2	-10.8±8.9	0.13
Membranous septum	-13.1±5.4	-12.3±4.7	-8.1±4.6	0.34
Inlet septum	-18.6±4.5	-13.8±7.2	-8.3±7.4	0.09
Trabecular septum	-13.8±1.6	-12.9±5.6	-12.3±7.0	0.94
RV Longitudinal strain, %				
Global LS	-13.3±4.2	-14.2±5.7	-14.2±5.7	0.20
Anterior wall	-12.7±3.5	-11.2±5.6	-7.2±6.9	0.25
Inferior wall	-20.5±3.8	-19.7±5.0	-14.2±5.8	0.06
Lateral wall	-17.2±4.2	-13.6±3.4	-10.3±4.2	**0.02**
RVOT anterior	-12.1±8.7	-14.7±7.1	-7.4±6.3	0.24
Infundibular septum	-10.2±5.9	-12.4±10.3	-5.5±8.0	0.34
Membranous septum	-8.0±5.9	-11.6±7.1	-9.7±5.7	0.63
Inlet septum	-10.9±7.2	-15.7±9.8	-13.7±4.9	0.72
Trabecular septum	-14.8±3.9	-14.8±2.7	-9.3±8.0	0.31

Significant differences are observed in circumferential strain: small ASD have increased global RV circumferential strain as compared to ASD-PAH patients. Differences are particularly significant at the lateral wall.

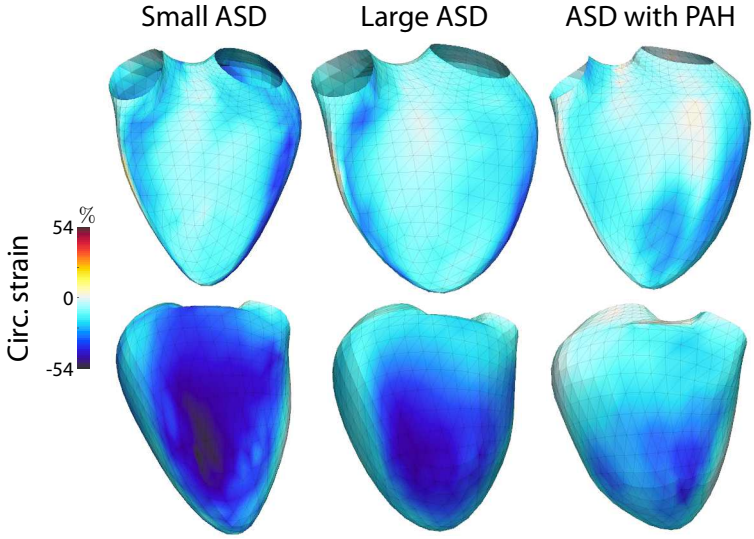

Figure 12: Circumferential strain represented over the mean RV shape in each group of ASD. As for area strain, a gradient is observed with the severity of the disease. Main changes occur at the basal level.

There was no significant difference in regional longitudinal strain between controls and all ASD patients, except in the lateral wall with lower LS in ASD-PH patients. However, over the mean LS pattern of ASD, there is a trend toward an increased septal LS strain in large ASD and an increased RV lateral and inferior wall LS in small ASD.

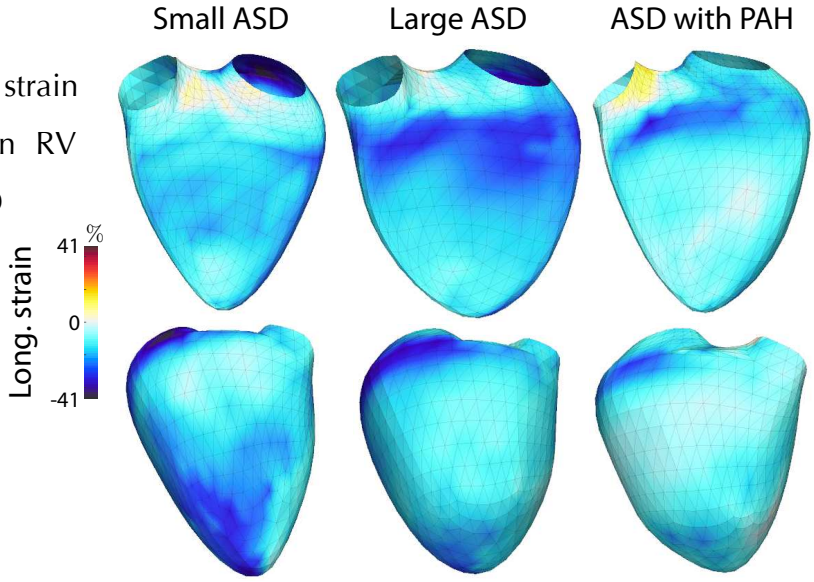

Figure 13: Longitudinal strain represented over the mean RV shape in each group of ASD

TOF patients

Patients with TOF were divided according to the presence of severe pulmonary regurgitation. However, no significant difference in terms of RV dilatation, ejection fraction or strain (either area, circumferential or longitudinal strain) was identified. Table 6 presents the results from 3D analysis.

Table 6: 3D data for TOF patients

	No severe pulmonary regurgitation n=7	**Severe pulmonary regurgitation n=8**	**p-value**
RV EDV, mL	120.1±41.3	165.6±87.0	0.23
RV EF, %	45.2±9.2	46.8±10.9	0.77
RV Area strain, %			
global AS	-23.8±6.6	-25.4±6.3	0.63
Anterior wall	-25.3±8.0	-23.4±7.2	0.64
Inferior wall	-28.7±8.5	-31.2±10.8	0.63
Lateral wall	-30.0±8.2	-29.3±7.8	0.87
RVOT anterior	-19.1±7.9	-23.0±6.1	0.27
Infundibular septum	-23.9±6.3	-28.8±6.7	0.17
Membranous septum	-20.3±7.7	-21.4±8.5	0.79
Inlet septum	-23.7±8.6	-27.4±7.4	0.39
Trabecular septum	-19.1±6.3	-18.4±6.3	0.83
RV Circumferential strain, %			
Global CS	-15.3±3.8	-15.1±4.5	0.93
Anterior wall	-18.2±7.3	-14.8±7.7	0.40
Inferior wall	-16.7±4.8	-17.6±8.5	0.81
Lateral wall	-20.3±5.2	-20.0±5.8	0.88
RVOT anterior	-12.2±5.9	-14.1±5.5	0.54
Infundibular septum	-17.4±4.4	-20.3±6.0	0.31
Membranous septum	-12.7±3.8	-11.1±4.6	0.49
Inlet septum	-14.4±4.6	-14.2±4.9	0.94
Trabecular septum	-10.1±3.3	-8.5±4.8	0.47
RV Longitudinal strain, %			

Global LS	-9.3±3.5	-10.9±3.1	0.36
Anterior wall	-7.5±1.7	-9.7±3.1	0.12
Inferior wall	-13.7±5.6	-14.8±4.2	0.66
Lateral wall	-11.0±4.1	-10.4±3.4	0.75
RVOT anterior	-7.4±3.9	-10.3±2.6	0.11
Infundibular septum	-6.1±5.0	-9.2±4.4	0.21
Membranous septum	-8.4±5.6	-10.0±5.3	0.59
Inlet septum	-9.7±5.4	-13.3±5.2	0.22
Trabecular septum	-10.1±4.1	-9.2±3.7	0.68

Association with QRS duration

In the whole population, QRS duration has been correlated with RV end-diastolic volume (r=0.60, p=0.0002), RV ejection fraction (r=0.51, p=0.002) and RV area strain (r=0.51, p=0.002). In the subset of TOF patients, RV ejection fraction and AS were not significantly correlated to QRS duration but RV end-diastolic volume was (r=0.76, p=0.0009). While the septum curvature was not significantly correlated to QRS duration, a strong correlation was found between RV inferior (r=0.85, p=0.0001), lateral (r=0.78, p=0.0006), anterior wall curvature (r=0.65, p=0.009) and QRS duration.

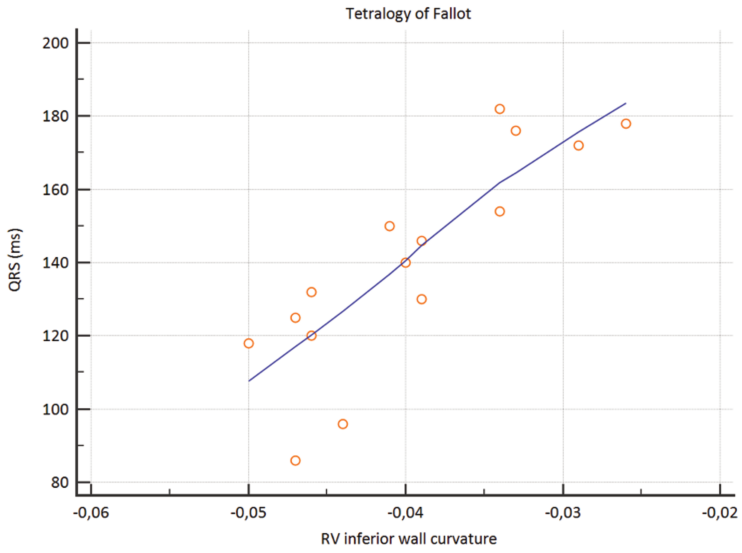

Figure 14: Correlation between RV inferior wall curvature and QRS duration

DISCUSSION

Volume overload results in different adaptation according to the underlying congenital heart disease. Our results illustrate differences in RV deformation and shape between patients with different kinds of RV volume overload and a control population. RV shape in ASD and TOF patients is quite similar but highly diverse from the control group. Although longitudinal strain is significantly altered, circumferential strain is predominant (even if impaired) in TOF patients and area strain is only mildly impaired as compared to a control group. No significant difference in strain was observed between ASD and control patients but a gradient in area strain and especially circumferential strain was observed according to the type and evolution of the ASD. The lack of association between shape and deformation underlines the complementarity of those 2 indicators, relating to different RV adaptation mechanisms.

RV strain in ASD patients and comparison with TOF

RV deformation was different between ASD and TOF patients. This difference has already been suggested in children using 2D-strain but analyzing only the longitudinal strain (69). While ASD patients (except those with pulmonary hypertension) had similar circumferential strain and even a trend toward a higher longitudinal strain as compared to controls, TOF patients had clearly reduced longitudinal strain and area strain with a relatively preserved circumferential strain (except at the lateral wall). This is in agreement with other echocardiographic data: 3D ejection fraction, TAPSE and tricuspid valve s' which are all reduced in TOF patients under the influence of the reduced global RV deformation. In contrast, TAPSE in ASD patients is higher than in the general population. Volume overload in ASD seems to slightly increase RV longitudinal deformation as previously reported (208, 209). Our study demonstrates that both longitudinal and circumferential are preserved in atrial septal defect, this might be related to the wall shear stress. However, only little is known about RV remodeling after ASD closure. Some authors suggest that RV function after ASD closure (either surgical or interventional closure) declines as compared with the pre-intervention assessment (209, 210). Regional differences in patients with open ASD have also been described (211) using 2D

echocardiography, with increased apical longitudinal strain that also correlates with volume load severity. As we chose to use the RV segmentation according to Haddad, et al. (13), the apex is not entirely included within one region. However, looking at local patterns on the RV meshes, we can clearly see in small ASD an increased longitudinal strain within the apical area of the inferior and lateral wall, which was not observed in patients with large ASD presenting a trend toward higher basal longitudinal strain.

RV characteristics in TOF patients

ASD patients present a better RV remodeling pattern than TOF patients. TOF patients have an increased circumferential / longitudinal strain ratio, with a more hypertrophic RV. An increased radial strain pattern could be a physiological adaptation to chronic pressure loading as previously demonstrated in systemic right ventricles (151) and in Eisenmenger syndrome where transverse strain has been related to outcomes (68). However, radial strain estimation is less precise (either by 2D or 3D echocardiography) (106) as the spatial motion gradient is calculated over a small region with limited spatial resolution, especially in the RV wall, thinner as compared to the left ventricle. Given that our 3D software only authorized the delineation of the endocardium, radial strain has not been computed. Instead, area strain has been studied, integrating both longitudinal and circumferential strain data. The reduced longitudinal RV strain and predominance of circumferential strain might thus be explained by prior pre-op RV pressure overload and RV hypertrophy, observed in our cohort. Although we observed a significant degree of circumferential deformation in normal RVs, usually the RV is known to be a thin ventricle without any histologic middle layer (containing circumferential fibers) as seen on the left side. However, there is experimental evidence in animals subject to pulmonary artery banding (RV pressure overload) that RV fibers reorient from oblique to circumferential (212). This suggests that there is a potential for a post-natal RV remodeling with development of this middle layer under the influence of pressure overload. The question, whether this remodeling is adaptative or (at least partly) innate remains unclear as Sanchez-Quintana *et al* (9) described a middle layer in post-mortem hearts of TOF, even in neonates. Thus, it is more likely that RV remodeling observed in TOF patients is from

diverse origins: both related to their abnormal cardiac development, to the postnatal response to pressure overload and influenced by myocardial damage related to prolonged cyanosis or surgery. Regarding the impact of surgery on the regional level, the difference in RV strain as compared to other groups was not only observed within the infundibular area, but also and predominantly at the lateral wall suggesting a more global remodeling.

Differential regional effects of RV overload have been observed in TOF. During the last decade, authors emphasized the importance of regional differences within the RV of TOF patients (213), as suggested also by our study, with a variable adaptive response to isolated volume overload as opposed to combined pressure / volume overload. The role of the apex has been previously underlined with a loss of function in TOF patients (69), but the use of 3D ultrasound allows us to analyze more precisely differences in TOF patients and to highlight the role of the RV lateral and inferior wall for strain as well as curvature. The absence of difference within TOF between patients with severe pulmonary regurgitation and those without was anticipated given the relatively small group of TOF patients and the presence in the group without severe PR of patients with pulmonary valve replacement > 1 month.

RV shape

We hypothesize that RV pathology would affect RV shape differently depending on the underlying defect and thus, that our indicators of RV shape would allow us to differentiate TOF from ASD. It was not the case. Using our curvature index, even with a small neighborhood (radius of 2) to improve the sensitivity, there was no significant difference in RV shape between ASD and TOF. However, patients with volume overload were very different from controls. The curvature in RV volume overload patients was less important as compared to controls. Thus, even in patients with previous ventriculotomy, the degree of volume overload will determine RV curvature and shape. In TOF patients, the infundibular septum is significantly less curved than in ASD patients,

this was expected given the history of ventricular septal defect surgical closure by patch during the initial complete correction in these patients.

A strong correlation has been identified between RV curvature; especially in the inferior wall; and RV volumes. It is particularly important in TOF patients. We observed a strong correlation between RV inferior wall curvature and QRS duration in TOF patients. QRS duration is one of the strongest predictors of ventricular arrhythmias and death in adult patients with TOF (214, 215), thus, RV shape might provide outcome information. Prolonged electrical intra-ventricular delay seems to be related to RV shape but not RV deformation and function. Therefore, in the assessment of TOF patients, RV deformation and shape appear complementary and further evaluation in a larger cohort is required to assess their prognostic role.

As opposed to Addetia, *et al*. who studied RV shape in pulmonary arterial hypertension patients (132), we chose not to index curvature to the volume of the area of interest as in our view, the volume is already part of the shape and indexed values would have diluted the information of curvature. However, there is no standard in appreciating RV shape, especially using 3D echocardiography. The neighborhood of 2 used in our study for the calculation of curvature has been chosen a priori, reflecting local changes, but not too small to allow an interpretation of the area of interest. The same neighborhood has been studied in (132) and (216).

Below, figure 15 illustrates an example of curvature computations using different neighborhood: 1 ring (NN=1), 2 rings (NN=2) … in a representative TOF patient and a control. When the neighborhood is very small (for example NN=1), the computation is more sensitive to very local changes: as curvature is calculated using only the direct circle of the point of interest, interpretation of those values could be difficult within a region. On the opposite, when the neighborhood is important (a radius of 5 points for example, which represents the radius of the entire posterior wall of the RV), the computation highlights curvature changes at a much larger scale and the curvature information is diluted. The choice of 2 appeared as the more coherent given the analyzed structure.

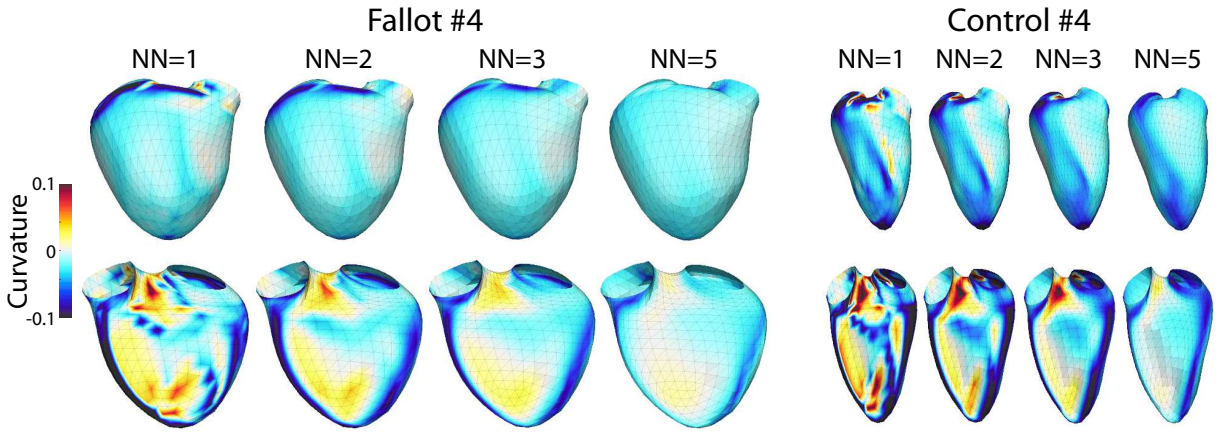

Figure 15: Illustration of RV shape according to curvature calculated using different neighborhood.

Previous authors concluded that mechanical wall stress is inversely proportional to the local RV curvature. The characterization of RV shape indirectly reflects the effects of volume overload and allows better understanding of RV remodeling. While marked differences in strain data are observed in the trabecular septum, no significant difference is observed using curvature index between TOF and ASD, highlighting the independent information provided by RV shape.

Limitations

3D RV study was feasible in all patients, however given anticipated difficulties, this method will not be applicable, in particular in case of poor acoustic window. Cardiac magnetic resonance data, the gold standard for RV volume assessment, have not been presented in our study as the timing of 3D echocardiography and cardiac magnetic resonance was variable and patients with ASD usually did not undergo CMR study.

Even if we investigated a relatively rare pathology, our study suffers from a lack of power given the small cohort. This was only a monocentric study and our results need to be confirmed using the same methodology in a larger multicentric cohort.

CONCLUSION

Our study illustrates differences in both RV strain and shape in TOF and ASD patients as compared to healthy volunteers. We believe these innovative methods will allow us to gain further insights into RV failure in different loading conditions.

CHAPTER 5.
MODELLING STUDY IN PULMONARY HYPERTENSION PATIENTS

Personalized 0D modelling of cardiovascular circulation: disease characterization and drug effect

CONTENTS

ABSTRACT

A Personalised model of the circulation consists in the creation of a virtual simulation of a patient's cardiovascular system: it is a powerful tool that integrates flow and pressure information. Once a personalised simulation created, it can be used to simulate or analyse several conditions and even predict the cardiac behaviour. In this last chapter, we focused on the personalisation of a 0D model of the circulation from volume and pressure information, in order to estimate mechanical parameters such as resistances and compliances. The aim of this study was to evaluate the added value of such personalised model parameters to characterise pulmonary arterial hypertension (PAH) and predict the response to PAH therapy. The model was personalised to 11 PAH patients' data before and after advanced PAH therapy. The model reproduces with accuracy the cardiovascular circulation of the patients, and the estimated parameters reflected well the expected changes with therapy.

INTRODUCTION

The circulatory system, also called the cardio-vascular system, allows the blood to circulate and carry oxygen, carbon dioxide, nutrients (electrolytes, amino acids), hormones and blood cells to and from each cell in the human body to provide for nutrition and cellular homeostasis. We will exclude from our topic the lymphatic system that recycles the excessive blood plasma that has been filtered from the interstitial fluid.

The main components of the human cardiovascular system are the heart, the blood and blood vessels. It includes the pulmonary circulation (also called small circulation) which makes a "loop" through the lungs to oxygenate the blood and the systemic circulation, a "loop" through the body to provide oxygenated blood. This system can be seen as a double pump (the heart) connected in series. The left heart is composed of the left atrium and left ventricle, separated by the mitral valve. Contraction of the left ventricle is responsible for pumping blood to all systemic organs. Blood exits the ventricle through the aortic valve into the aorta, the larger artery in the body. The aorta branches into successively smaller arteries, that in turn branch into millions of very small vessels that terminate into billions of capillaries, the main site of transport of water, gases, electrolytes, substrates, and waste products between the bloodstream and the extracellular fluid. Blood from the capillaries comes back into venules, merging into veins. The veins will merge to form the 2 main veins of the systemic circulation: the superior vena cava and the inferior vena cava. These veins drain into the right atrium which is separated from the right ventricle by the tricuspid valve. The right ventricle pumps blood through the pulmonary valve into the pulmonary arteries and the lungs. Oxygenated blood exiting the lungs is returned to the left atrium, completing the circulatory loop (217).

First developed for biology and as a demonstration tool, circulatory models are evolving toward clinical applications (218). Several approaches over the last decades have been developed to describe and simulate the cardiovascular system, including cardiac mechanics and electrophysiology (219-228) with the identification of the

mathematical laws underlying biological mechanisms derived or verified using experimental data. They differ in their choice of hyperelastic material, electrophysiological properties or electromechanical coupling. Multi-scale mathematical frameworks have been developed to simulate the cardiac function at the whole-organ scale (226, 229-233). Additionally, 0D models of the circulation are powerful tools to integrate flow and pressure information at a more global level and estimate mechanical parameters, like resistance or compliance. Personalization of the model consists in optimizing its mechanical parameters so that the simulation behaves in accordance to patient- specific datasets (Figure 1, from Marchesseau *et al*. (234)). It is the main challenge for all these models (235).

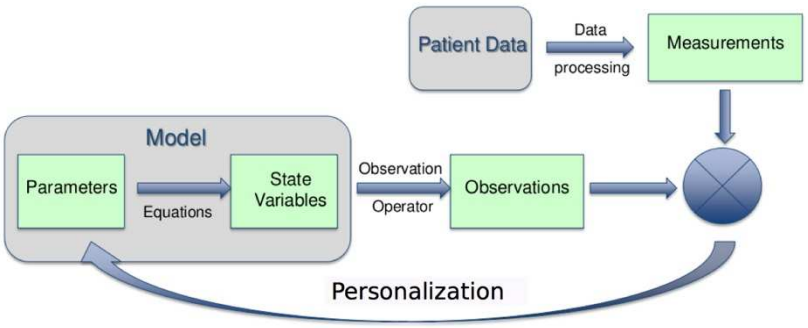

Figure 1: representation of the personalization pipeline

In PAH, the principal indicators of severity of the disease are the mean PA pressure, the cardiac output and the pulmonary vascular resistance (PVR) / compliance (PVC).

Formulas to calculate PVR are the following:

$$PVR = (PAPm - PCWP)/Q$$

$$PVR = \frac{l.\eta.8}{\pi.r^4}$$

where η is the blood viscosity, l and r the length and radius of the vessel (the pulmonary artery in our case), PAPm, the mean pulmonary arterial pressure; PCWP the pulmonary capillary wedge pressure and Q, the cardiac output.

Compliance (or capacitance) is a measure of arterial distensibility. The formula to compute the PVC is:

$$PVC = \frac{SV}{PP}$$

where PP is the increase in pressure, SV the stroke volume and PVC the pulmonary vascular compliance (mL/mmHg, the change in volume associated with a given change in pressure).

Cross-sectional compliance (236) is defined by the absolute change in lumen area for a given change in pressure:

$$CC = \frac{AA}{PP}$$

where AA is the change in pulmonary artery area. CC is expressed in mm^2/mmHg.

From a mechanical point of view, differences in compliance refer to structural changes occurring in the pulmonary vasculature as a consequence of pulmonary diseases (237), which make the vessels stiffer than normal. In PAH, small increases in PVR are accompanied by large decreases in PVC, likely accounting for the important prognostic ability of PVC (238, 239). The decrease in pulmonary artery pressure during diastole depends both on PVR and PVC (Figure 2). Elevated PVR slows down flow through the peripheral circulation, while a preserved PVC determines a good volume accumulation in systole and release in diastole, contributing to a slow reduction in diastolic pulmonary artery pressure. This combined effect is summarized by the product of PVR and PVC, the time constant "τ", called the RC-time: $\tau = R.C$.

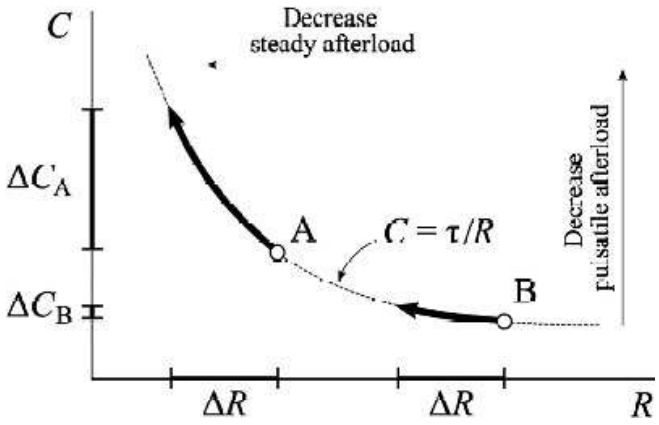

Figure 2: changes in PVC for a similar reduction in PVR in patients with different PVR at baseline illustrating the inverse hyperbolic relationship between PVR and PVC (240)

From a clinical point of view, we were wondering whether patient-specific cardiac modelling could help understand the hemodynamic in pulmonary arterial hypertension (PAH) and predict the response to therapy (pulmonary vasodilators, PAH advanced therapy).

METHODS

Study

We performed a case study in patients with PAH. Patients with PAH undergo regular assessment in our institution (CHU de Nice, Hôpital Pasteur, Service de Cardiologie) including clinical assessment, echocardiography and right heart catheterization. We identified from our patients' database 11 patients with right heart catheterization performed in our centre before instauration and after 3 to 6 months of advanced therapy.

Pre-capillary pulmonary hypertension was considered according to right heart catheterization data, when mean resting pulmonary artery pressure was ≥25 mmHg with pulmonary capillary wedge pressure ≤15 mmHg. Patients with significant left heart disease, arrhythmias or congenital heart disease were excluded as it would have challenged hemodynamic laws and potentially led to a misinterpretation of measured hemodynamic data.

For each patient, a 0D model of the cardiovascular system was personalised from the patient data. Personalisation means the estimation of the model parameters that generate the simulations that are the closest to the patient measurements. A description of the model and its personalization are provided below.

The 0D Circulation Model

The circulation model is a lumped model of the cardiovascular circulation, made of 4 main components: the left heart, the systemic circulation, the right heart and the pulmonary circulation.

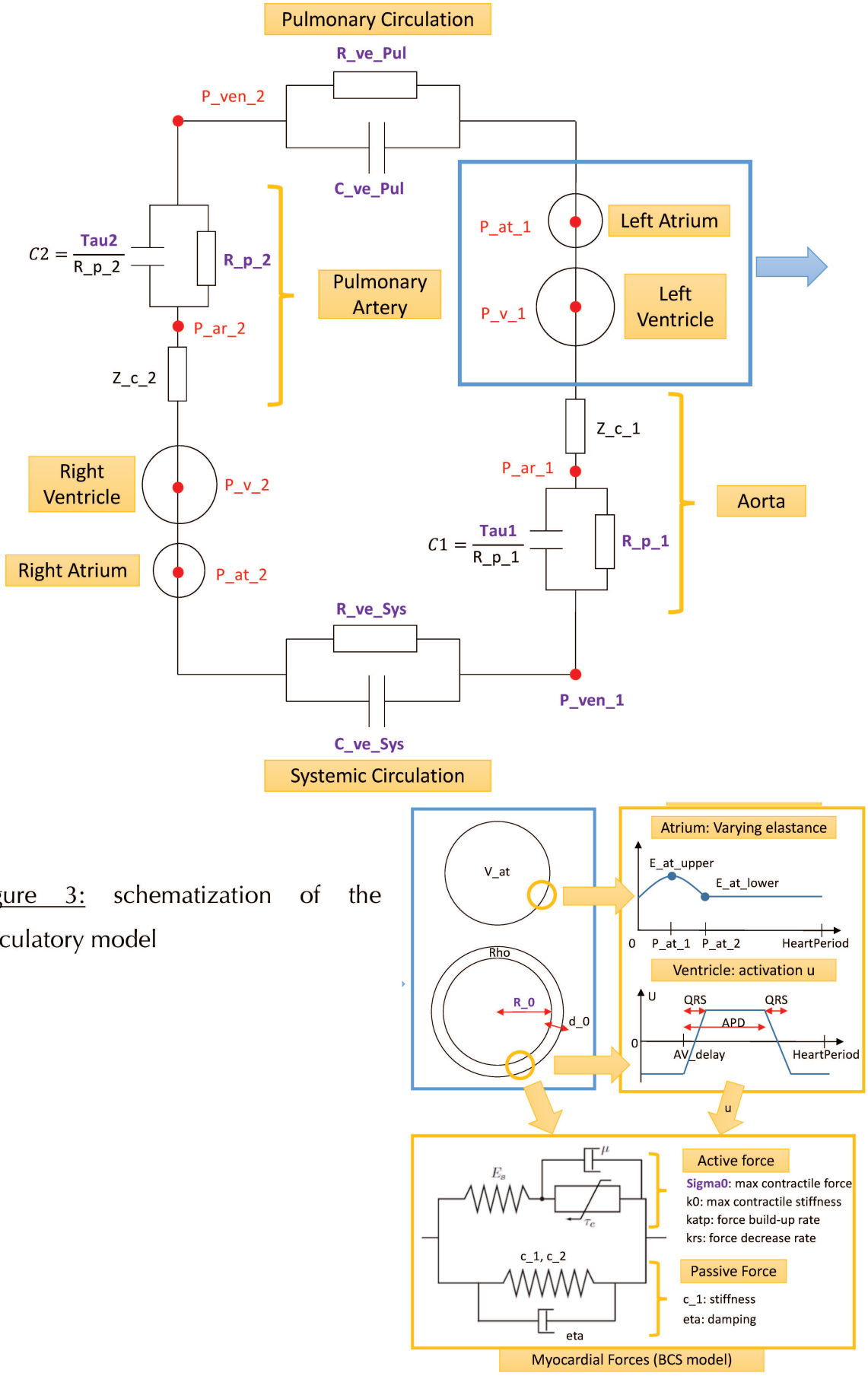

Figure 3: schematization of the circulatory model

The "heart" components are based on the "0D" simplified model of ventricular mechanics presented in (241) (Figure 3). This model consists in a fast version of Inria in-house 3D electromechanical model, based on the implementation of the Bestel-Clément-Sorine (BCS) model (242) by (234) (see figure below) in the SOFA software (www.sofa-framework.org).

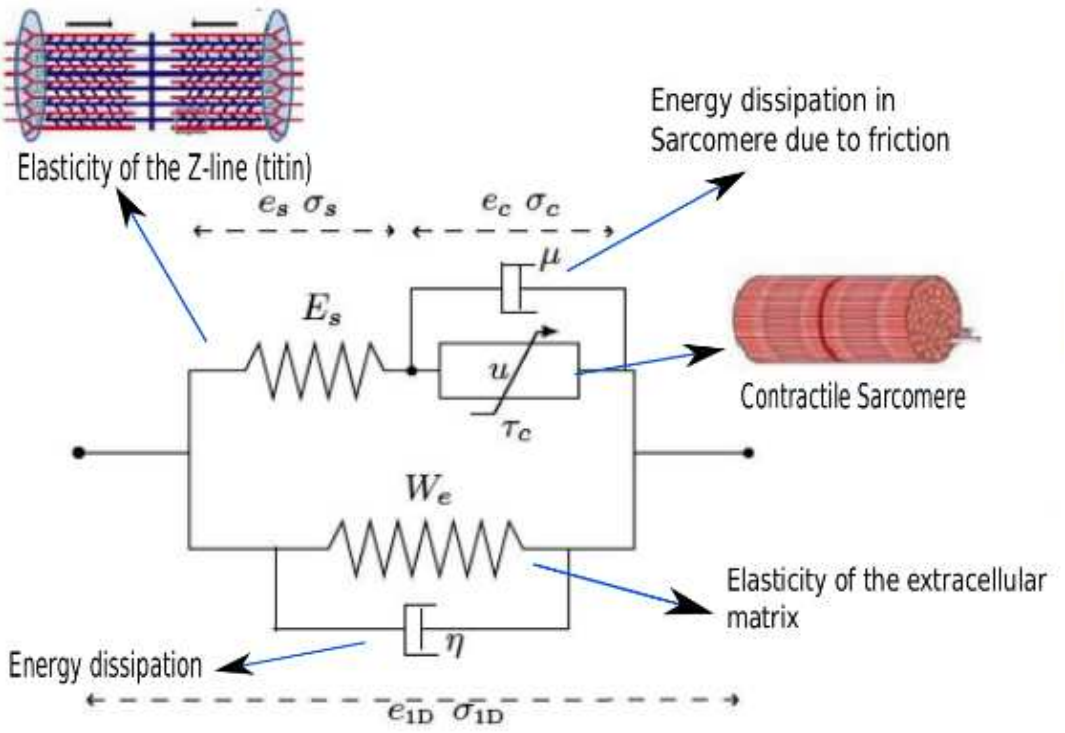

Figure 4: Electromechanical model. W_e is the strain energy of the extracellular matrix considered here as an isotropic material, associated with a dissipative term η. u is a control variable which is driven by changes in transmembrane potential. It controls the contraction stress τ_c. μ deals with the friction in the sarcomere while E_s is a linear spring to enforce elasticity of the titin. From (234).

As described in (241), both the 3D and 0D model share the same mechanical and hemodynamic equations, but simplifying assumptions are made on the geometry to obtain the simplified equations of the 0D model. This leads to a very fast model made of around 18 equations described in the Appendix B of (241), which can simulate around 15 beats per second.

To simulate the cardiovascular pulmonary circulation, the parameter P_{ven_2} ("Distal Arterial Pressure") is connected to the pulmonary circulation component, which is made of a resistance R_{ve_Pul} and compliance C_{ve_Pul} that model the total vascular resistance and compliance of the pulmonary circulation. This circulation component is then connected to the left atrial pressure P_{at_1} of the left heart component. The pulmonary vascular resistance (PVR) as measured using right heart catheterization corresponds to the sum of Z_{c_2} (proximal resistance), pulmonary artery resistance R_{p_2} and R_{ve_Pul}.

The pulmonary circulation components take the flow going out of the pulmonary artery as input ($\boldsymbol{Q_{circul\_in}}$). They successively output the flow going into the left atrium ($\boldsymbol{Q_{circul\_out}}$) with the formula:

$$Q_{circul\_out} = \frac{P_{ven\_2} - P_{at\_1}}{R_{ve\_Pul}}$$

and updates the Distal Arterial Pressure with the formula:

$$\frac{dP_{ven\_2}}{dt} = \frac{(Q_{circul\_in} - Q_{circul\_out})}{C_{ve\_Pul}}$$

Instead of a prescribed time-varying atrial pressure (as originally described in (241)), a time-varying elastance E_{last} is used to model the atrial contraction and the increase of atrial pressure during contraction (see figure 1, bottom). The atrial pressure is then derived from the ventricular volume through the equation:

$$P_{at\_1} = E_{last} (V_{at\_1} - V_{at\_1\_0})$$

where $V_{at\_1\_0}$ is the initial left atrial volume. The left atrial volume V_{at} is then updated with the formula:

$$\frac{dV_{at\_1}}{dt} = Q_{circul\_out} - Q_{at\_out}$$

where Q_{at_out} is the flow from the atrium to the ventricle as computed in (241)

Overall, the circulation model contains 87 parameters. As in (241) it is solved with the Euler Forward Method and a temporal discretization of 0.01ms, and can simulate 50 seconds of cardiovascular circulation in 4 seconds of computation.

Personalization of the model

From the available patient data, 3 parameters were imposed (the heart rate, obtained from the patient, the duration of the action potential and the atrio-ventricular delay from default values of the restitution curve), 13 parameters were estimated and the 71 remaining parameters were set to default values.

At each iteration of the personalization algorithm, 50 heartbeats were simulated in order to get a stable cardiovascular simulation, then the following 10 values were extracted from the 50th beat (10 observations):

Diastolic pulmonary artery pressure	#PAPdiast1
Mean pulmonary artery pressure	#PAPmean1
Pulmonary wedge pressure	#Pcapillary1
Right atrial pressure	#RAP1
Diastolic aortic pressure	#Paodiast1
Mean aortic pressure	#Paomean1
Maximum left ventricular pressure	#Max_LV
Maximum right ventricular pressure	#Max_RV
Left ventricular stroke volume	#SV_LV
Right ventricular stroke volume	#SV_RV

Then we estimate relevant values of 13 parameters of the model so that the simulated values match the clinical measured values of these quantities (personalization). The 13 estimated parameters are presented in the following table (in purple on Figure 1):

Pulmonary compliance	#C_ven_Pul
Systemic compliance	#C_ven_Sys
Pulmonary resistance	#R_ven_Pul
Systemic resistance	#R_ven_Sys
Left ventricular radius	#R_0_1
Aortic resistance	#R_p_
Aortic compliance	#Tau1
Left ventricular contractility	#sigma_0_1
Right ventricular radius	#R_0_2
Pulmonary arterial resistance	#R_p_2
Pulmonary arterial time constant	#Tau2
Right ventricular contractility	#sigma_0_2 (LV contractility)
Initial resting pressure value of the venous system	#P_ve

Parameters estimation was performed as in (243), through the minimization of a regularized cost function $(\hat{S}(x,\hat{O}) = S(x, \hat{O}) + \lambda R(x))$, made first of a data-fit term S (also called goodness of fit), which computes a (normalized) distance between the vector of simulated values (O(x)) and the vector of clinical (target) values Ô:

$$S(x, \hat{O}) = \| (O_M(x) - \hat{O}) \oslash N \|$$

where $\oslash$ is the coordinate by coordinate division with the normalization vector N.

The normalization coefficients in the normalization vector N are 200Pa for the pressures values and 10ml for the volume values. The vector N is

[200,200,200,200,200,200,10,10,10,10]. It provides the scale at which the different quantities are considered well fitted.
The cost function also contains a regularization term R, as described in (243)

$$(R(x) = (x - \mu_R)\Delta^{-1}(x - \mu_R)^T)$$

which depends on a mean μ and a covariance Δ in order to provide prior knowledge. With this formulation, minimizing the regularized cost function leads to the estimation of a Maximum A Posteriori, with a Gaussian prior probability (defined by μ and Δ) and a Gaussian data fit term (or likelihood) defined by the formula of S.

Here we use population-based priors, namely we first perform a personalization on the whole database without priors (without regularization), then we use the distribution of estimated parameter values in this first personalization as prior probability for a second personalization of the whole database (μ and Δ are respectively set to the mean and covariance of estimated parameters at the first personalization). The use of prior probabilities enables to guide the estimation of parameters for which the values are not completely determined from the data. In particular, when multiple sets of parameter values are possible for the same simulated value, the use of prior probabilities promotes the selection of a parameter set for which the variation of individual parameters (from the mean of the population parameters) is minimal, limiting the estimation of extreme values of physiological parameters.

Hemodynamic assessment of PAH patients

Right heart catheterization was performed in the catheterization laboratory at rest in the supine position. The femoral vein approach was commonly used. A balloon-tipped catheter was used to obtain mean right atrial pressure, pulmonary artery systolic and diastolic pressures, as well as PCWP. All measurements were obtained at end expiration at steady state with the patient in a supine position. PCWP was calculated by the computer as the integrated mean. Cardiac output was measured by thermodilution. PVR and systemic vascular resistance, cardiac index, stroke volume, and transpulmonary

gradient were calculated using the standard formulas. Systolic and diastolic blood pressures were obtained using a digital sphygmomanometer at the time of the procedure. PVC is related to the stroke volume and inversely proportional to the difference between pulmonary artery systolic and diastolic pressures. The product of resistance and compliance (PVR × PVC) is referred to as the pulmonary arterial time constant τ.

Statistical analysis

Data were summarized as mean ± standard deviation for continuous variables with normal distribution; median [95% confidence interval] for other continuous variables and number of subjects (%) for categorical variables. The goodness of fit, which describes how well the model fits a set of observations, summarizes the discrepancy between measured or observed values and simulated values. To assess the goodness of fit, the method already described in (243) was used. Correlation coefficients were assessed to test the relation between measured and simulated values as well as Bland-Altman graphs to assess the agreement between simulation and invasive patient data. For all analyses, statistical significance was defined as a p value <0.05. Statistical analyses were performed using MedCalc 16.1 (MedCalc Software, Mariakerke, BE).

RESULTS

Eleven patients with PAH were included. All patients suffered from group 1 PAH (148), 5 patients suffered from idiopathic PAH, 3 from porto-pulmonary hypertension, 2 from PAH associated to connective tissue disease, and 1 from HIV associated PAH. Main characteristics of our population are listed in Table 1. Among these patients, 6 (54.5%) were considered as improving under specific advanced therapy using a classic outcome measure: improvement in WHO class, 6-minute walking test distance and improvement in pulmonary vascular resistance and cardiac output.

Table 1: Main characteristics of our cohort of patients

PAH patients n=11	Baseline	2nd assessment
Age, y	54.1±21	
Female sex, n(%)	5 (45.5)	
WHO class, I/II/II/IV	0/2/6/3	1/4/6/0
Heart rate, bpm	76.1±14.3	78.6±15.6
Mean PA pressure, mmHg	48.6±9.8	42.1±11.3
PCWP, mmHg	10.7±3.0	9.6±2.8
PVR, Wood Unit	8.1±2.5	5.9±3.1
RV echocardiographic diameter, mm	47.3±5.7	46.3±5.5
RV EDV, mL	122.5±44.9	159.2±46.5

Examples of invasive measurements and curves obtained using the circulatory model

Patient 1: 1st assessment with right heart catheterization

RV pressure during right heart catheterization

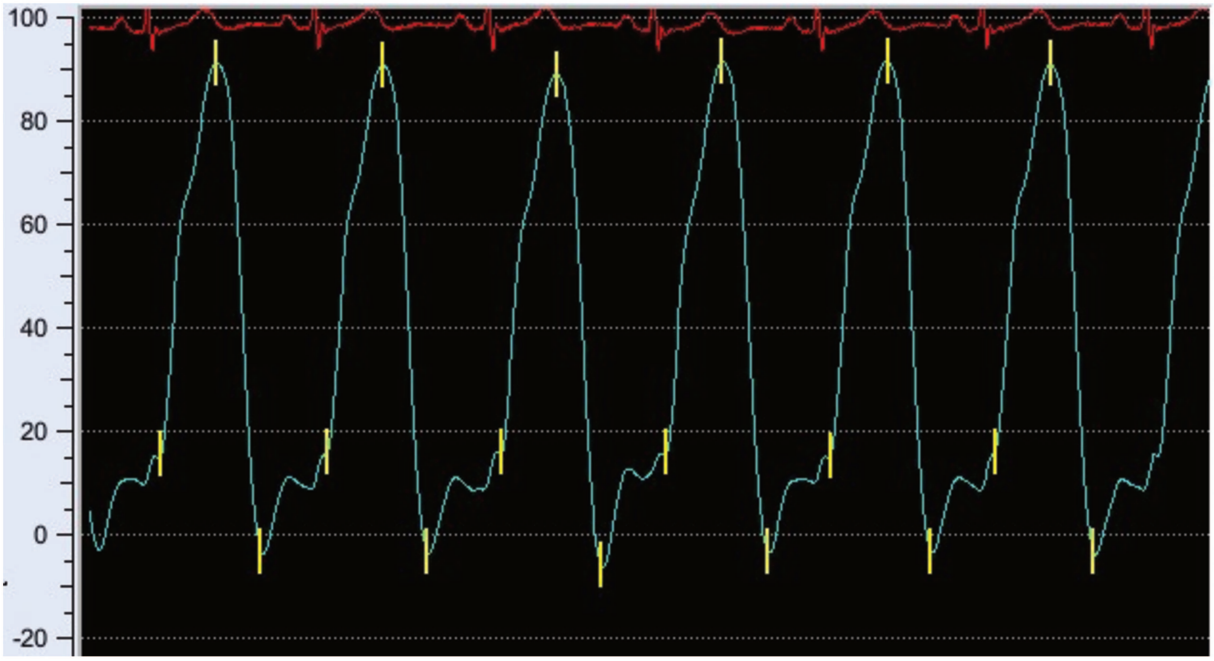

Right atrial pressure

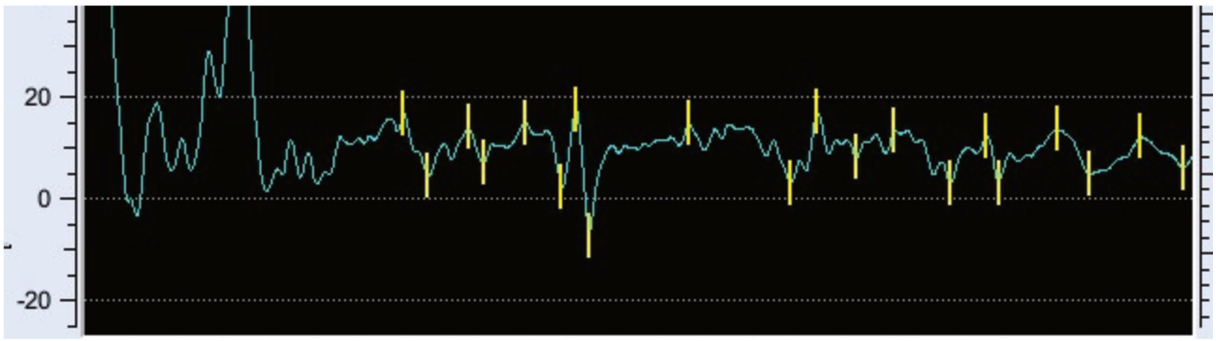

Simulation of the baseline condition in patient 1

Pressure-time curves of right atrial pressure, RV pressure and PA pressure

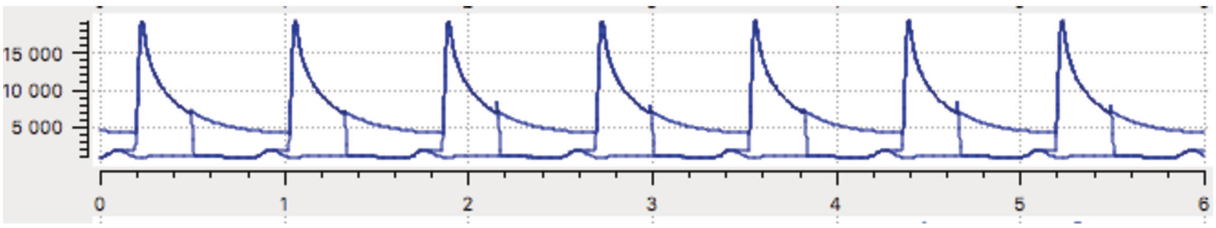

Patient 2

RV pressures:

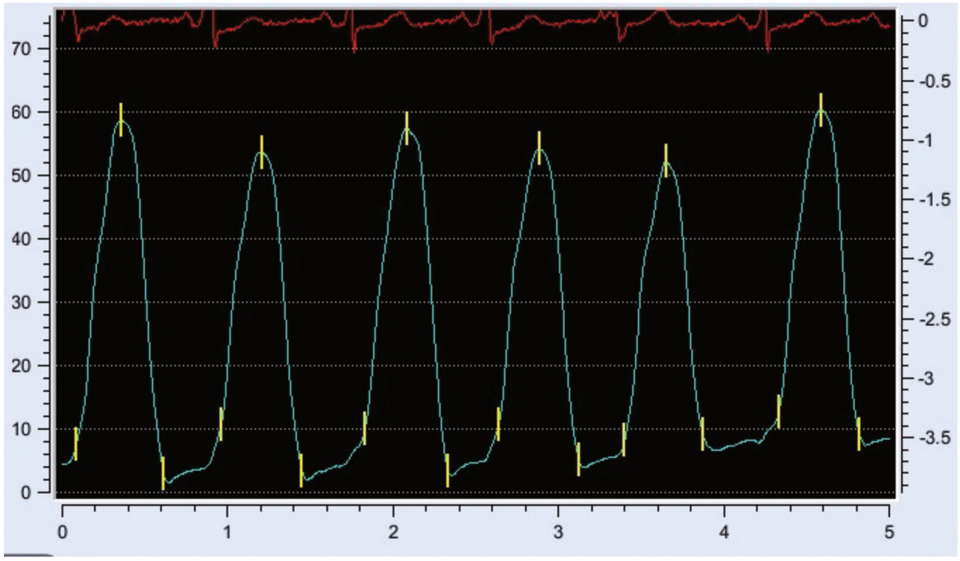

PA pressures:

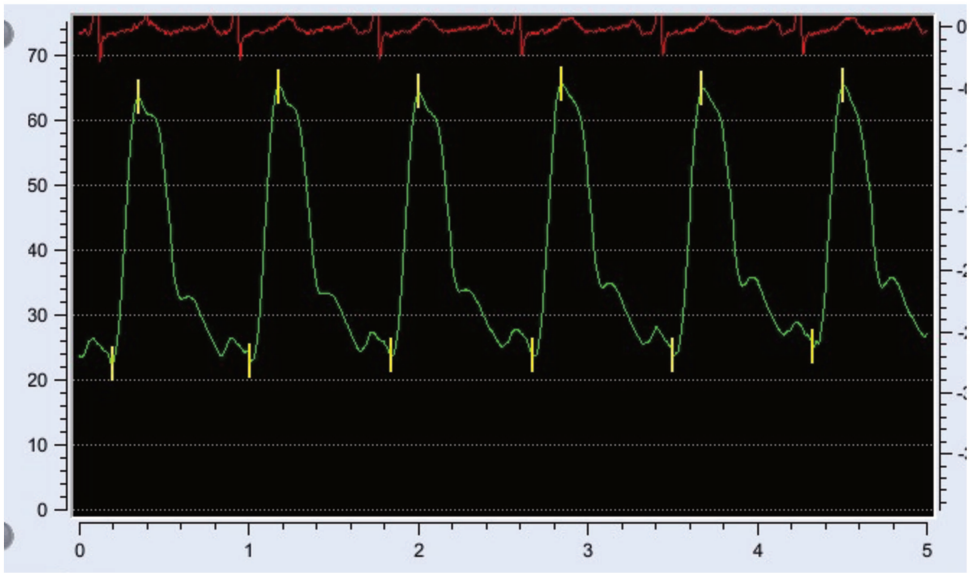

Simulated curves (RV – PA and RA pressures)

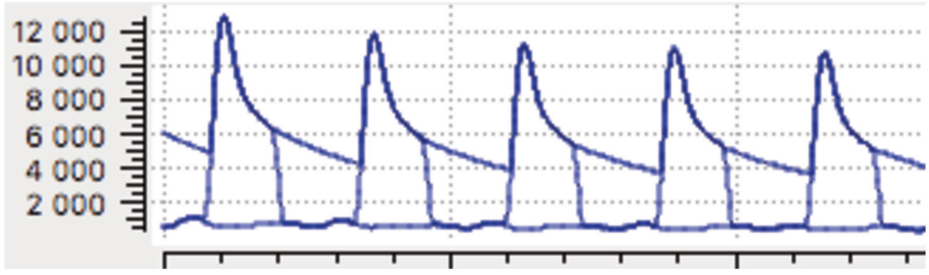

Correlation between simulated values and measures:

After personalisation, an excellent agreement was observed between measured and simulated mean, diastolic PA pressure, pulmonary capillary wedge pressure (r=1 with significant p-values) and between PVR measured by right heart catheterization and simulated in the model (r=0.97; p<0.0001) (Figure 3). The correlation was only modest for tau (r=0.47; p=0.03). There was no relationship between the measured capacitance and the estimated compliance and regarding only simulated measures, no significant correlation was observed between pulmonary compliance and resistance.

The following table 2 presents the goodness of fit in percentage of the target value for each simulation (baseline data / after advanced therapy). The values indicate an excellent fit except in patient 8 regarding baseline assessment.

Table 2: Comparison between simulated and measured parameters in each patient

	LV SV	RV SV	mAo P	dAo P	mPAP	dPAP	RAP
Patient 1	0,6	0,3	0,0	0,0	0,0	0,0	0,3
Patient 2	0,3	0,2	0,0	0,1	0,0	0,1	0,5
Patient 3	0,3	0,6	0,0	0,0	0,0	0,1	0,5
Patient 4	0,2	1,0	0,0	0,0	0,1	0,0	0,0
Patient 5	0,1	0,2	0,1	0,0	0,1	0,1	0,0
Patient 6	0,6	1,4	0,0	0,0	0,1	0,0	0,0
Patient 7	0,4	0,8	0,0	0,0	0,1	0,0	0,2
Patient 8	4,3	88,5	0,1	0,1	0,1	0,1	11,4
Patient 9	0,4	0,8	0,0	0,0	0,0	0,0	0,1
Patient 10	0,7	0,5	0,0	0,0	0,0	0,0	0,1
Patient 11	0,3	0,2	0,0	0,0	0,0	0,0	0,1

Ao, aortic; d, diastolic; LV, left ventricular; m, mean; P, pressure; PAP, pulmonary artery pressure; RAP, right atrial pressure; RV right ventricular; SV, stroke volume.

Figure 5: Correlation of mean PA pressures, pulmonary capillary wedge pressure and pulmonary vascular resistance with simulated observations

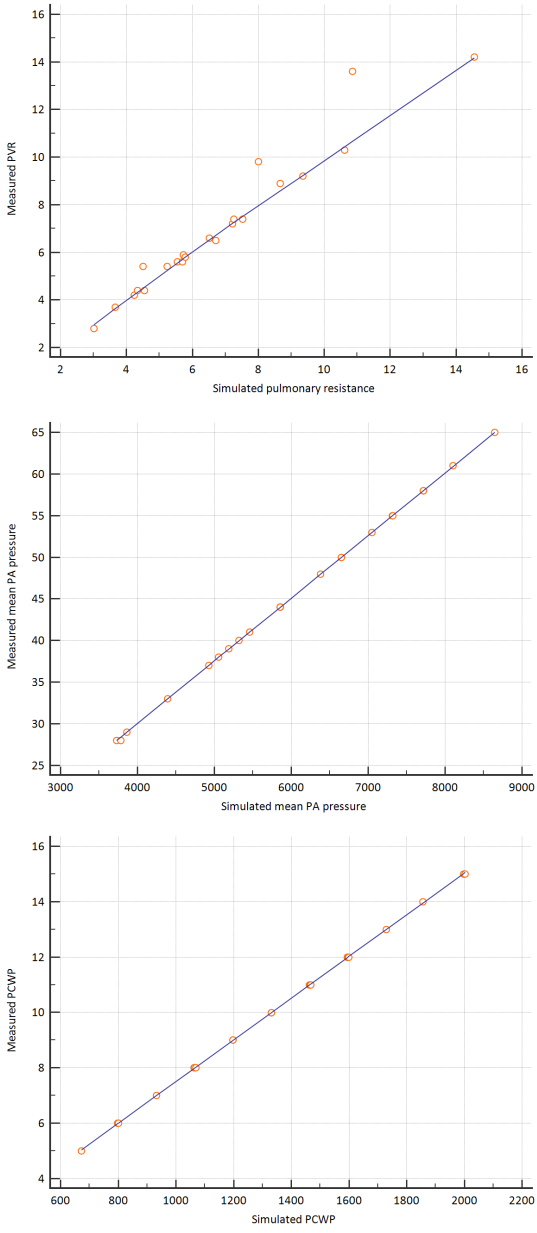

Bland and Altman graph (Figure 6) show an excellent agreement between simulated and measured parameters

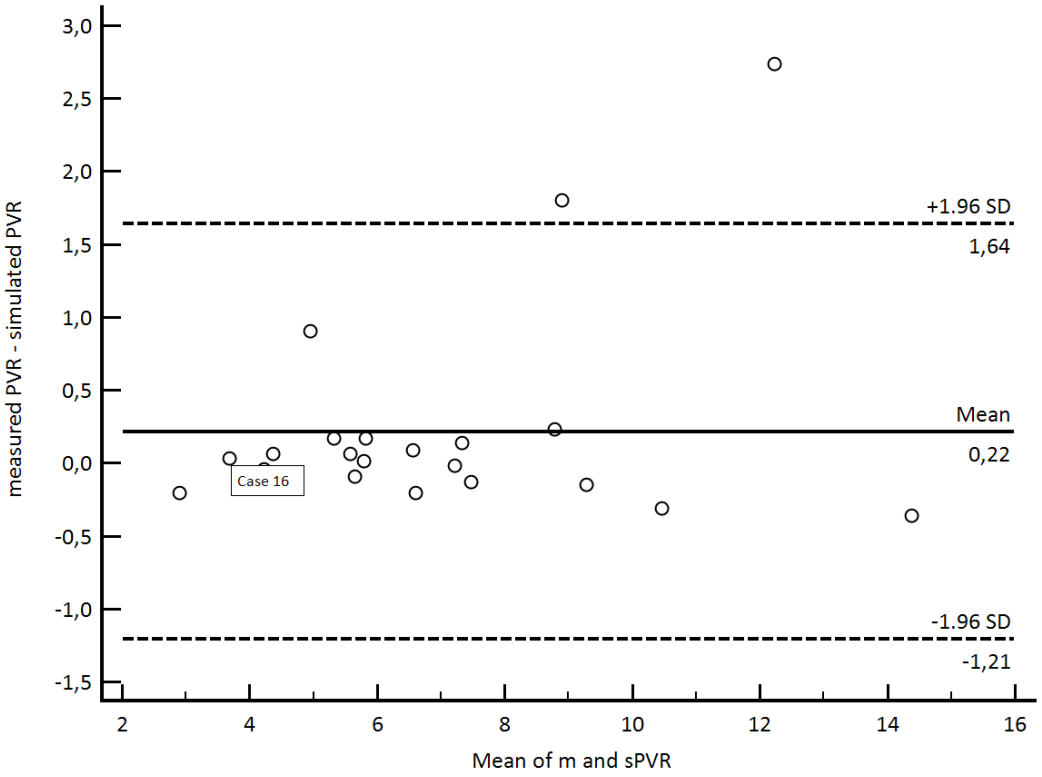

Figure 6: *PVR values:* simulated values are in all cases but 2 within the range [-1.96 SD - +1.96SD]

Evolution of measured and simulated parameters after advanced therapy

Patients 3, 8, 9, 10 and 11 were considered non-responders to advanced therapy because they failed to improve either their WHO class, 6-minute walk test or according to right heart catheterization data.

The observed evolution of hemodynamic parameters is described in the figures below (Figure 7, 8, 9 and 10) where "serie 1" represent the data before therapy and "serie 2", after therapy.

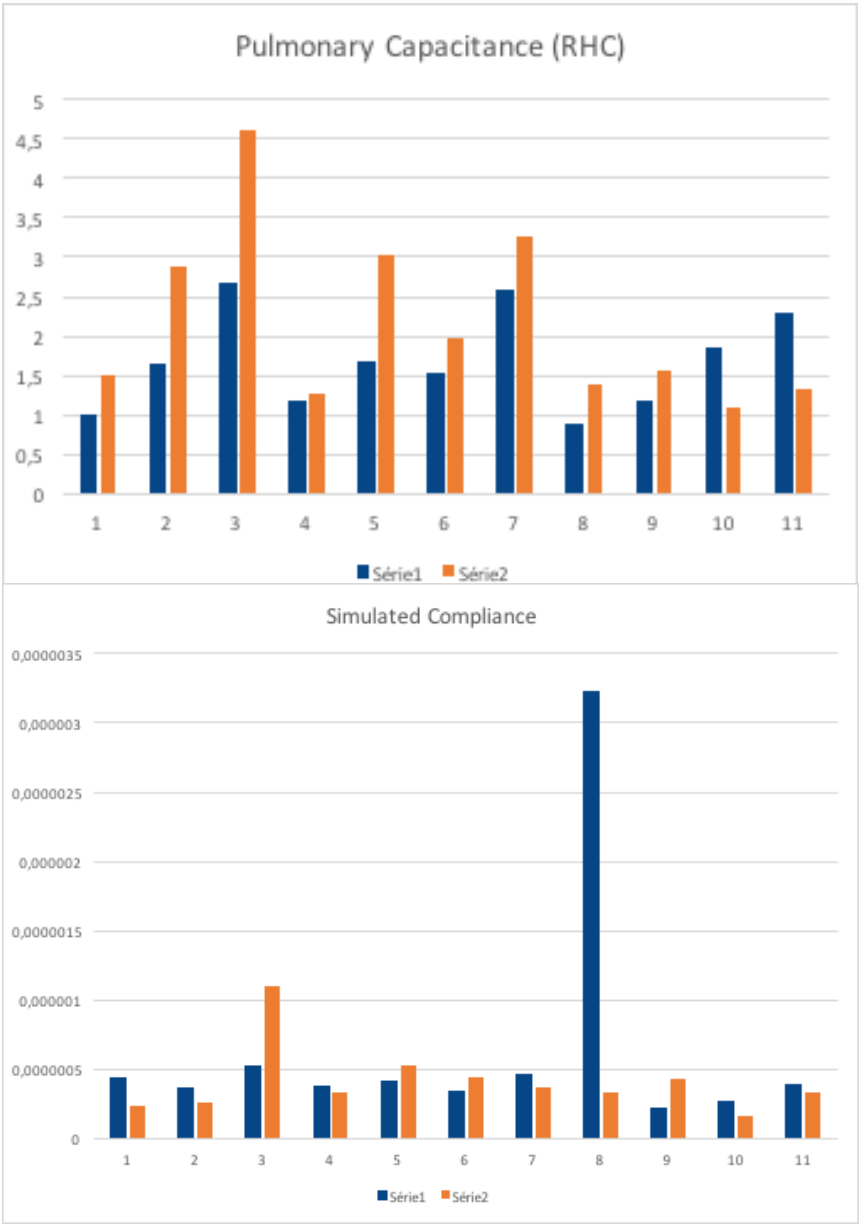

Figure 7: Trends for measured and estimated pulmonary compliance.

The same pattern is observed for the evolution of invasive and estimated compliance, except in patient 8 for whom the model was not correctly fitted.

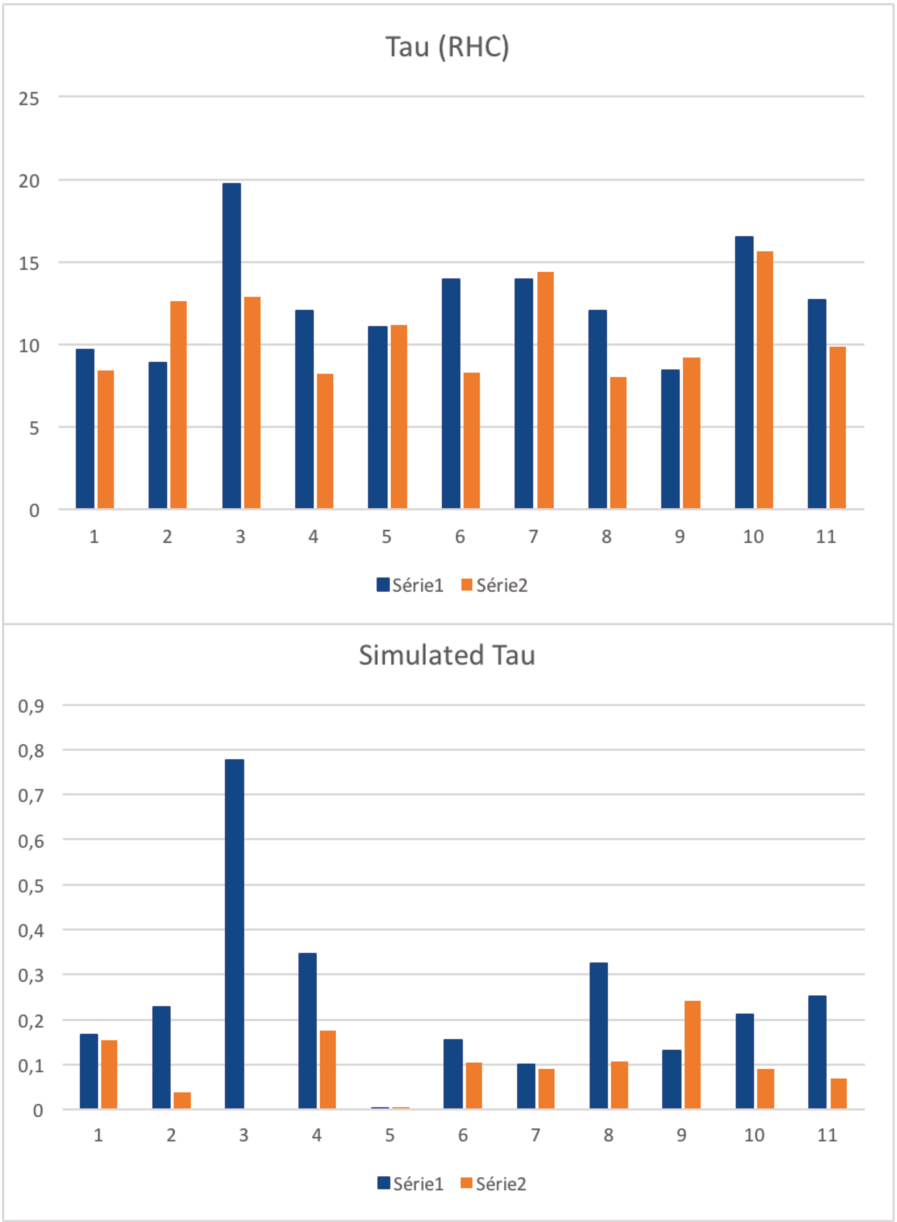

Figure 8: Evolution of the time constant of the pulmonary circulation τ

Overall, the constant τ seems to follow the measured parameters. However, we can notice that advanced therapy seems to have little influence on this constant even in responder patients.

Mean PA pressure only increases in non-responders and Figure 9 illustrates the trend toward lower mean PA pressure after advanced therapy.

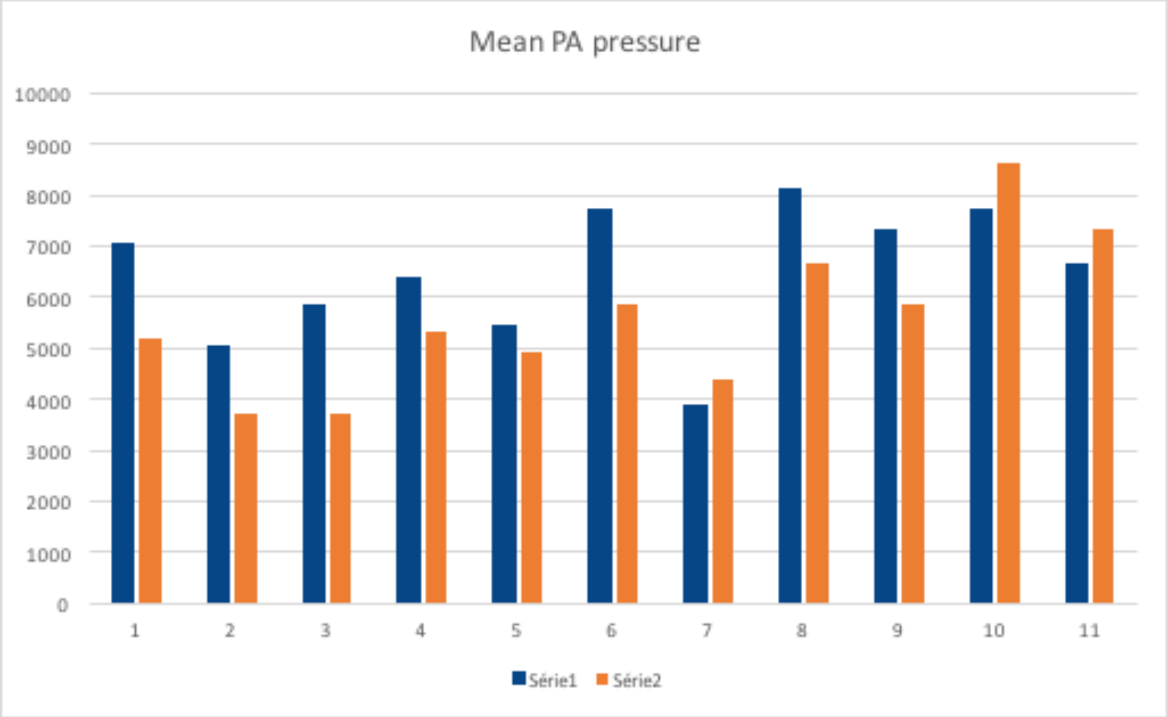

Figure 9: Evolution of mean PA pressure

In general, measured PVR decreases under advanced therapy, except in non-responders. This is clearly illustrated by measured PVR, but also as clearly by simulated PVR (Figure 10).

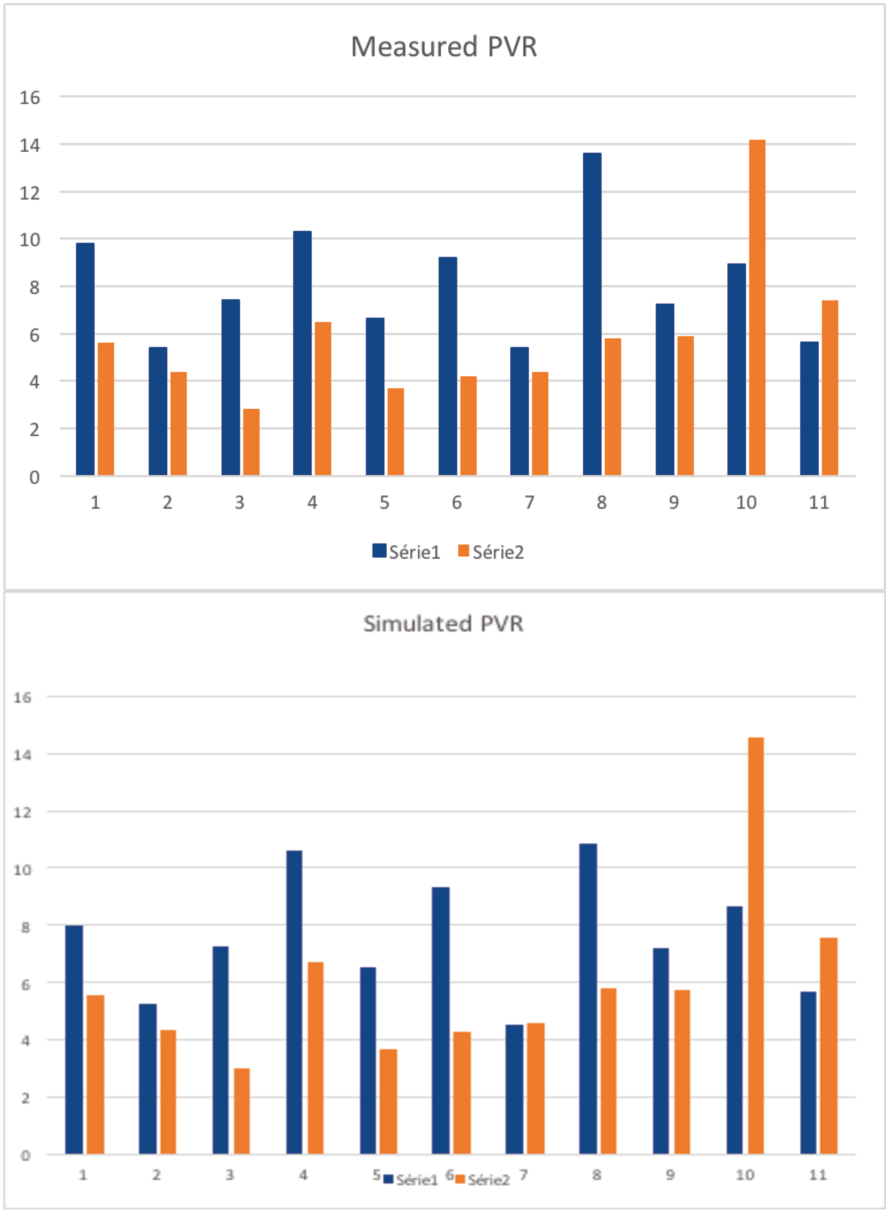

Figure 10: Evolution of PVR under advanced therapy

DISCUSSION

Our results show generally a very good fit of simulated hemodynamic variables as compared with the invasive reference value. We were able to clinically detect the same trends toward improvement under advanced therapy in all patients but one (patient 8), confirming the ability of the model to capture and integrate haemodynamic laws of circulation.

The model allowed an estimation of pulmonary vascular resistance with an excellent agreement with clinically used formulas. This estimation comes from a personalized model using invasive measurements of pulmonary pressure. As these measurements are also available from echocardiography, one could estimate the pulmonary vascular resistance using this circulatory model only on the basis of echocardiographic data. Indeed, peak pulmonary regurgitation (PR) velocity can estimate the mean PA Pressure using the equation mPAP = 4 × PR $Vmax^2$ + right atrial pressure, whereas end-diastolic PR enables the calculation of diastolic PA pressure using the equation dPAP = 4 × end-diastolic PR $velocity^2$ + right atrial pressure. Echocardiography itself can help predict if PVR are elevated or not: dividing tricuspid regurgitation velocity peak (m/s) by pulmonary velocity-time integral (VTI) (in cm) allows differentiation between high PA pressure related to high pulmonary vascular resistance (ratio ≥0.2) or to increased pulmonary blood flow (<0.2) (as in atrial septal defect for example). However, a reliable estimation of PVR using a formula that includes this ratio (PVR = TR Vmax /VTI × 10 + 0.16) is not valid in patients with elevated pulmonary vascular resistance (244). Cardiac magnetic resonance, studying pulmonary blood flows could also be helpful in non-invasively measuring pulmonary pressures (245, 246). Those applications of models could help reducing the number of invasive procedures, especially in children for example.

An excellent correlation has been found between invasive and simulated parameters. Another group studied a OD-model in pulmonary hypertension with a different methodology (247). The authors aimed to extrapolate unavailable haemodynamic data using the model and have also demonstrated a correlation between

their model estimated values and measured patients parameters. However, personalisation of this model has not been presented.

During a hemodynamic study, capacitance can be assessed and relates to compliance, which cannot directly be assessed using right heart catheterization. However, the model allows us to analyse pulmonary compliance, These data are of interest in PAH (239, 240, 248, 249), group II pulmonary hypertension (250), group IV pulmonary hypertension (251) but also in heart failure related to systolic dysfunction (252) or in patients with preserved systolic function (253) in whom pulmonary capacitance is a strong and earlier marker of prognosis. In our study, even if not significantly correlated, simulated compliance exhibits the same profile as measured capacitance indicating the potential importance of this observation. In particular, as it is now recognized that patients with heart failure should not undergo regular right heart catheterization for evaluation purpose, simulation of pulmonary compliance using a circulatory model might be a future possibility that needs further investigation.

Using our model, we tried to simulate the evolution of haemodynamic parameters under the effect of targeted advanced PAH therapy. This method, with the help of a larger patient database, could help simulate and predict the evolution of a patient under advanced therapy, integrating not only haemodynamic parameters but also imaging, electrophysiology data and background data for example. Examples of large studies including multi-modality model simulation (235) have been recently published.

Modeling and simulation enable us to perform investigations where experimentation does not exist, or is costly or unethical. This is of critical importance in the field of therapeutic research, if evaluated in a model, we can thus theoretically perform an unlimited number of experiments. Indeed, there would not be any recruitment difficulties. Several pediatric issues exist regarding the participation of children in a research, models could be a solution, creating an infinity of virtual physiological patients. Recently, a noninvasive personalization of a cardiac electrophysiology model from body surface potential mapping has been used to predict the response to different pacing conditions (254). The use of computational modeling in pharmaceutical or even device research will allow less reliance on animal and human data. This solution will also be

cost-effective especially when trying to develop new therapies. The validity and direct applicability of model simulation, as in our study, will help foster confidence and increase the acceptance of this method.

To conclude, this preliminary work allowed a solid reproduction of measured PVR using a personalized model. It also allowed to emphasise the limitations of the model, in order to improve some of its components. This is a new step toward the generalization of personalised models in medicine.

CONCLUSION AND PERSPECTIVES

CONTENTS

Despite major advances in the field of physiology and cardiology research, the right ventricle remains the “grey” area of the heart for many physicians. Even with this reputation of being the “less informative” ventricle, imaging and modelling the right ventricle can provide substantial data in various diseases. Usually when the RV fails, there is a rise in poor clinical outcomes. Studying the RV function is challenging but of critical importance, especially in conditions such as pulmonary hypertension or congenital heart disease. This was the main focus of our work. Main results and conclusions are presented in the next section.

SUMMARY OF THE MAIN CONTRIBUTIONS

Strain study in pulmonary hypertension patients.

In chapter 2, we describe for the first time with a dedicated RV software the analysis of RV strain in patients with pulmonary hypertension as compared to healthy controls. Our results highlight the role of dominant regions of the RV using deformation analysis: the inferior and lateral wall. We observed a gradient in RV area strain alteration according to the severity of the disease (World Health Organization (WHO) classification). We also demonstrated in this large cohort of patients, the prognostic role of RV area strain in pulmonary hypertension. Indeed, the mortality rate of patients with RV area strain > -18% was almost multiplied by 2.

Longitudinal study of strain in pulmonary hypertension patients.

In chapter 3, our study demonstrates the added value of serial 3D echocardiographic assessment as compared to baseline only in pulmonary hypertension patients. Indeed, changes in RV function (area strain) were strongly associated with outcomes. The most significant decrease in RV strain occurred within the septum, especially in patients with clinical outcomes such as mortality related to pulmonary hypertension, lung transplantation, hospitalization for heart failure related to pulmonary hypertension, need to start therapies targeting the PGI2 pathway. A composite score

including changes in WHO function class, BNP and RV global AS identified a high-risk population with increased mortality.

Shape and strain study in congenital heart disease patients.

In chapter 4, we studied both RV strain and shape in RV volume overload patients (tetralogy of Fallot (TOF) and atrial septal defect (ASD)) as compared to healthy volunteers. We observed differences in both TOF and ASD patients versus controls in terms of RV shape using curvature indices. However, except in the infundibulum, almost no difference in RV shape appeared between TOF and ASD patients using curvature. In TOF patients, the inferior wall curvature was strongly correlated to QRS duration, a known prognostic marker in TOF. Regarding deformation data, RV strain in ASD patients was almost similar to the one in controls. In TOF patients, both strain were altered, especially in the septum, lateral and inferior wall. The RV in TOF patients tolerates probably less volume overload than in ASD patients, given the history of ventriculotomy with myocardial damage and previous pressure overload. We believe these innovative methods will allow us to gain further insights into RV failure in different loading conditions.

Modelling study in pulmonary hypertension patients

In chapter 5, a model was personalised to 11 pulmonary arterial hypertension patients' data before and after advanced pulmonary arterial hypertension advanced therapy. The model consistently reproduced the cardiovascular circulation of the patients, and the estimated parameters reflected well the expected changes with therapy. Estimated pulmonary vascular resistances were strongly correlated with measured pulmonary resistances.

PERSPECTIVES

Our work illustrates how imaging together with computational statistics can help characterize the right ventricle in various loading conditions.

Clearly, deformation imaging using 3D echocardiography provides clinically relevant data, especially in the setting of pulmonary hypertension. In a multi-centric study, we are currently assessing RV strain in adult patients with pulmonary arterial hypertension associated with congenital heart defects, in comparison with other causes as their prognosis is better and seems related to a relatively preserved RV function. We hope that 3D RV studies such as ours will help better understand right ventricular adaptation.

In chapter 3, the hypothesis that a change in RV function has more prognostic significance than a baseline measurement has been verified. Although expected, this is an innovative message supporting the need to standardize all the measurements performed in a patient to increase the comparability.

In chapter 4, we observed differences in RV shape and strain in tetralogy of Fallot patients. In these patients, the question of the timing of pulmonary valve replacement remains controversial. Studying RV function using strain and probably shape has potential to help clinical decision making, together with cardiac magnetic resonance data, the current reference. In congenital cardiology, the methods demonstrated in this work could be extended to patients with Ebstein's anomaly, systemic right ventricle or hypoplastic left heart syndrome, who would all benefit from a thorough investigation of the RV.

Assessing the shape of the RV is challenging. Standard parameters with 2D-echocardiography are already helpful but investigating curvature indices using 3D echocardiography is promising. Given the various approaches of ventricular shape estimation, a multimodal assessment of shape including both local indices such as curvature and global measurements such as shape variability encoded in a computational atlas are promising to better understand RV remodelling according to various loading conditions.

However, the lack of standardisation of the features extraction methods might be a limitation, as notably pointed out by the scientific community when analysing the strain. Efforts to homogenise strain and shape calculations as well as transparency from manufacturers might help increase and develop the applicability of these methods.

Furthermore, as described using classic RV function parameters, RV strain and shape data could help provide additional information and risk stratification in patients with left heart disease a very frequent condition. Thus, the development of validated tools to assess the RV is of critical importance in cardiology.

In chapter 5, we present the preliminary results of a circulatory model personalisation in patients with pulmonary arterial hypertension. The development and validation of this multiscale model might help avoid invasive hemodynamic measurement. This requires further investigation and might be particularly helpful in young patients.

We expect in the next future the development of research and applications combining both imaging, electrophysiological data but also integrating bio-cellular information together with advanced models to allow better understanding of RV function and earlier detection of RV failure.

REFERENCES

1. Harvey W. Exercitatio Anatomica de Motu Cordis et Sanguinis in Animalibus. 1628.

2. Starr I, Jeffers W, Meade R. The absence of conspicuous increments of venous pressure after severe damage to the right ventricle of the dog, with a discussion of the relation between clinical congestive failure and heart disease. *Am Heart J*. 1943;26:291-301.

3. Bakos A. The question of the function of the right ventricular myocardium: an experimental study. *Circulation*. 1950;1:724-31.

4. Kagan A. Dynamic responses of the right ventricle following extensive damage by cauterization. *Circulation*. 1952;5:816-23.

5. Ho SY, Nihoyannopoulos P. Anatomy, echocardiography, and normal right ventricular dimensions. *Heart*. 2006;92 Suppl 1:i2-13.

6. Kjaergaard J, Iversen KK, Vejlstrup NG, Smith J, Bonhoeffer P, Sondergaard L, *et al*. Impacts of acute severe pulmonary regurgitation on right ventricular geometry and contractility assessed by tissue-Doppler echocardiography. *Eur J Echocardiogr*. 2009;11:19-26.

7. Yamasaki Y, Nagao M, Kamitani T, Yamanouchi T, Kawanami S, Yamamura K, *et al*. Clinical impact of left ventricular eccentricity index using cardiac MRI in assessment of right ventricular hemodynamics and myocardial fibrosis in congenital heart disease. *Eur Radiol*. 2016;26:3617-25.

8. Ryan T, Petrovic O, Dillon JC, Feigenbaum H, Conley MJ, Armstrong WF. An echocardiographic index for separation of right ventricular volume and pressure overload. *J Am Coll Cardiol*. 1985;5:918-27.

9. Sanchez-Quintana D, Anderson RH, Ho SY. Ventricular myoarchitecture in tetralogy of Fallot. *Heart*. 1996;76:280-6.

10. Agger P, Lakshminrusimha S, Laustsen C, Gugino S, Frandsen JR, Smerup M, *et al*. The myocardial architecture changes in persistent pulmonary hypertension of the newborn in an ovine animal model. *Pediatr Res*. 2016;79:565-74.

11. Rallidis LS, Makavos G, Nihoyannopoulos P. Right ventricular involvement in coronary artery disease: role of echocardiography for diagnosis and prognosis. *J Am Soc Echocardiogr*. 2014;27:223-9.

12. Tabima DM, Philip JL, Chesler NC. Right Ventricular-Pulmonary Vascular Interactions. *Physiology (Bethesda)*. 2017;32:346-56.

13. Haddad F, Hunt SA, Rosenthal DN, Murphy DJ. Right ventricular function in cardiovascular disease, part I: Anatomy, physiology, aging, and functional assessment of the right ventricle. *Circulation*. 2008;117:1436-48.

14. Vonk-Noordegraaf A, Westerhof N. Describing right ventricular function. *Eur Respir J*. 2013;41:1419-23.

15. Voelkel NF, Quaife RA, Leinwand LA, Barst RJ, McGoon MD, Meldrum DR, *et al*. Right Ventricular Function and Failure: Report of a National Heart, Lung, and Blood Institute Working Group on Cellular and Molecular Mechanisms of Right Heart Failure. *Circulation*. 2006;114:1883-91.

16. Guazzi M, Bandera F, Pelissero G, Castelvecchio S, Menicanti L, Ghio S, *et al*. Tricuspid annular plane systolic excursion and pulmonary arterial systolic pressure relationship in heart failure: an index of right ventricular contractile function and prognosis. *Am J Physiol Heart Circ Physiol*. 2013;305:H1373-81.

17. Sabe MA, Sabe SA, Kusunose K, Flamm SD, Griffin BP, Kwon DH. Predictors and Prognostic Significance of Right Ventricular Ejection Fraction in Patients With Ischemic Cardiomyopathy. *Circulation*. 2016;134:656-65.

18. Gorter TM, van Veldhuisen DJ, Bauersachs J, Borlaug BA, Celutkiene J, Coats AJS, *et al*. Right heart dysfunction and failure in heart failure with preserved ejection fraction: mechanisms and management. Position statement on behalf of the Heart Failure Association of the European Society of Cardiology. *Eur J Heart Fail*. 2017. *In Press*.

19. Melenovsky V, Hwang SJ, Lin G, Redfield MM, Borlaug BA. Right heart dysfunction in heart failure with preserved ejection fraction. *Eur Heart J*. 2014;35:3452-62.

20. Haddad F, Fisher P, Pham M, Berry G, Weisshaar D, Kuppahally S, *et al*. Right ventricular dysfunction predicts poor outcome following hemodynamically compromising rejection. *J Heart Lung Transplant*. 2009;28:312-9.

21. Tamborini G, Muratori M, Brusoni D, Celeste F, Maffessanti F, Caiani EG, *et al*. Is right ventricular systolic function reduced after cardiac surgery? A two- and three-dimensional echocardiographic study. *Eur J Echocardiogr*. 2009;10:630-4.

22. D'Andrea A, Salerno G, Scarafile R, Riegler L, Gravino R, Castaldo F, *et al.* Right ventricular myocardial function in patients with either idiopathic or ischemic dilated cardiomyopathy without clinical sign of right heart failure: effects of cardiac resynchronization therapy. *Pacing Clin Electrophysiol*. 2009;32:1017-29.

23. Baumgartner H, Falk V, Bax JJ, De Bonis M, Hamm C, Holm PJ, *et al*. 2017 ESC/EACTS Guidelines for the management of valvular heart disease. *Eur Heart J*. 2017;38:2739-91.

24. Koifman E, Didier R, Patel N, Jerusalem Z, Kiramijyan S, Ben-Dor I, *et al.* Impact of right ventricular function on outcome of severe aortic stenosis patients undergoing transcatheter aortic valve replacement. *Am Heart J*. 2017;184:141-7.

25. Le Tourneau T, Deswarte G, Lamblin N, Foucher-Hossein C, Fayad G, Richardson M, *et al.* Right ventricular systolic function in organic mitral regurgitation: impact of biventricular impairment. *Circulation*. 2013;127:1597-608.

26. Moceri P, Baudouy D, Chiche O, Cerboni P, Bouvier P, Chaussade C, *et al.* Imaging in pulmonary hypertension: Focus on the role of echocardiography. *Arch Cardiovasc Dis*. 2014;107:261-71.

27. Sutendra G, Dromparis P, Paulin R, Zervopoulos S, Haromy A, Nagendran J, *et al*. A metabolic remodeling in right ventricular hypertrophy is associated with decreased angiogenesis and a transition from a compensated to a decompensated state in pulmonary hypertension. *J Mol Med (Berl)*. 2013;91:1315-27.

28. Burgess MI, Mogulkoc N, Bright-Thomas RJ, Bishop P, Egan JJ, Ray SG. Comparison of echocardiographic markers of right ventricular function in determining prognosis in chronic pulmonary disease. *J Am Soc Echocardiogr*. 2002;15:633-9.

29. van Wolferen SA, Marcus JT, Boonstra A, Marques KM, Bronzwaer JG, Spreeuwenberg MD, *et al*. Prognostic value of right ventricular mass, volume, and function in idiopathic pulmonary arterial hypertension. *Eur Heart J*. 2007;28:1250-7.

30. Zylkowska J, Kurzyna M, Florczyk M, Burakowska B, Grzegorczyk F, Burakowski J, *et al*. Pulmonary artery dilatation correlates with the risk of unexpected death in chronic arterial or thromboembolic pulmonary hypertension. *Chest*. 2012;142:1406-16.

31. Hinderliter AL, Willis PWt, Long WA, Clarke WR, Ralph D, Caldwell EJ, *et al*. Frequency and severity of tricuspid regurgitation determined by Doppler echocardiography in primary pulmonary hypertension. *Am J Cardiol*. 2003;91:1033-7, A9.

32. Lang RM, Bierig M, Devereux RB, Flachskampf FA, Foster E, Pellikka PA, *et al*. Recommendations for chamber quantification. *Eur J Echocardiogr*. 2006;7:79-108.

33. Mauritz GJ, Kind T, Marcus JT, Bogaard HJ, van de Veerdonk M, Postmus PE*, et al*. Progressive changes in right ventricular geometric shortening and long-term survival in pulmonary arterial hypertension. *Chest*. 2012;141:935-43.

34. Brown SB, Raina A, Katz D, Szerlip M, Wiegers SE, Forfia PR. Longitudinal shortening accounts for the majority of right ventricular contraction and improves after pulmonary vasodilator therapy in normal subjects and patients with pulmonary arterial hypertension. *Chest*. 2011;140:27-33.

35. Sato T, Tsujino I, Ohira H, Oyama-Manabe N, Yamada A, Ito YM, *et al*. Validation study on the accuracy of echocardiographic measurements of right ventricular systolic function in pulmonary hypertension. *J Am Soc Echocardiogr*. 2012;25:280-6.

36. Ueti OM, Camargo EE, Ueti Ade A, de Lima-Filho EC, Nogueira EA. Assessment of right ventricular function with Doppler echocardiographic indices derived from tricuspid annular motion: comparison with radionuclide angiography. *Heart*. 2002;88:244-8.

37. Forfia PR, Fisher MR, Mathai SC, Housten-Harris T, Hemnes AR, Borlaug BA, *et al*. Tricuspid Annular Displacement Predicts Survival in Pulmonary Hypertension. *Am J Respir Crit Care Med*. 2006;174:1034-41.

38. Mathai SC, Sibley CT, Forfia PR, Mudd JO, Fisher MR, Tedford RJ, *et al*. Tricuspid annular plane systolic excursion is a robust outcome measure in systemic sclerosis-associated pulmonary arterial hypertension. *J Rheumatol*. 2011;38:2410-8.

39. Moceri P, Dimopoulos K, Liodakis E, Germanakis I, Kempny A, Diller G-P, *et al*. Echocardiographic Predictors of Outcome in Eisenmenger Syndrome. *Circulation*. 2012;126:1461-8.

40. Koestenberger M, Nagel B, Ravekes W, Everett AD, Stueger HP, Heinzl B, *et al*. Tricuspid annular plane systolic excursion and right ventricular ejection fraction in pediatric and adolescent patients with tetralogy of Fallot, patients with atrial septal defect, and age-matched normal subjects. *Clin Res Cardiol*. 2011;100:67-75.

41. Koestenberger M, Nagel B, Ravekes W, Everett AD, Stueger HP, Heinzl B, *et al*. Systolic right ventricular function in pediatric and adolescent patients with tetralogy of Fallot: echocardiography versus magnetic resonance imaging. *J Am Soc Echocardiogr*. 2011;24:45-52.

42. Lopez-Candales A, Rajagopalan N, Saxena N, Gulyasy B, Edelman K, Bazaz R. Right ventricular systolic function is not the sole determinant of tricuspid annular motion. *Am J Cardiol*. 2006;98:973-7.

43. Meluzin J, Spinarova L, Bakala J, Toman J, Krejci J, Hude P, *et al*. Pulsed Doppler tissue imaging of the velocity of tricuspid annular systolic motion; a new, rapid, and non-invasive method of evaluating right ventricular systolic function. *Eur Heart J*. 2001;22:340-8.

44. Rudski LG, Lai WW, Afilalo J, Hua L, Handschumacher MD, Chandrasekaran K, *et al*. Guidelines for the Echocardiographic Assessment of the Right Heart in Adults: A Report from the American Society of Echocardiography. *J Am Soc Echocardiogr*. 2010;23:685-713.

45. Calcutteea A, Chung R, Lindqvist P, Hodson M, Henein MY. Differential right ventricular regional function and the effect of pulmonary hypertension: three-dimensional echo study. *Heart*. 2011;97:1004-11.

46. Vogel M, Schmidt MR, Kristiansen SB, Cheung M, White PA, Sorensen K, *et al*. Validation of myocardial acceleration during isovolumic contraction as a novel noninvasive index of right ventricular contractility: comparison with ventricular pressure-volume relations in an animal model. *Circulation*. 2002;105:1693-9.

47. Kjaergaard J, Snyder EM, Hassager C, Oh JK, Johnson BD. Impact of preload and afterload on global and regional right ventricular function and pressure: a quantitative echocardiography study. *J Am Soc Echocardiogr*. 2006;19:515-21.

48. Yang T, Liang Y, Zhang Y, Gu Q, Chen G, Ni XH, *et al*. Echocardiographic parameters in patients with pulmonary arterial hypertension: correlations with right ventricular ejection fraction derived from cardiac magnetic resonance and hemodynamics. *PLoS One*. 2013;8:e71276.

49. Ernande L, Cottin V, Leroux PY, Girerd N, Huez S, Mulliez A, *et al*. Right isovolumic contraction velocity predicts survival in pulmonary hypertension. *J Am Soc Echocardiogr*. 2013;26:297-306.

50. Toyono M, Harada K, Tamura M, Yamamoto F, Takada G. Myocardial acceleration during isovolumic contraction as a new index of right ventricular contractile function and its relation to pulmonary regurgitation in patients after repair of tetralogy of Fallot. *J Am Soc Echocardiogr*. 2004;17:332-7.

51. Tei C, Dujardin KS, Hodge DO, Bailey KR, McGoon MD, Tajik AJ, *et al*. Doppler echocardiographic index for assessment of global right ventricular function. *J Am Soc Echocardiogr*. 1996;9:838-47.

52. Rojo EC, Rodrigo JL, Perez de Isla L, Almeria C, Gonzalo N, Aubele A, *et al*. Disagreement between tissue Doppler imaging and conventional pulsed wave Doppler in the measurement of myocardial performance index. *Eur J Echocardiogr*. 2006;7:356-64.

53. Sebbag I, Rudski LG, Therrien J, Hirsch A, Langleben D. Effect of chronic infusion of epoprostenol on echocardiographic right ventricular myocardial performance

index and its relation to clinical outcome in patients with primary pulmonary hypertension. *Am J Cardiol*. 2001;88:1060-3.

54. Blanchard DG, Malouf PJ, Gurudevan SV, Auger WR, Madani MM, Thistlethwaite P, *et al*. Utility of right ventricular Tei index in the noninvasive evaluation of chronic thromboembolic pulmonary hypertension before and after pulmonary thromboendarterectomy. *JACC Cardiovasc imaging*. 2009;2:143-9.

55. Dyer KL, Pauliks LB, Das B, Shandas R, Ivy D, Shaffer EM, *et al*. Use of myocardial performance index in pediatric patients with idiopathic pulmonary arterial hypertension. *J Am Soc Echocardiogr*. 2006;19:21-7.

56. Norozi K, Buchhorn R, Alpers V, Arnhold JO, Schoof S, Zoege M, *et al.* Relation of systemic ventricular function quantified by myocardial performance index (Tei) to cardiopulmonary exercise capacity in adults after Mustard procedure for transposition of the great arteries. *Am J Cardiol*. 2005;96:1721-5.

57. Eidem BW, O'Leary PW, Tei C, Seward JB. Usefulness of the myocardial performance index for assessing right ventricular function in congenital heart disease. *Am J Cardiol*. 2000;86:654-8.

58. Yasuoka K, Harada K, Toyono M, Tamura M, Yamamoto F. Tei index determined by tissue Doppler imaging in patients with pulmonary regurgitation after repair of tetralogy of Fallot. *Pediatr Cardiol*. 2004;25:131-6.

59. Mercer-Rosa L, Yang W, Kutty S, Rychik J, Fogel M, Goldmuntz E. Quantifying pulmonary regurgitation and right ventricular function in surgically repaired tetralogy of Fallot: a comparative analysis of echocardiography and magnetic resonance imaging. *Circ Cardiovasc Imaging*. 2012;5:637-43.

60. Babu-Narayan SV, Prati D, Rydman R, Dimopoulos K, Diller GP, Uebing A, *et al*. Dyssynchrony and electromechanical delay are associated with focal fibrosis in the systemic right ventricle - Insights from echocardiography. *Int J Cardiol.* 2016;220:382-8.

61. Lindqvist P, Waldenstrom A, Wikstrom G, Kazzam E. Right ventricular myocardial isovolumic relaxation time and pulmonary pressure. *Clin Physiol Funct Imaging.* 2006;26:1-8.

62. Mauritz GJ, Marcus JT, Westerhof N, Postmus PE, Vonk-Noordegraaf A. Prolonged right ventricular post-systolic isovolumic period in pulmonary arterial hypertension is not a reflection of diastolic dysfunction. *Heart*. 2011;97:473-8.

63. Alkon J, Humpl T, Manlhiot C, McCrindle BW, Reyes JT, Friedberg MK. Usefulness of the right ventricular systolic to diastolic duration ratio to predict functional capacity and survival in children with pulmonary arterial hypertension. *Am J Cardiol*. 2010;106:430-6.

64. Friedberg MK, Silverman NH. The systolic to diastolic duration ratio in children with hypoplastic left heart syndrome: a novel Doppler index of right ventricular function. *J Am Soc Echocardiogr*. 2007;20:749-55.

65. Fukuda Y, Tanaka H, Sugiyama D, Ryo K, Onishi T, Fukuya H, *et al*. Utility of right ventricular free wall speckle-tracking strain for evaluation of right ventricular performance in patients with pulmonary hypertension. *J Am Soc Echocardiogr*. 2011;24:1101-8.

66. Haeck ML, Scherptong RW, Marsan NA, Holman ER, Schalij MJ, Bax JJ*, et al*. Prognostic value of right ventricular longitudinal peak systolic strain in patients with pulmonary hypertension. *Circ Cardiovasc Imaging*. 2012;5:628-36.

67. Moceri P, Iriart X, Bouvier P, Baudouy D, Gibelin P, Saady R, *et al*. Speckle-tracking imaging in patients with Eisenmenger syndrome. *Arch Cardiovasc Dis*. 2016;109:104-12.

68. Moceri P, Bouvier P, Baudouy D, Dimopoulos K, Cerboni P, Wort SJ*, et al*. Cardiac remodelling amongst adults with various aetiologies of pulmonary arterial hypertension including Eisenmenger syndrome-implications on survival and the role of right ventricular transverse strain. *Eur Heart J Cardiovasc Imaging*. 2017;18:1262-70

69. Dragulescu A, Grosse-Wortmann L, Redington A, Friedberg MK, Mertens L. Differential effect of right ventricular dilatation on myocardial deformation in patients with atrial septal defects and patients after tetralogy of Fallot repair. *Int J Cardiol*. 2013;168:803-10.

70. Friedberg MK, Fernandes FP, Roche SL, Slorach C, Grosse-Wortmann L, Manlhiot C, *et al*. Relation of right ventricular mechanics to exercise tolerance in children after tetralogy of Fallot repair. *Am Heart J*. 2013;165:551-7.

71. Menting ME, van den Bosch AE, McGhie JS, Eindhoven JA, Cuypers JA, Witsenburg M, *et al*. Assessment of ventricular function in adults with repaired Tetralogy of Fallot using myocardial deformation imaging. *Eur Heart J Cardiovasc Imaging*. 2015;16:1347-57.

72. Valente AM, Cook S, Festa P, Ko HH, Krishnamurthy R, Taylor AM, *et al*. Multimodality imaging guidelines for patients with repaired tetralogy of fallot: a report from the AmericanSsociety of Echocardiography: developed in collaboration with the Society for Cardiovascular Magnetic Resonance and the Society for Pediatric Radiology. *J Am Soc Echocardiogr*. 2014;27:111-41.

73. Seguela PE, Hascoet S, Brierre G, Bongard V, Acar P. Feasibility of three-dimensional transthoracic echocardiography to evaluate right ventricular volumes in children and comparison to left ventricular values. *Echocardiography*. 2012;29:492-501.

74. Simpson J, Lopez L, Acar P, Friedberg M, Khoo N, Ko H, *et al*. Three-dimensional echocardiography in congenital heart disease: an expert consensus document from the European Association of Cardiovascular Imaging and the American Society of Echocardiography. *Eur Heart J Cardiovasc Imaging*. 2016;17:1071-97.

75. Niemann PS, Pinho L, Balbach T, Galuschky C, Blankenhagen M, Silberbach M, *et al*. Anatomically oriented right ventricular volume measurements with dynamic three-dimensional echocardiography validated by 3-Tesla magnetic resonance imaging. *J Am Coll Cardiol*. 2007;50:1668-76.

76. Jenkins C, Chan J, Bricknell K, Strudwick M, Marwick TH. Reproducibility of right ventricular volumes and ejection fraction using real-time three-dimensional echocardiography: comparison with cardiac MRI. *Chest*. 2007;131:1844-51.

77. Leibundgut G, Rohner A, Grize L, Bernheim A, Kessel-Schaefer A, Bremerich J, *et al*. Dynamic assessment of right ventricular volumes and function by real-time three-dimensional echocardiography: a comparison study with magnetic resonance imaging in 100 adult patients. *J Am Soc Echocardiogr*. 2010;23:116-26.

78. Bhave NM, Patel AR, Weinert L, Yamat M, Freed BH, Mor-Avi V, *et al*. Three-dimensional modeling of the right ventricle from two-dimensional transthoracic echocardiographic images: utility of knowledge-based reconstruction in pulmonary arterial hypertension. *J Am Soc Echocardiogr*. 2013;26:860-7.

79. Dragulescu A, Grosse-Wortmann L, Fackoury C, Riffle S, Waiss M, Jaeggi E, et al. Echocardiographic assessment of right ventricular volumes after surgical repair of tetralogy of Fallot: clinical validation of a new echocardiographic method. *J Am Soc Echocardiogr*. 2011;24:1191-8.

80. Simpson J, Lopez L, Acar P, Friedberg M, Khoo N, Ko H, *et al*. Three-dimensional echocardiography in congenital heart disease: an expert consensus document from the European Association of Cardiovascular Imaging and the American Society of Echocardiography. *Eur Heart J Cardiovasc Imaging*. 2016;17:1071-97.

81. Iriart X, Montaudon M, Lafitte S, Chabaneix J, Reant P, Balbach T, *et al*. Right ventricle three-dimensional echography in corrected tetralogy of fallot: accuracy and variability. *Eur J Echocardiogr*. 2009;10:784-92.

82. Dragulescu A, Grosse-Wortmann L, Fackoury C, Mertens L. Echocardiographic assessment of right ventricular volumes: a comparison of different techniques in children after surgical repair of tetralogy of Fallot. *Eur Heart J Cardiovasc Imaging*. 2012;13:596-604.

83. Yu HK, Li SJ, Ip JJ, Lam WW, Wong SJ, Cheung YF. Right Ventricular Mechanics in Adults after Surgical Repair of Tetralogy of Fallot: Insights from Three-Dimensional Speckle-Tracking Echocardiography. *J Am Soc Echocardiogr*. 2014;27:423-9.

84. Galie N, Rubin L, Simonneau G. Developing a heart score: next steps. *Am J Cardiol*. 2012;110(6 Suppl):49S-51S.

85. Opotowsky AR, Ojeda J, Rogers F, Prasanna V, Clair M, Moko L, *et al*. A simple echocardiographic prediction rule for hemodynamics in pulmonary hypertension. *Circ Cardiovasc Imaging*. 2012;5:765-75.

86. D'Hooge J, Heimdal A, Jamal F, Kukulski T, Bijnens B, Rademakers F, *et al*. Regional strain and strain rate measurements by cardiac ultrasound: principles, implementation and limitations. *Eur J Echocardiogr*. 2000;1:154-70.

87. Voigt JU, Pedrizzetti G, Lysyansky P, Marwick TH, Houle H, Baumann R, *et al*. Definitions for a common standard for 2D speckle tracking echocardiography: consensus document of the EACVI/ASE/Industry Task Force to standardize deformation imaging. *Eur Heart J Cardiovasc Imaging*. 2015;16:1-11.

88. Perk G, Tunick PA, Kronzon I. Non-Doppler two-dimensional strain imaging by echocardiography--from technical considerations to clinical applications. *J Am Soc Echocardiogr*. 2007;20:234-43.

89. Leitman M, Lysyansky P, Sidenko S, Shir V, Peleg E, Binenbaum M, *et al*. Two-dimensional strain-a novel software for real-time quantitative echocardiographic assessment of myocardial function. *J Am Soc Echocardiogr*. 2004;17:1021-9.

90. Crosby J, Amundsen BH, Hergum T, Remme EW, Langeland S, Torp H. 3-D speckle tracking for assessment of regional left ventricular function. *Ultrasound Med Biol*. 2009;35:458-71.

91. Reant P, Barbot L, Touche C, Dijos M, Arsac F, Pillois X, *et al*. Evaluation of global left ventricular systolic function using three-dimensional echocardiography speckle-tracking strain parameters. *J Am Soc Echocardiogr*. 2012;25:68-79.

92. Zhang L, Gao J, Xie M, Yin P, Liu W, Li Y, *et al*. Left ventricular three-dimensional global systolic strain by real-time three-dimensional speckle-tracking in children: feasibility, reproducibility, maturational changes, and normal ranges. *J Am Soc Echocardiogr*. 2013;26:853-9.

93. Kleijn SA, Aly MF, Terwee CB, van Rossum AC, Kamp O. Reliability of left ventricular volumes and function measurements using three-dimensional speckle tracking echocardiography. *Eur Heart J Cardiovasc Imaging*. 2012;13:159-68.

94. Perez de Isla L, Balcones DV, Fernandez-Golfin C, Marcos-Alberca P, Almeria C, Rodrigo JL, *et al*. Three-dimensional-wall motion tracking: a new and faster tool for myocardial strain assessment: comparison with two-dimensional-wall motion tracking. *J Am Soc Echocardiogr*. 2009;22:325-30.

95. Jasaityte R, Heyde B, D'Hooge J. Current state of three-dimensional myocardial strain estimation using echocardiography. *J Am Soc Echocardiogr*. 2013;26:15-28.

96. Heyde B, Cygan S, Choi HF, Lesniak-Plewinska B, Barbosa D, Elen A, *et al*. Regional cardiac motion and strain estimation in three-dimensional echocardiography: a validation study in thick-walled univentricular phantoms. *IEEE Trans Ultrason Ferroelectr Freq Control*. 2012;59:668-82.

97. Heyde B, Bouchez S, Thieren S, Vandenheuvel M, Jasaityte R, Barbosa D, *et al*. Elastic image registration to quantify 3-D regional myocardial deformation from volumetric ultrasound: experimental validation in an animal model. *Ultrasound Med Biol*. 2013;39:1688-97.

98. Elen A, Choi HF, Loeckx D, Gao H, Claus P, Suetens P, *et a*l. Three-dimensional cardiac strain estimation using spatio-temporal elastic registration of ultrasound images: a feasibility study. *IEEE Trans Med Imaging*. 2008;27:1580-91.

99. Yang L, Georgescu B, Zheng Y, Wang Y, Meer P, Comaniciu D. Prediction based collaborative trackers (PCT): a robust and accurate approach toward 3D medical object tracking. *IEEE Trans Med Imaging*. 2011;30:1921-32.

100. De Craene M, Piella G, Camara O, Duchateau N, Silva E, Doltra A*, et al*. Temporal diffeomorphic free-form deformation: application to motion and strain estimation from 3D echocardiography. *Med Image Anal*. 2012;16:427-50.

101. Hjertaas JJ, Fossa H, Dybdahl GL, Gruner R, Lunde P, Matre K. Accuracy of real-time single- and multi-beat 3-d speckle tracking echocardiography in vitro. *Ultrasound Med Biol*. 2013;39:1006-14.

102. Seo Y, Ishizu T, Enomoto Y, Sugimori H, Yamamoto M, Machino T, *et al*. Validation of 3-dimensional speckle tracking imaging to quantify regional myocardial deformation. *Circ Cardiovasc Imaging*. 2009;2:451-9.

103. Seo Y, Ishizu T, Enomoto Y, Sugimori H, Aonuma K. Endocardial surface area tracking for assessment of regional LV wall deformation with 3D speckle tracking imaging. *JACC Cardiovasc Imaging*. 2011;4:358-65.

104. Ashraf M, Myronenko A, Nguyen T, Inage A, Smith W, Lowe RI, *et al*. Defining left ventricular apex-to-base twist mechanics computed from high-resolution 3D echocardiography: validation against sonomicrometry. *JACC Cardiovasc imaging*. 2010;3:227-34.

105. Bouchez S, Heyde B, Barbosa D, Vandenheuvel M, Houle H, Wang Y*, et al*. In-vivo validation of a new clinical tool to quantify three-dimensional myocardial strain using ultrasound. *Int J Cardiovasc Imaging*. 2016;32:1707-14.

106. Maffessanti F, Nesser HJ, Weinert L, Steringer-Mascherbauer R, Niel J, Gorissen W, *et al*. Quantitative evaluation of regional left ventricular function using three-dimensional speckle tracking echocardiography in patients with and without heart disease. *Am J Cardiol*. 2009;104:1755-62.

107. Hayat D, Kloeckner M, Nahum J, Ecochard-Dugelay E, Dubois-Rande JL, Jean-Francois D, *et al*. Comparison of real-time three-dimensional speckle tracking to magnetic resonance imaging in patients with coronary heart disease. *Am J Cardiol*. 2012;109:180-6.

108. Kleijn SA, Aly MF, Terwee CB, van Rossum AC, Kamp O. Three-dimensional speckle tracking echocardiography for automatic assessment of global and regional left ventricular function based on area strain. *J Am Soc Echocardiogr*. 2011;24:314-21.

109. Kleijn SA, Brouwer WP, Aly MF, Russel IK, de Roest GJ, Beek AM, *et al*. Comparison between three-dimensional speckle-tracking echocardiography and cardiac magnetic resonance imaging for quantification of left ventricular volumes and function. *Eur Heart J Cardiovasc Imaging*. 2012;13:834-9.

110. Ng A, Consultant A, Lung CentreRoyal Wolverhampton Hospitals NHST, University of BirminghamWest Midlands WVQeF, Swanevelder. Resolution in ultrasound imaging. *Continuing Education in Anaesthesia Critical Care & Pain*. 2017;11:186-92.

111. Mitchell GF, Lamas GA, Vaughan DE, Pfeffer MA. Left ventricular remodeling in the year after first anterior myocardial infarction: a quantitative analysis of contractile segment lengths and ventricular shape. *J Am Coll Cardiol*. 1992;19:1136-44.

112. Douglas PS, Morrow R, Ioli A, Reichek N. Left ventricular shape, afterload and survival in idiopathic dilated cardiomyopathy. *J Am Coll Cardiol*. 1989;13:311-5.

113. Maffessanti F, Caiani EG, Tamborini G, Muratori M, Sugeng L, Weinert L, *et al*. Serial changes in left ventricular shape following early mitral valve repair. *Am J Cardiol*. 2010;106:836-42.

114. Tischler MD, Niggel J, Borowski DT, LeWinter MM. Relation between left ventricular shape and exercise capacity in patients with left ventricular dysfunction. *J Am Coll Cardiol*. 1993;22:751-7.

115. Cohn JN, Ferrari R, Sharpe N. Cardiac remodeling--concepts and clinical implications: a consensus paper from an international forum on cardiac remodeling. Behalf of an International Forum on Cardiac Remodeling. *J Am Coll Cardiol*. 2000;35:569-82.

116. Ambale-Venkatesh B, Yoneyama K, Sharma RK, Ohyama Y, Wu CO, Burke GL, *et al*. Left ventricular shape predicts different types of cardiovascular events in the general population. *Heart*. 2017;103:499-507.

117. Lamata P, Lazdam M, Ashcroft A, Lewandowski AJ, Leeson P, Smith N. Computational mesh as a descriptor of left ventricular shape for clinical diagnosis. Computing in Cardiology; Zaragoza, Spain: IEEE; 2013. p. 571-4.

118. Medrano-Gracia P, Cowan BR, Ambale-Venkatesh B, Bluemke DA, Eng J, Finn JP, *et al*. Left ventricular shape variation in asymptomatic populations: the Multi-Ethnic Study of Atherosclerosis. *J Cardiovasc Magn Reson*. 2014;16:56.

119. Young AA, Frangi AF. Computational cardiac atlases: from patient to population and back. *Exp Physiol*. 2009;94:578-96.

120. Mansi T, Voigt I, Leonardi B, Pennec X, Durrleman S, Sermesant M*, et al*. A statistical model for quantification and prediction of cardiac remodelling: application to tetralogy of Fallot. *IEEE Trans Med Imaging*. 2011;30:1605-16.

121. Leonardi B, Taylor AM, Mansi T, Voigt I, Sermesant M, Pennec X, *et al*. Computational modelling of the right ventricle in repaired tetralogy of Fallot: can it provide insight into patient treatment? *Eur Heart J: Cardiovasc Imaging*. 2012;14:381-6.

122. Peyrat JM, Sermesant M, Pennec X, Delingette H, Xu C, McVeigh E, *et al*. Towards a statistical atlas of cardiac fiber structure. *Med Image Comput Comput Assist Interv*. 2006;9:297-304.

123. Guibert R, McLeod K, Caiazzo A, Mansi T, Fernandez MA, Sermesant M, *et al*. Group-wise construction of reduced models for understanding and characterization of pulmonary blood flows from medical images. *Med Image Anal*. 2014;18:63-82.

124. Maffessanti F, Sugeng L, Takeuchi M, Weinert L, Mor-Avi V, Lang RM, *et al*. Feasibility of regional and global left ventricular shape analysis from real-time 3d echocardiography. *Conf Proc IEEE Eng Med Biol Soc*. 2009:3641-4.

125. Duann JR, Chiang SH, Lin SB, Lin CC, Chen JH, Su JL. Assessment of left ventricular cardiac shape by the use of volumetric curvature analysis from 3D echocardiography. *Comput Med Imaging Graph*. 1999;23:89-101.

126. Salgo IS, Tsang W, Ackerman W, Ahmad H, Chandra S, Cardinale M, *et al*. Geometric assessment of regional left ventricular remodeling by three-dimensional echocardiographic shape analysis correlates with left ventricular function. *J Am Soc Echocardiogr*. 2012;25:80-8.

127. Nielsen JC, Kamenir SA, Ko HS, Lai WW, Parness IA. Ventricular septal flattening at end systole falsely predicts right ventricular hypertension in patients with ostium primum atrial septal defects. *J Am Soc Echocardiogr*. 2002;15:247-52.

128. Lee CM, Sheehan FH, Bouzas B, Chen SS, Gatzoulis MA, Kilner PJ. The shape and function of the right ventricle in Ebstein's anomaly. *Int J Cardiol*. 2013;167:704-10.

129. Sheehan FH, Ge S, Vick GW, 3rd, Urnes K, Kerwin WS, Bolson EL, *et al*. Three-dimensional shape analysis of right ventricular remodeling in repaired tetralogy of Fallot. *Am J Cardiol*. 2008;101:107-13.

130. Zhong L, Gobeawan L, Su Y, Tan JL, Ghista D, Chua T, *et al*. Right ventricular regional wall curvedness and area strain in patients with repaired tetralogy of Fallot. *Am J Physiol Heart Circ Physiol*. 2012;302:H1306-16.

131. Leary PJ, Kurtz CE, Hough CL, Waiss MP, Ralph DD, Sheehan FH. Three-dimensional analysis of right ventricular shape and function in pulmonary hypertension. *Pulm Circ*. 2012;2:34-40.

132. Addetia K, Maffessanti F, Yamat M, Weinert L, Narang A, Freed BH, *et al*. Three-dimensional echocardiography-based analysis of right ventricular shape in pulmonary arterial hypertension. *Eur Heart J Cardiovasc Imaging*. 2016;17:564-75.

133. Moceri P, Duchateau N, Baudouy D, Schouver E, Leroy S, Squara F, *et al*. Three-dimensional right-ventricular regional deformation and survival in pulmonary hypertension. *Eur Heart J Cardiovasc Imaging*. 2017. *In Press*

134. Raymond RJ, Hinderliter AL, Willis PW, Ralph D, Caldwell EJ, Williams W, *et al*. Echocardiographic predictors of adverse outcomes in primary pulmonary hypertension. *J Am Coll Cardiol*. 2002;39:1214-9.

135. Mertens LL, Friedberg MK. Imaging the right ventricle--current state of the art. *Nat Rev Cardiol*. 2010;7:551-63.

136. Reisner SA, Azzam Z, Halmann M, Rinkevich D, Sideman S, Markiewicz W, *et al*. Septal/free wall curvature ratio: a noninvasive index of pulmonary arterial pressure. *J Am Soc Echocardiogr*. 1994;7:27-35.

137. Sciancalepore MA, Maffessanti F, Patel AR, Gomberg-Maitland M, Chandra S, Freed BH, et al. Three-dimensional analysis of interventricular septal curvature from cardiac magnetic resonance images for the evaluation of patients with pulmonary hypertension. *Int J Cardiovasc Imaging*. 2012;28:1073-85.

138. Pirat B, McCulloch ML, Zoghbi WA. Evaluation of global and regional right ventricular systolic function in patients with pulmonary hypertension using a novel speckle tracking method. *Am J Cardiol*. 2006;98:699-704.

139. Hardegree EL, Sachdev A, Villarraga HR, Frantz RP, McGoon MD, Kushwaha SS, *et al*. Role of serial quantitative assessment of right ventricular function by strain in pulmonary arterial hypertension. *Am J Cardiol*. 2013;111:143-8.

140. Motoji Y, Tanaka H, Fukuda Y, Ryo K, Emoto N, Kawai H, *et a*l. Efficacy of right ventricular free-wall longitudinal speckle-tracking strain for predicting long-term outcome in patients with pulmonary hypertension. *Circ J*. 2013;77:756-63.

141. Fine NM, Chen L, Bastiansen PM, Frantz RP, Pellikka PA, Oh JK, *et al*. Outcome prediction by quantitative right ventricular function assessment in 575 subjects evaluated for pulmonary hypertension. *Circ Cardiovasc Imaging*. 2013;6:711-21.

142. Smith BC, Dobson G, Dawson D, Charalampopoulos A, Grapsa J, Nihoyannopoulos P. Three-dimensional speckle tracking of the right ventricle: toward optimal quantification of right ventricular dysfunction in pulmonary hypertension. *J Am Coll Cardiol*. 2014;64:41-51.

143. Reichek N. Right ventricular strain in pulmonary hypertension: flavor du jour or enduring prognostic index? *Circ Cardiovasc Imaging*. 2013;6:609-11.

144. Abidov A, Rischard F. Quantitative Right Ventricular Function in Pulmonary Arterial Hypertension: A Quest for a More Reliable Metric. *Echocardiography*. 2016;33:174-6.

145. Douglas PS, DeCara JM, Devereux RB, Duckworth S, Gardin JM, Jaber WA, *et al*. Echocardiographic Imaging in Clinical Trials: American Society of Echocardiography Standards for Echocardiography Core Laboratories. *J Am Soc Echocardiogr*. 2009;22:755-65.

146. Lang RM, Badano LP, Mor-Avi V, Afilalo J, Armstrong A, Ernande L, *et al*. Recommendations for cardiac chamber quantification by echocardiography in adults: an update from the American Society of Echocardiography and the European Association of Cardiovascular Imaging. *Eur Heart J Cardiovasc Imaging*. 2015;16:233-70.

147. Duchateau N, De Craene M, Allain P, Saloux E, Sermesant M. Infarct Localization From Myocardial Deformation: Prediction and Uncertainty Quantification by Regression From a Low-Dimensional Space. *IEEE Trans Med Imaging*. 2016;35:2340-52.

148. Galie N, Humbert M, Vachiery JL, Gibbs S, Lang I, Torbicki A*, et al*. 2015 ESC/ERS Guidelines for the diagnosis and treatment of pulmonary hypertension: The Joint Task Force for the Diagnosis and Treatment of Pulmonary Hypertension of the European Society of Cardiology (ESC) and the European Respiratory Society (ERS): Endorsed by: Association for European Paediatric and Congenital Cardiology (AEPC), International Society for Heart and Lung Transplantation (ISHLT). *Eur Heart J*. 2016;37:67-119.

149. Prati G, Vitrella G, Allocca G, Muser D, Buttignoni SC, Piccoli G, *et al*. Right Ventricular Strain and Dyssynchrony Assessment in Arrhythmogenic Right Ventricular Cardiomyopathy: Cardiac Magnetic Resonance Feature-Tracking Study. *Circ Cardiovasc Imaging*. 2015;8:e003647

150. Cho EJ, Jiamsripong P, Calleja AM, Alharthi MS, McMahon EM, Khandheria BK, *et al*. Right ventricular free wall circumferential strain reflects graded elevation in acute right ventricular afterload. *Am J Physiol Heart Circ Physiol*. 2009;296:H413-20.

151. Pettersen E, Helle-Valle T, Edvardsen T, Lindberg H, Smith H-J, Smevik B, *et al*. Contraction Pattern of the Systemic Right Ventricle. *J Am Coll Cardiol*. 2007;49:2450-6.

152. Bove T, Vandekerckhove K, Devos D, Panzer J, De Groote K, De Wilde H, *et al*. Functional analysis of the anatomical right ventricular components: should assessment of right ventricular function after repair of tetralogy of Fallot be refined? *Eur J Cardiothorac Surg*. 2014;45:e6-12.

153. Wald RM, Haber I, Wald R, Valente AM, Powell AJ, Geva T. Effects of regional dysfunction and late gadolinium enhancement on global right ventricular function and exercise capacity in patients with repaired tetralogy of Fallot. *Circulation*. 2009;119:1370-7.

154. Kutty S, Zhou J, Gauvreau K, Trincado C, Powell AJ, Geva T. Regional dysfunction of the right ventricular outflow tract reduces the accuracy of Doppler tissue imaging assessment of global right ventricular systolic function in patients with repaired tetralogy of Fallot. *J Am Soc Echocardiogr*. 2011;24:637-43.

155. Mediratta A, Addetia K, Medvedofsky D, Gomberg-Maitland M, Mor-Avi V, Lang RM. Echocardiographic Diagnosis of Acute Pulmonary Embolism in Patients with McConnell's Sign. *Echocardiography*. 2016;33:696-702.

156. Platz E, Hassanein AH, Shah A, Goldhaber SZ, Solomon SD. Regional right ventricular strain pattern in patients with acute pulmonary embolism. *Echocardiography*. 2012;29:464-70.

157. Medvedofsky D, Addetia K, Patel AR, Sedlmeier A, Baumann R, Mor-Avi V, *et al*. Novel Approach to Three-Dimensional Echocardiographic Quantification of

Right Ventricular Volumes and Function from Focused Views. *J Am Soc Echocardiogr*. 2015;28:1222-31.

158. Muraru D, Spadotto V, Cecchetto A, Romeo G, Aruta P, Ermacora D, *et al*. New speckle-tracking algorithm for right ventricular volume analysis from three-dimensional echocardiographic data sets: validation with cardiac magnetic resonance and comparison with the previous analysis tool. *Eur Heart J Cardiovasc Imaging*. 2016;17:1279-89.

159. Vitarelli A, Mangieri E, Terzano C, Gaudio C, Salsano F, Rosato E, *et al*. Three-Dimensional Echocardiography and 2D-3D Speckle-Tracking Imaging in Chronic Pulmonary Hypertension: Diagnostic Accuracy in Detecting Hemodynamic Signs of Right Ventricular (RV) Failure. *J Am Heart Assoc*. 2015;4(3):e001584-e.

160. Ryo K, Goda A, Onishi T, Delgado-Montero A, Tayal B, Champion HC, *et al*. Characterization of right ventricular remodeling in pulmonary hypertension associated with patient outcomes by 3-dimensional wall motion tracking echocardiography. *Circ Cardiovasc Imaging*. 2015;8(6).

161. Sitbon O, Benza RL, Badesch DB, Barst RJ, Elliott CG, Gressin V, *et al*. Validation of two predictive models for survival in pulmonary arterial hypertension. *Eur Respir J*. 2015;46:152-64.

162. Guihaire J, Noly PE, Schrepfer S, Mercier O. Advancing knowledge of right ventricular pathophysiology in chronic pressure overload: Insights from experimental studies. *Arch Cardiovasc Dis*. 2015; 108:519-29.

163. Vanderpool RR, Pinsky MR, Naeije R, Deible C, Kosaraju V, Bunner C, *et al*. RV-pulmonary arterial coupling predicts outcome in patients referred for pulmonary hypertension. *Heart*. 2015;101:37-43.

164. Maffessanti F, Muraru D, Esposito R, Gripari P, Ermacora D, Santoro C, *et al*. Age-, body size-, and sex-specific reference values for right ventricular volumes and ejection fraction by three-dimensional echocardiography: a multicenter echocardiographic study in 507 healthy volunteers. *Circ Cardiovasc Imaging*. 2013;6:700-10.

165. Grapsa J, Gibbs JS, Cabrita IZ, Watson GF, Pavlopoulos H, Dawson D, *et al*. The association of clinical outcome with right atrial and ventricular remodelling in patients with pulmonary arterial hypertension: study with real-time three-dimensional echocardiography. *Eur Heart J Cardiovasc Imaging*. 2012;13:666-72.

166. Grapsa J, Gibbs JSR, Dawson D, Watson G, Patni R, Athanasiou T*, et al*. Morphologic and Functional Remodeling of the Right Ventricle in Pulmonary Hypertension by Real Time Three Dimensional Echocardiography. *Am J Cardiol*. 2012;109:906-13.

167. Van De Bruaene A, De Meester P, Voigt JU, Delcroix M, Pasquet A, De Backer J, *et al*. Worsening in oxygen saturation and exercise capacity predict adverse outcome in patients with Eisenmenger syndrome. *Int J Cardiol*. 2013;168:1386-92.

168. Schuijt MTU, Blok IM, Zwinderman AH, van Riel A, Schuuring MJ, de Winter RJ, *et al*. Mortality in pulmonary arterial hypertension due to congenital heart disease: Serial changes improve prognostication. *Int J Cardiol*. 2017;243:449-53.

169. Lang RM, Badano LP, Mor-Avi V, Afilalo J, Armstrong A, Ernande L*, et al*. Recommendations for cardiac chamber quantification by echocardiography in adults: an update from the American Society of Echocardiography and the European Association of Cardiovascular Imaging. *J Am Soc Echocardiogr*. 2015;28:1-39.

170. Rudski LG, Lai WW, Afilalo J, Hua L, Handschumacher MD, Chandrasekaran K, *et al*. Guidelines for the echocardiographic assessment of the right heart in adults: a report from the American Society of Echocardiography endorsed by the European Association of Echocardiography, a registered branch of the European Society of Cardiology, and the Canadian Society of Echocardiography. *J Am Soc Echocardiogr*. 2010;23:685-713.

171. Sitbon O, Channick R, Chin KM, Frey A, Gaine S, Galie N, *et al*. Selexipag for the Treatment of Pulmonary Arterial Hypertension. *N Engl J Med*. 2015;373:2522-33.

172. Pulido T, Adzerikho I, Channick RN, Delcroix M, Galie N, Ghofrani HA, *et al*. Macitentan and morbidity and mortality in pulmonary arterial hypertension. *N Engl J Med*. 2013;369:809-18.

173. DeLong ER, DeLong DM, Clarke-Pearson DL. Comparing the areas under two or more correlated receiver operating characteristic curves: a nonparametric approach. *Biometrics*. 1988;44:837-45.

174. Van De Bruaene A, De Meester P, Voigt J-U, Delcroix M, Pasquet A, De Backer J, *et al*. Worsening in oxygen saturation and exercise capacity predict adverse outcome in patients with Eisenmenger syndrome. *Int J Cardiol*. 2013;168:1386-92.

175. Ghofrani HA, Grimminger F, Grunig E, Huang Y, Jansa P, Jing ZC, *et al*. Predictors of long-term outcomes in patients treated with riociguat for pulmonary arterial hypertension: data from the PATENT-2 open-label, randomised, long-term extension trial. *Lancet Respir Med*. 2016;4:361-71.

176. Medrek SK, Kloefkorn C, Nguyen DTM, Graviss EA, Frost AE, Safdar Z. Longitudinal change in pulmonary arterial capacitance as an indicator of prognosis and response to therapy and in pulmonary arterial hypertension. *Pulm Circ*. 2017;7:399-408.

177. Puwanant S, Park M, Popovic ZB, Tang WH, Farha S, George D, *et al*. Ventricular geometry, strain, and rotational mechanics in pulmonary hypertension. *Circulation*. 2010;121:259-66.

178. Hardegree EL, Sachdev A, Fenstad ER, Villarraga HR, Frantz RP, McGoon MD, *et al*. Impaired left ventricular mechanics in pulmonary arterial hypertension: identification of a cohort at high risk. *Circ Heart Fail*. 2013;6:748-55.

179. Nielsen EA, Okumura K, Sun M, Hjortdal VE, Redington AN, Friedberg MK. Regional septal hinge-point injury contributes to adverse biventricular interactions in pulmonary hypertension. *Physiol Rep*. 2017;5(14).

180. Nagata Y, Wu VC, Kado Y, Otani K, Lin FC, Otsuji Y, *et al*. Prognostic Value of Right Ventricular Ejection Fraction Assessed by Transthoracic 3D Echocardiography. *Circ Cardiovasc Imaging*. 2017;10(2).

181. Reddy S, Bernstein D. Molecular Mechanisms of Right Ventricular Failure. *Circulation*. 2015;132:1734-42.

182. Zaffran S, Kelly RG, Meilhac SM, Buckingham ME, Brown NA. Right ventricular myocardium derives from the anterior heart field. *Circ Res*. 2004;95:261-8.

183. Friedberg MK, Redington AN. Right versus left ventricular failure: differences, similarities, and interactions. *Circulation*. 2014;129:1033-44.

184. Giardini A, Lovato L, Donti A, Formigari R, Gargiulo G, Picchio FM, *et al*. A pilot study on the effects of carvedilol on right ventricular remodelling and exercise tolerance in patients with systemic right ventricle. *Int J Cardiol*. 2007;114:241-6.

185. Hoffman JI, Kaplan S. The incidence of congenital heart disease. *J Am Coll Cardiol*. 2002;39:1890-900.

186. Geva T, Martins JD, Wald RM. Atrial septal defects. *Lancet*. 2014;383:1921-32.

187. Caputo S, Capozzi G, Russo MG, Esposito T, Martina L, Cardaropoli D*, et al*. Familial recurrence of congenital heart disease in patients with ostium secundum atrial septal defect. *Eur Heart J*. 2005;26:2179-84.

188. McElhinney DB, Geiger E, Blinder J, Benson DW, Goldmuntz E. NKX2.5 mutations in patients with congenital heart disease. *J Am Coll Cardiol*. 2003;42:1650-5.

189. Warnes CA, Williams RG, Bashore TM, Child JS, Connolly HM, Dearani JA, *et al*. ACC/AHA 2008 Guidelines for the Management of Adults with Congenital Heart Disease: a report of the American College of Cardiology/American Heart Association Task Force on Practice Guidelines (writing committee to develop guidelines on the management of adults with congenital heart disease). *Circulation*. 2008;118:e714-833.

190. Baumgartner H, Bonhoeffer P, De Groot NMS, de Haan F, Deanfield JE, Galie N, *et al*. ESC Guidelines for the management of grown-up congenital heart disease (new version 2010): The Task Force on the Management of Grown-up Congenital Heart Disease of the European Society of Cardiology (ESC). *Eur Heart J*. 2010;31:2915-57.

191. Anderson RH, Weinberg PM. The clinical anatomy of tetralogy of fallot. *Cardiol Young*. 2005;15:38-47.

192. Marelli AJ, Mackie AS, Ionescu-Ittu R, Rahme E, Pilote L. Congenital heart disease in the general population: changing prevalence and age distribution. *Circulation*. 2007;115:163-72.

193. Marelli AJ, Ionescu-Ittu R, Mackie AS, Guo L, Dendukuri N, Kaouache M. Lifetime prevalence of congenital heart disease in the general population from 2000 to 2010. *Circulation*. 2014;130:749-56.

194. Starr JP. Tetralogy of fallot: yesterday and today. *World J Surg*. 2010;34:658-68.

195. Kawashima Y, Kitamura S, Nakano S, Yagihara T. Corrective surgery for tetralogy of Fallot without or with minimal right ventriculotomy and with repair of the pulmonary valve. *Circulation*. 1981;64:II147-53.

196. Van Arsdell GS, Maharaj GS, Tom J, Rao VK, Coles JG, Freedom RM, *et al*. What is the optimal age for repair of tetralogy of Fallot? *Circulation*. 2000;102:III123-9.

197. Pacifico AD, Sand ME, Bargeron LM, Jr., Colvin EC. Transatrial-transpulmonary repair of tetralogy of Fallot. *J Thorac Cardiovasc Surg*. 1987;93:919-24.

198. Karl TR, Sano S, Pornviliwan S, Mee RB. Tetralogy of Fallot: favorable outcome of nonneonatal transatrial, transpulmonary repair. *Ann Thorac Surg*. 1992;54:903-7.

199. Silvestry FE, Cohen MS, Armsby LB, Burkule NJ, Fleishman CE, Hijazi ZM, *et al*. Guidelines for the Echocardiographic Assessment of Atrial Septal Defect and Patent Foramen Ovale: From the American Society of Echocardiography and Society for Cardiac Angiography and Interventions. *J Am Soc Echocardiogr*. 2015;28:910-58.

200. Li W, Davlouros PA, Kilner PJ, Pennell DJ, Gibson D, Henein MY, *et al*. Doppler-echocardiographic assessment of pulmonary regurgitation in adults with repaired tetralogy of Fallot: comparison with cardiovascular magnetic resonance imaging. *Am Heart J*. 2004;147:165-72.

201. Renella P, Aboulhosn J, Lohan DG, Jonnala P, Finn JP, Satou GM, *et al*. Two-dimensional and Doppler echocardiography reliably predict severe pulmonary regurgitation as quantified by cardiac magnetic resonance. *J Am Soc Echocardiogr*. 2010;23:880-6.

202. Ma L, Zou B, Yan H. Identifying EGFR mutation-induced drug resistance based on alpha shape model analysis of the dynamics. *Proteome Sci*. 2016;14:12.

203. Loriot S, Cazals F. Modeling macro-molecular interfaces with Intervor. *Bioinformatics*. 2010;26:964-5.

204. Board CE. CGAL 4.11, Computational Geometry Algorithms Library, http://www.cgal.org/. 2017.

205. Hotelling H. The generalization of Student's ratio. *Annals of Mathematical Statistics*. 1931;2:360-78.

206. Duchateau N, De Craene M, Piella G, Silva E, Doltra A, Sitges M*, et al*. A spatiotemporal statistical atlas of motion for the quantification of abnormal myocardial tissue velocities. *Med Image Anal*. 2011;15:316-28.

207. Duchateau N, Doltra A, Silva E, De Craene M, Piella G, Castel MA, *et al.* Atlas-based quantification of myocardial motion abnormalities: added-value for understanding the effect of cardiac resynchronization therapy. *Ultrasound Med Biol*. 2012;38:2186-97.

208. Eyskens B, Ganame J, Claus P, Boshoff D, Gewillig M, Mertens L. Ultrasonic strain rate and strain imaging of the right ventricle in children before and after percutaneous closure of an atrial septal defect. *J Am Soc Echocardiogr*. 2006;19:994-1000.

209. Jategaonkar SR, Scholtz W, Butz T, Bogunovic N, Faber L, Horstkotte D. Two-dimensional strain and strain rate imaging of the right ventricle in adult patients before and after percutaneous closure of atrial septal defects. *Eur J Echocardiogr*. 2009;10:499-502.

210. Ko HK, Yu JJ, Cho EK, Kang SY, Seo CD, Baek JS, *et al*. Segmental Analysis of Right Ventricular Longitudinal Deformation in Children before and after Percutaneous Closure of Atrial Septal Defect. *J Cardiovasc Ultrasound*. 2014;22:182-8.

211. Van De Bruaene A, Buys R, Vanhees L, Delcroix M, Voigt JU, Budts W. Regional right ventricular deformation in patients with open and closed atrial septal defect. *Eur J Echocardiogr*. 2010;12:206-13.

212. Tezuka F, Hort W, Lange PE, Nurnberg JH. Muscle fiber orientation in the development and regression of right ventricular hypertrophy in pigs. *Acta Pathol Jpn.* 1990;40:402-7.

213. Bodhey NK, Beerbaum P, Sarikouch S, Kropf S, Lange P, Berger F, *et al*. Functional analysis of the components of the right ventricle in the setting of tetralogy of Fallot. *Circ Cardiovasc Imaging*. 2008;1:141-7.

214. Muller J, Hager A, Diller GP, Derrick G, Buys R, Dubowy KO, *et al*. Peak oxygen uptake, ventilatory efficiency and QRS-duration predict event free survival in patients late after surgical repair of tetralogy of Fallot. *Int J Cardiol*. 2015;196:158-64.

215. Gatzoulis MA, Till JA, Somerville J, Redington AN. Mechanoelectrical interaction in tetralogy of Fallot. QRS prolongation relates to right ventricular size and predicts malignant ventricular arrhythmias and sudden death. *Circulation*. 1995;92:231-7.

216. Addetia K, Uriel N, Maffessanti F, Sayer G, Adatya S, Kim GH, *et al*. 3D Morphological Changes in LV and RV During LVAD Ramp Studies. *JACC Cardiovasc imaging*. 2017. *In Press*

217. Rhoades RA, Bell DR. Medical Phisiology: Principles for Clinical Medicine: Wolters Kluwer Health; 2012.

218. Trayanova NA. Whole-heart modeling: applications to cardiac electrophysiology and electromechanics. *Circ Res*. 2011;108:113-28.

219. Humphrey JD, Strumpf RK, Yin FC. Determination of a constitutive relation for passive myocardium: I. A new functional form. *J Biomech Eng*. 1990;112:333-9.

220. Nash MP, Hunter PJ. Computational Mechanics of the Heart. *J. Elast*. 2000;61:113-41.

221. Bestel J, Clément F, Sorine M. A Biomechanical Model of Muscle Contraction. In: Niessen WJ, Viergever MA, editors. Medical Image Computing and Computer-Assisted Intervention – MICCAI 2001: 4th International Conference Utrecht, The Netherlands, October 14–17, 2001 Proceedings. Berlin, Heidelberg: Springer Berlin Heidelberg; 2001. p. 1159-61.

222. Sachse FB. Computational Cardiology: Modeling of Anatomy, Electrophysiology, and Mechanics: Springer; 2004.

223. Tobon-Gomez C, Duchateau N, Sebastian R, Marchesseau S, Camara O, Donal E*, et al*. Understanding the mechanisms amenable to CRT response: from pre-

operative multimodal image data to patient-specific computational models. *Med Biol Eng Comput*. 2013; 51:1235-50.

224. Land S, Niederer SA, Louch WE, Sejersted OM, Smith NP. Integrating multi-scale data to create a virtual physiological mouse heart. *Interface Focus*. 2013;3:20120076.

225. Campbell SG, McCulloch AD. Multi-scale computational models of familial hypertrophic cardiomyopathy: genotype to phenotype. *J R Soc Interface*. 2011;8:1550-61.

226. Sermesant M, Chabiniok R, Chinchapatnam P, Mansi T, Billet F, Moireau P, *et al*. Patient-specific electromechanical models of the heart for the prediction of pacing acute effects in CRT: a preliminary clinical validation. *Med Image Anal*. 2012;16:201-15.

227. Huntjens PR, Walmsley J, Ploux S, Bordachar P, Prinzen FW, Delhaas T, *et al*. Influence of left ventricular lead position relative to scar location on response to cardiac resynchronization therapy: a model study. *Europace*. 2014;16:iv62-iv8.

228. Ashikaga H, Arevalo H, Vadakkumpadan F, Blake RC, 3rd, Bayer JD, Nazarian S, *et al*. Feasibility of image-based simulation to estimate ablation target in human ventricular arrhythmia. *Heart Rhythm*. 2013;10:1109-16.

229. Hunter PJ, Borg TK. Integration from proteins to organs: the Physiome Project. *Nat Rev Mol Cell Biol*. 2003;4:237-43.

230. Niederer SA, Smith NP. An improved numerical method for strong coupling of excitation and contraction models in the heart. *Prog Biophys Mol Biol*. 2008;96:90-111.

231. Relan J, Chinchapatnam P, Sermesant M, Rhode K, Ginks M, Delingette H, *et al*. Coupled personalization of cardiac electrophysiology models for prediction of ischaemic ventricular tachycardia. *Interface Focus*. 2011;1:396-407.

232. Xi J, Lamata P, Niederer S, Land S, Shi W, Zhuang X, *et al*. The estimation of patient-specific cardiac diastolic functions from clinical measurements. *Med Image Anal*. 2013;17:133-46.

233. Nielsen PM, Le Grice IJ, Smaill BH, Hunter PJ. Mathematical model of geometry and fibrous structure of the heart. *Am J Physiol*. 1991;260:H1365-78.

234. Marchesseau S, Delingette H, Sermesant M, Ayache N. Fast parameter calibration of a cardiac electromechanical model from medical images based on the unscented transform. *Biomech Model Mechanobiol*. 2013;12:815-31.

235. Kayvanpour E, Mansi T, Sedaghat-Hamedani F, Amr A, Neumann D, Georgescu B, *et al*. Towards Personalized Cardiology: Multi-Scale Modeling of the Failing Heart. *PLoS One*. 2015;10:e0134869.

236. Reuben SR. Compliance of the human pulmonary arterial system in disease. *Circ Res*. 1971;29:40-50.

237. Ghio S, Schirinzi S, Pica S. Pulmonary arterial compliance: How and why should we measure it? *Glob Cardiol Sci Pract*. 2015;4:58.

238. Mahapatra S, Nishimura RA, Oh JK, McGoon MD. The prognostic value of pulmonary vascular capacitance determined by Doppler echocardiography in patients with pulmonary arterial hypertension. *J Am Soc Echocardiogr*. 2006;19:1045-50.

239. Mahapatra S, Nishimura RA, Sorajja P, Cha S, McGoon MD. Relationship of pulmonary arterial capacitance and mortality in idiopathic pulmonary arterial hypertension. *J Am Coll Cardiol*. 2006;47:799-803.

240. Lankhaar JW, Westerhof N, Faes TJ, Gan CT, Marques KM, Boonstra A*, et al*. Pulmonary vascular resistance and compliance stay inversely related during treatment of pulmonary hypertension. *Eur Heart J*. 2008;29:1688-95.

241. Mollero R, Pennec X, Delingette H, Garny A, Ayache N, Sermesant M. Multifidelity-CMA: a multifidelity approach for efficient personalisation of 3D cardiac electromechanical models. *Biomech Model Mechanobiol*. 2017. *In Press*

242. Chapelle D, Le Tallec P, Moireau P, Sorine M. Energy-preserving muscle tissue model: Formulation and compatible discretizations. *Int J Mult Comp Eng*. 2012;10:189-211.

243. Mollero R, Delingette H, Datar M, Heimann T, Hauser JA, Panesar D, et al. Longitudinal Analysis using Personalised 3D Cardiac Models with Population-Based

Priors: Application to Paediatric Cardiomyopathies. Medical Image Computing and Computer Assisted Intervention (MICCAI); Quebec City, Canada.: MICCAI 2017; 2017.

244. Abbas AE, Fortuin FD, Schiller NB, Appleton CP, Moreno CA, Lester SJ. A simple method for noninvasive estimation of pulmonary vascular resistance. *J Am Coll Cardiol*. 2003;41:1021-7.

245. Mousseaux E, Tasu JP, Jolivet O, Simonneau G, Bittoun J, Gaux JC. Pulmonary arterial resistance: noninvasive measurement with indexes of pulmonary flow estimated at velocity-encoded MR imaging--preliminary experience. *Radiology*. 1999;212:896-902.

246. Swift AJ, Rajaram S, Condliffe R, Capener D, Hurdman J, Elliot CA, *et al*. Diagnostic accuracy of cardiovascular magnetic resonance imaging of right ventricular morphology and function in the assessment of suspected pulmonary hypertension results from the ASPIRE registry. *J Cardiovasc Magn Reson*. 2012;14:40.

247. Kheyfets VO, Dunning J, Truong U, Ivy D, Hunter K, Shandas R. A Zero-Dimensional Model and Protocol for Simulating Patient-Specific Pulmonary Hemodynamics From Limited Clinical Data. J Biomech Eng. 2016;138: 121001-1-8.

248. Bonderman D, Martischnig AM, Vonbank K, Nikfardjam M, Meyer B, Heinz G, *et al*. Right ventricular load at exercise is a cause of persistent exercise limitation in patients with normal resting pulmonary vascular resistance after pulmonary endarterectomy. *Chest*. 2011;139:122-7.

249. de Perrot M, McRae K, Shargall Y, Thenganatt J, Moric J, Mak S, et al. Early postoperative pulmonary vascular compliance predicts outcome after pulmonary endarterectomy for chronic thromboembolic pulmonary hypertension. *Chest*. 2011;140:34-41.

250. Sugimoto K, Yoshihisa A, Nakazato K, Jin Y, Suzuki S, Yokokawa T, *et al*. Pulmonary Arterial Capacitance Predicts Cardiac Events in Pulmonary Hypertension Due to Left Heart Disease. *PLoS One*. 2016;11:e0165603.

251. Castelain V, Herve P, Lecarpentier Y, Duroux P, Simonneau G, Chemla D. Pulmonary artery pulse pressure and wave reflection in chronic pulmonary

thromboembolism and primary pulmonary hypertension. *J Am Coll Cardiol*. 2001;37:1085-92.

252. Dupont M, Mullens W, Skouri HN, Abrahams Z, Wu Y, Taylor DO, *et al*. Prognostic role of pulmonary arterial capacitance in advanced heart failure. *Circ Heart Fail*. 2012;5:778-85.

253. Al-Naamani N, Preston IR, Paulus JK, Hill NS, Roberts KE. Pulmonary Arterial Capacitance Is an Important Predictor of Mortality in Heart Failure With a Preserved Ejection Fraction. *JACC Heart Fail*. 2015;3:467-74.

254. Giffard-Roisin S, Jackson T, Fovargue L, Lee J, Delingette H, Razavi R, *et al*. Noninvasive Personalization of a Cardiac Electrophysiology Model From Body Surface Potential Mapping. *IEEE Trans Biomed Eng*. 2017;64:2206-18.